

Ab Initio Study of Low pH Vanadium (V)

by

Yaoting Zhang

A Thesis Submitted to

Saint Mary's University, Halifax, Nova Scotia

In Partial Fulfillment of the Requirement for

the Degree of the Masters of Science in Applied Science (Chemistry)

March 2012, Halifax, NS

Copyright Yaoting Zhang, 2012

Approved:	Dr. Cory Pye Supervisor
Approved:	Dr. Katherine Darvesh External Examine
Approved:	Dr. Jason Masuda Supervisor Committee Member
Approved:	Dr. Ron Russell Supervisor Committee Member
Approved:	Dr. Jason Clyburne Program Representative
Approved:	Dr. Zhongming Dong Graduate Studies Representative
Date:	March 12 th , 2012



Library and Archives
Canada

Published Heritage
Branch

395 Wellington Street
Ottawa ON K1A 0N4
Canada

Bibliothèque et
Archives Canada

Direction du
Patrimoine de l'édition

395, rue Wellington
Ottawa ON K1A 0N4
Canada

Your file Votre référence
ISBN: 978-0-494-83805-1

Our file Notre référence
ISBN: 978-0-494-83805-1

NOTICE:

The author has granted a non-exclusive license allowing Library and Archives Canada to reproduce, publish, archive, preserve, conserve, communicate to the public by telecommunication or on the Internet, loan, distribute and sell theses worldwide, for commercial or non-commercial purposes, in microform, paper, electronic and/or any other formats.

The author retains copyright ownership and moral rights in this thesis. Neither the thesis nor substantial extracts from it may be printed or otherwise reproduced without the author's permission.

In compliance with the Canadian Privacy Act some supporting forms may have been removed from this thesis.

While these forms may be included in the document page count, their removal does not represent any loss of content from the thesis.

AVIS:

L'auteur a accordé une licence non exclusive permettant à la Bibliothèque et Archives Canada de reproduire, publier, archiver, sauvegarder, conserver, transmettre au public par télécommunication ou par l'Internet, prêter, distribuer et vendre des thèses partout dans le monde, à des fins commerciales ou autres, sur support microforme, papier, électronique et/ou autres formats.

L'auteur conserve la propriété du droit d'auteur et des droits moraux qui protègent cette thèse. Ni la thèse ni des extraits substantiels de celle-ci ne doivent être imprimés ou autrement reproduits sans son autorisation.

Conformément à la loi canadienne sur la protection de la vie privée, quelques formulaires secondaires ont été enlevés de cette thèse.

Bien que ces formulaires aient inclus dans la pagination, il n'y aura aucun contenu manquant.

Canada

Table of Contents

Abstract.....	i
Acknowledgements.....	ii
List of Abbreviations	iii
List of Figures.....	iv
List of Tables	vi
Chapter I: Introduction	1
Part I: Vanadium (V).....	1
<i>Vanadium in Nature</i>	1
<i>Aqueous Vanadium Chemistry</i>	1
<i>Importance of the Aqueous Chemistry of Vanadium</i>	5
<i>Diabetes</i>	5
<i>Diabetes and Vanadium Compounds</i>	6
<i>Diabetic Activities of Vanadium Compounds</i>	9
<i>Energy : Vanadium Redox Flow Battery</i>	10
<i>Challenges of Instrumental Analysis of Aqueous Chemistry of Vanadium</i>	11
Part II: Computational Chemistry.....	14
<i>Quantum Theory Basics: Schrödinger Equation</i>	14
<i>Hartree-Fock Theory</i>	16
<i>Basis Sets</i>	18
<i>Post Hartree-Fock Methods</i>	20
<i>Density Functional Theory</i>	21
<i>Polarizable Continuum Model</i>	23
<i>Natural Bond-Order Analysis</i>	24
<i>Car-Parrinello Molecular Dynamics</i>	24
Chapter II: Objective and Methods.....	26
<i>Equipment</i>	29
Chapter III: $\text{VO}_2(\text{H}_2\text{O})_4^+$	31
<i>Introduction</i>	31

<i>Results and Discussions</i>	32
Geometries.....	32
Energies	34
Bond Lengths.....	37
Vibrational Frequencies.....	39
Charges	44
<i>Conclusion</i>	45
Chapter IV: H_3VO_4	46
<i>Introduction</i>	46
<i>Results and Discussions</i>	47
Geometries.....	47
Energies	49
Bond Lengths.....	52
Vibrational Frequencies	56
Charges	58
<i>Conclusion</i>	59
Chapter V: H_2VO_4^-	61
<i>Introduction</i>	61
<i>Results and Discussions</i>	63
Geometries and Energies	63
Bond Lengths.....	68
Vibrational Frequencies	73
Charges	75
<i>Conclusion</i>	76
Chapter VI: The H_2VO_4^- to VO_2^+ Conversion	78
<i>Introduction</i>	78
<i>Results and Discussions</i>	80
Mechanism I: Vanadic Acid Cation	82
Mechanism II : Direct Double Protonation of Dihydrogen Vanadate	85
Mechanism II: The CPMD Attempt.....	87

The Solvation Effect	87
<i>Conclusion</i>	96
References.....	98
Appendix.....	101

***Ab Initio* Study of Low pH Vanadium (V)**

by Yaoting Zhang

March 12th, 2012

Abstract

The aqueous chemistry of the low pH vanadium (V) species is complex. These low concentration species of vanadium (V) cannot be studied by conventional experimental methods to obtain the important structural information of vanadium compounds. This project studied three compounds of vanadium (V): VO_2^+ , H_3VO_4 and H_2VO_4^- using *ab initio* computational methods (HF, MP2, B3LYP, CCSD(T) and CPMD). The geometries of hydrated (up to six water molecules) VO_2^+ , H_3VO_4 and H_2VO_4^- were calculated using the *ab initio* methods. The effects of hydration on the bond lengths and vibrational frequencies of these compounds were established. The coordination of water molecules weakened the bonds and decreased their corresponding vibrational frequencies. The hydrogen bonded water molecules strengthened the bonds and increased their corresponding vibrational frequencies. The mechanism of the conversion of H_2VO_4^- to VO_2^+ was studied. The complete hydration of H_2VO_4^- increased the coordination number to five and the double protonation of its hydroxo ligands produced the VO_2^+ .

Acknowledgements

I would like to thank Dr. Cory Pye for supervising this project. Having had this opportunity to work on this project allowed me to develop my skills as a chemist and as a researcher. I would like to thank my enthusiastic lab mates Jane Ferguson, Barbara Goodall, Liwei Cheng, Rajesh Satyamurti and especially Mr. Daniel Whynot for many valuable discussions. I would like to thank the faculty and staff members of the Department of Chemistry, Saint Mary's University, for their support. I am very grateful to Dr. Jason Clyburne and Dr. Katherine Robertson, for their invaluable insights in inorganic chemistry and wonderful suggestions for this thesis. I also express my gratitude to Drs. Ronald Russell and Jason Masuda for acting as members of my supervisory committee and Dr. Katherine Darvesh for reappearing as my external reader. I wish to acknowledge The Atlantic Computational Excellence network (ACEnet) for the access to the state of art computational hardware. I would like to thank Ross Dickson and Sergiy Khan, the ACEnet staff members, who were very prompt and helpful to solve any occurring computational issues. I would like to acknowledge the Department of Chemistry, Faculty of Graduate Studies and Research and ACEnet for the financial support.

Lastly, I would like to extend my thanks to my family and friends for their support over these years and hope one day they will read this thesis.

List of Abbreviations

ACEnet	Atlantic Computational Excellence network
BEOV	Bis(ethyl maltolato) oxovanadium IV
B3LYP	Becke-3 parameter LeeYang Parr
BLYP	Becke LeeYang Parr
CCSD(T)	Coupled Cluster Singles Doubles (Triples)
CPMD	Carr-Parrinello Molecular Dynamics
DFT	Density Functional Theory
IEFPCM	Integral-Equation-Formalism PCM
IR	Infrared Spectroscopy
GTO	Gaussian-Type Orbital
HF	Hartree-Fock
HPC	High Performance Computing
LCAO	Linear Combination of Atomic Orbitals
MP2	Second-Order Møller-Plesset Perturbation Theory
NBO	Natural Bond Orbital
NMR	Nuclear Magnetic Resonance
NPA	Natural Population Analysis
PCM	Polarizable Continuum Model
PES	Potential Energy Surface
SCF	Self-Consistent Field
STO	Slater-Type Orbital
STZ rats	Streptozocin-Treated rats
TS	Transition Structure
VRFB	Vanadium Redox Flow Battery

List of Figures

Figure 1.1. Stability domains of various vanadates and polyvanadates as a function of the pH and vanadium concentration, by Sadoc <i>et al</i>	2
Figure 1.2. Decavanadate structure in the form of $\text{Na}_6\text{V}_{10}\text{O}_{28} \cdot 18\text{H}_2\text{O}$	4
Figure 1.3. Structure of Bis(ethyl maltolato) oxovanadium IV.....	8
Figure 1.4. Structure of $\text{VO}_2\text{dipic}^-$	9
Figure 3.1. The B3LYP/6-31+G* optimized structures of oxovanadyl cation $\text{VO}_2(\text{H}_2\text{O})_n^+$, where $n=0-4$	33
Figure 3.2. The PCM B3LYP/6-31+G* optimized $\text{VO}_2(\text{H}_2\text{O})_n^+$, where $n=1-4$	34
Figure 3.3. The B3LYP/6-31+G* Optimized Structure of $\text{VO}_2(\text{H}_2\text{O})_3^+ \cdot \text{H}_2\text{O}$	35
Figure 3.4. The V=O and V-O bond lengths calculated at the HF/6-31+G* level for $\text{VO}_2(\text{H}_2\text{O})_n^+$, with $n=0-4$	38
Figure 3.5. The V=O and V-O bond lengths calculated at the B3LYP/6-31+G* level for $\text{VO}_2(\text{H}_2\text{O})_n^+$, with $n=0-4$	38
Figure 3.6. Vibrational frequencies calculated at the HF/6-31+G* level for $\text{VO}_2(\text{H}_2\text{O})_n^+$, with $n=0-4$	41
Figure 3.7. Vibrational frequencies calculated at the B3LYP/6-31+G* level for $\text{VO}_2(\text{H}_2\text{O})_n^+$, with $n=0-4$	42
Figure 4.1. B3LYP/6-31+G* Optimized Structures of $\text{H}_3\text{VO}_4 \cdot n\text{H}_2\text{O}$, where $n=0-6$	48
Figure 4.2. B3LYP/6-31+G* optimized global minima of the $\text{H}_3\text{VO}_4 \cdot 5\text{H}_2\text{O}$ and $\text{H}_3\text{VO}_4 \cdot 6\text{H}_2\text{O}$ structures.	49
Figure 4.3. The B3LYP/cc-pVTZ optimized structure of $\text{V}(\text{OH})_5$	51
Figure 4.4. The V=O and V-O bond lengths calculated at the MP2/6-31+G* level for $\text{H}_3\text{VO}_4 \cdot n\text{H}_2\text{O}$, with $n=0-6$	53
Figure 4.5. The V=O and V-O bond lengths calculated at the B3LYP/6-31+G* level for $\text{H}_3\text{VO}_4 \cdot n\text{H}_2\text{O}$, with $n=0-6$	54
Figure 4.6. The V- -O distances calculated at the MP2/6-31+G* level for $\text{H}_3\text{VO}_4 \cdot n\text{H}_2\text{O}$, with $n=0-6$	55
Figure 4.7. The V- -O distances calculated at the B3LYP/6-31+G* level for $\text{H}_3\text{VO}_4 \cdot n\text{H}_2\text{O}$, with $n=0-6$	55
Figure 4.8. Vibrational Frequencies calculated at the MP2/6-31+G* level for $\text{H}_3\text{VO}_4 \cdot n\text{H}_2\text{O}$, with $n=0-6$	57
Figure 4.9. Vibrational Frequencies calculated at the B3LYP/6-31+G* level for $\text{H}_3\text{VO}_4 \cdot n\text{H}_2\text{O}$, with $n=0-6$	57
Figure 5.1. Two possible orientations of dihydrogen vanadate: A (C_2) and B (C_s) orientations.	63

Figure 5.2. The optimized structures of $\text{H}_2\text{VO}_4^- \cdot n\text{H}_2\text{O}$, $n=0-6$, calculated by B3LYP/6-31+G*. Solid boxes denote the MP2/6-31+G* global minima.	65
Figure 5.3. The B3LYP/cc-pVTZ Optimized Structure of $\text{VO}(\text{OH})_4^-$	68
Figure 5.4. The V=O and V-O bond lengths calculated at the MP2/6-31+G* level for $\text{H}_2\text{VO}_4^- \cdot n\text{H}_2\text{O}$, with $n=0-6$	70
Figure 5.5. The V=O and V-O bond lengths calculated at the B3LYP/6-31+G* level for $\text{H}_2\text{VO}_4^- \cdot n\text{H}_2\text{O}$, with $n=0-6$	70
Figure 5.6. The V--O distances calculated at the MP2/6-31+G* level for $\text{H}_2\text{VO}_4^- \cdot n\text{H}_2\text{O}$, with $n=0-6$	72
Figure 5.7. The V--O distances calculated at the B3LYP/6-31+G* level for $\text{H}_2\text{VO}_4^- \cdot n\text{H}_2\text{O}$, with $n=0-6$	72
Figure 5.8. Vibrational Frequencies calculated at the MP2/6-31+G* level for $\text{H}_2\text{VO}_4^- \cdot n\text{H}_2\text{O}$, with $n=0-6$	74
Figure 5.9. Vibrational Frequencies calculated at the B3LYP/6-31+G* level for $\text{H}_2\text{VO}_4^- \cdot n\text{H}_2\text{O}$, with $n=0-6$	75
Figure 6.1. The proposed reaction pathway (mechanism I) for the formation of the oxovanadyl cation by protonation of vanadic acid.	83
Figure 6.2. The proposed reaction pathway mechanism II for the formation of the oxovanadyl cation by the double protonations of dihydrogen vanadate.	86
Figure 6.3. The B3LYP/6-31+G* Optimized Structure of $\text{H}_4\text{VO}_5^- \cdot 24\text{H}_2\text{O}$ <A>	89
Figure 6.4. The B3LYP/6-31+G* Optimized Structure of $\text{H}_2\text{VO}_4^- \cdot 25\text{H}_2\text{O}$ 	90
Figure 6.5. The NBO charges of the vanadium atom and oxygens of H_2VO_4^- and H_4VO_5^-	92
Figure 6.6. The B3LYP/6-31+G* optimized structures of two possible hydrated $\text{VO}_2\text{OH}(\text{H}_2\text{O})_2$ conformations in $\text{H}_5\text{VO}_5 \cdot 24\text{H}_2\text{O}$	93
Figure 6.7. The structure of H_5VO_5 from <CI> with all of the water molecules removed.	95

List of Tables

Table 3.1. The relative energies of $\text{VO}_2(\text{H}_2\text{O})_4^+$ (A) and $\text{VO}_2(\text{H}_2\text{O})_3^+\cdot\text{H}_2\text{O}$ (B) .	35
Table 3.2. The PCM B3LYP/6-31+G* calculated energy of hydrogen bonded $\text{VO}_2(\text{H}_2\text{O})_3^+$ and $\text{VO}_2(\text{H}_2\text{O})_4^+$.	36
Table 3.3. The Gibbs energy of formation for the VO_2^+ complexes	37
Table 3.4. The summary tests of MPn (n=2-4) vibrational frequency for VO_2^+	40
Table 3.5. The B3LYP/6-31+G* calculated and experimental vibrational frequencies (cm^{-1}) of the oxovanadyl cation.	43
Table 3.6. NBO vanadium charges in gas/PCM phase calculated at the B3LYP/6-31+G* level for $\text{VO}_2(\text{H}_2\text{O})_n^+$, with n=0-4	44
Table 4.1. The incremental Gibbs energy of hydration for hydrated vanadic acid $\text{H}_3\text{VO}_4\cdot n\text{H}_2\text{O}$ n=1-6.	50
Table 4.2. NBO vanadium charges in gas/PCM phase calculated at the B3LYP/6-31+G* level for $\text{H}_3\text{VO}_4\cdot n\text{H}_2\text{O}$, n=0-6.	58
Table 5.1. The energy differences of the MP2 and B3LYP global minima for $\text{H}_2\text{VO}_4^- \cdot n\text{H}_2\text{O}$ structures, where n=1-3.	66
Table 5.2. The incremental Gibbs energy of hydration of $\text{H}_2\text{VO}_4^- \cdot n\text{H}_2\text{O}$, where n=0-6.	66
Table 5.3. NBO vanadium charges in gas/PCM phase calculated at the B3LYP/6-31+G* level for $\text{H}_2\text{VO}_4^- \cdot n\text{H}_2\text{O}$, with n=0-6.	76

Chapter I: Introduction

Part I: Vanadium (V)

Vanadium in Nature

Vanadium is a group V transition metal with an atomic number of 23 and the symbol V [1]. The concentration of vanadium in the Earth's crust is about 0.015 % and it is the twenty first most abundant metal. Vanadium does not exist in its pure form elemental form because of its high reactivity toward oxygen, carbon and nitrogen [2]. Vanadium is found in over 60 minerals and in crude oil [1]. Vanadium, in the form of $\text{Na}^+\text{H}_2\text{VO}_4^-$, is the second most abundant transition metal in sea water with the concentration of 30 nM, second only to molybdenum (100 nM). Vanadium concentration in air is low, ranging from 0.25 to 300 ng/m^3 [3].

Vanadium is known to exist in four oxidation states ranging from II to V [2]. In the biological systems, vanadium IV and V are the predominant species and are easily interconverted. Vanadium is an essential nutritional element for organisms such as ascidians and chicken but its nutritional value for humans is ambiguous [4]. Daily human intake of vanadium is estimated to be around 10-60 μg and mostly comes from following sources: black pepper, dill seeds, mushrooms, parsley, shellfish and spinach. These food products contain between 0.5 to 1.8 μg vanadium per gram.

Aqueous Vanadium Chemistry

In natural waters, vanadium exists predominantly in two forms, the IV and V oxidation states. Vanadium (V) is the more toxic form of the two because of its high mobility [5]. The aqueous chemistry of vanadium is very complex because of the ease

of conversion between its various oxidation states. Vanadium (V) is the main focus of this research and its chemistry will be discussed in greater detail. The aqueous chemistry of Vanadium (V) is the most complex of all vanadium species and it is highly dependent on concentration and pH level [1, 2, 5]. There are twelve known oxospecies of Vanadium (V) and they are shown in Figure 1.1 [6].

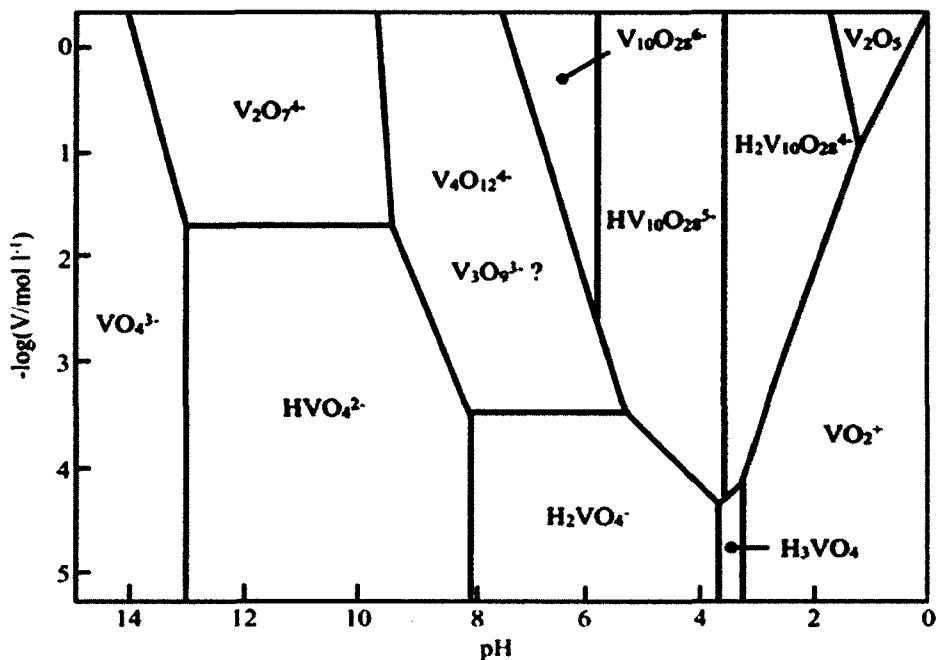


Figure 1.1. Stability domains of various vanadates and polyvanadates as a function of the pH and vanadium concentration, by Sadoc *et al* [6].

Monovanadates can exist only at low concentrations. If concentration increases the various polymerization reactions occur to form polyvanadates [2, 5, 6]. At both pH extremes mononuclear species dominate, at pH < 3 yellow $\text{VO}_2(\text{H}_2\text{O})_4^+$ is formed and above pH 13 colorless vanadate VO_4^{3-} exists. The speciation of Vanadium (V) below pH 13 becomes highly complicated. If the concentration stays low, the protonation of

vanadate leads to the formation of hydrogen vanadate HVO_4^{2-} , and if the concentration of vanadium significantly increases, newly formed hydrogen vanadates will dimerize to give $\text{V}_2\text{O}_7^{4-}$. In subneutral pH environments, hydrogen vanadate will go through a protonation to form dihydrogen vanadate H_2VO_4^- . Under similar pH conditions, vanadate dimer will react with itself to form larger polynuclear vanadium species such as trimer $\text{V}_3\text{O}_9^{3-}$ and the cyclic tetramer $\text{V}_4\text{O}_{12}^{4-}$.

In the pH range of 3 to 6, the common vanadate form is its decamer, the highly ordered decavanadate $\text{V}_{10}\text{O}_{28}^{6-}$ shown in Figure 1.2 [2, 5, 6]. Structure of decavanadate is revealed to have space $Pmmm$ and point D_{2h} groups [7]. All ten vanadium atoms tend to have distorted octahedral geometries and their connection with oxygen can be divided into seven categories ranging from terminal (double bonded or two coordinate) to six coordinate. There are many possible sites of protonation on decavanadate, so that the anions $\text{HV}_{10}\text{O}_{28}^{5-}$, $\text{H}_2\text{V}_{10}\text{O}_{28}^{4-}$ and $\text{H}_3\text{V}_{10}\text{O}_{28}^{3-}$ are known to form. Crystallographic studies of the $\text{H}_2\text{V}_{10}\text{O}_{28}^{4-}$ salt indicated that the hydrogen atoms are located at double linked oxygens of the decavanadate. This strongly yellow-coloured vanadate species is the predominant species at concentration above 0.2 nM [7]. At a constant concentration, depending on the pH change the following changes can happen: a) if the pH is increased it will decompose to smaller polyvanadates (trimers and tetramers) b) if the pH is decreased it will go through a protonation reaction to form $\text{H}_3\text{V}_{10}\text{O}_{28}^{3-}$ [2, 5-7].

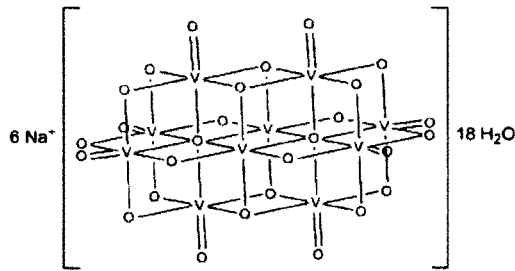
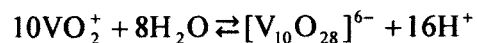


Figure 1.2. Decavanadate structure in the form of $\text{Na}_6\text{V}_{10}\text{O}_{28} \cdot 18\text{H}_2\text{O}$ [5].

Under dilute conditions, decavanadate dissociates to the pH dependent monomers, H_2VO_4^- or VO_2^+ [2, 5-7]. Clare and Kepert noticed that the pH plays a crucial part in the rate of decavanadate decomposition [8]. If the pH deviation is not significant from the stable pH range (3-6) of decavanadate, the half-life of decomposition is several hours. In extremely low pH environments, the decomposition takes only a few seconds.

In strongly acidic conditions (pH less than 3), decavanadate and H_2VO_4^- transform to the VO_2^+ cation [2, 5-7]. This decomposition reaction is reversible and decavanadate is proposed to be the hydrolysis product of VO_2^+ as the pH environment is increased (shown below) [2].



Vanadic acid (H_3VO_4) is a minor component of vanadium speciation [2, 5-7]. There is little information known about some Vanadium (V) compounds such as H_3VO_4 because of its narrow range of existence around the pH of 3.5. Most aqueous

mononuclear Vanadium (V) species exist at very low concentrations and they do not exist in solid form which causes extra challenges in determining its speciation.

Importance of the Aqueous Chemistry of Vanadium

The aqueous chemistry of vanadium has attracted a lot of attention because recent studies have revealed its biological role in plants, fungi and some sea creatures [1, 5]. Vanadium is believed to be an essential trace element for their normal cell growth. Vanadium is bioaccumulated in tunicates and the order of the bioaccumulation can reach 10^7 times more than its surrounding concentration. Vanadium is known to be important in the inhibition of phosphate-metabolising enzymes such as phosphatases, kinases and ribonucleases [1,7]. It has also been noted to have a stimulating effect on phosphomutase and isomerase enzymes. Also, Vanadium (V) is a well-established essential component for a number of mammalian haloperoxidases. Recently, the aqueous chemistry of vanadium has attracted the attention of researchers because of its potential to treat diabetes [9].

Diabetes

Diabetes is a disease that has been known since the first century CE [10]. One of the most famous Greek physicians, Aretaeus of Cappadocia, is believed to have named this disease. He used the ancient Greek words for “siphon” or “water pipe” and to “run through” to name diabetes mellitus.

Diabetes mellitus is a chronic metabolic disorder caused by defective insulin secretion, developed immunity to insulin action or a combination of both. Insulin is a

protein that regulates the glucose level in blood by stimulating cells in liver, muscle and fat tissues to absorb glucose and store it as glycogen in the liver and muscle [11]. Therefore, diabetes is characterized by hyperglycemia or high blood glucose levels. An above-normal level of glucose is defined as being above 7 mmol/L or 126 mg/dL [12]. There are two major types of diabetes, type 1 and type 2 [12, 13]. Type 1 diabetes is a metabolic disorder caused by the progressive destruction of insulin-secreting β -cells in the pancreas, which results in an insulin insufficiency, i.e. hyperglycemia. There is no cure for type 1 diabetes and people with this disease are dependent on insulin supplementation for life. Type 2 diabetes is a complex metabolic hyperglycemic disorder caused by relative insulin deficiency and insulin resistance. Insulin resistance in muscles and the liver, along with β -cell failure, represent the core pathophysiologic defects in type 2 diabetes. It is the most common type of diabetes (over 90% of total diabetes patients) due to the aging baby-boomers and massive rise of obesity in the general population [11-13].

Diabetes and Vanadium Compounds

The first anti-diabetic use of vanadium was by French physicians who administered sodium metavanadate (NaVO_3) to diabetic patients in 1899 [14]. This experiment improved the health of their patients. Unfortunately, the anti-diabetic action of vanadium was forgotten until it was rediscovered by Heyliger in 1985 [15]. He demonstrated that oral administration of metavanadate to streptozocin-treated (type 1) diabetic rats (STZ rats) lowered their blood sugar to normal levels. The concentration of sodium metavanadate administered in the drinking water of the rats was set at 0.2

mg/mL. After four days the blood sugar levels of the STZ rats returned to normal levels. This normoglycemia was stable for weeks as long as sodium metavanadate was supplied. Heyliger noted that metavanadate is a low molecular weight compound, and as a phosphate analogue, can easily permeate plasma membranes and intestinal walls.

In recent years vanadyl sulphate (VOSO_4) and NaVO_3 have been studied clinically to identify if they are capable of improving the health of diabetic patients [16]. Vanadyl sulphate has been proven to be a useful intervention for type 2 diabetic patients and has been reported to be 6-10 times less toxic than metavanadate [17].

In a single blind, placebo-controlled study, the diabetic effects of vanadyl sulphate were examined on eight male and female patients with type 2 diabetes [16]. Treated patients received vanadyl sulphate at 50 mg twice daily for two weeks, followed by a four week placebo phase. Results indicated moderate improvements in fasting glucose levels and insulin resistance following the treatment period that were retained throughout the placebo period.

Inorganic vanadium compounds do have an effect on the decline of hyperglycemia in diabetic patients. However, the toxic effects of these compounds limit their potential for drug use. Therefore, organic vanadium compounds have been synthesized in an effort to reduce these effects [4]. Other advantages of organic compounds are their increased lipophilicity and overall absorption efficiency into the gastrointestinal tract. Also, organic ligands have the potential to increase vanadium anti-diabetic efficacy [9]. The role of the ligand is to keep the organic vanadium molecule intact to a certain point for efficient bioavailability and pharmaceutical efficacy.

Bis(ethyl maltolato) oxovanadium IV (BEOV) shown in Figure 1.3, was designed at the University of British Columbia to be an orally active insulin mimetic agent [18].

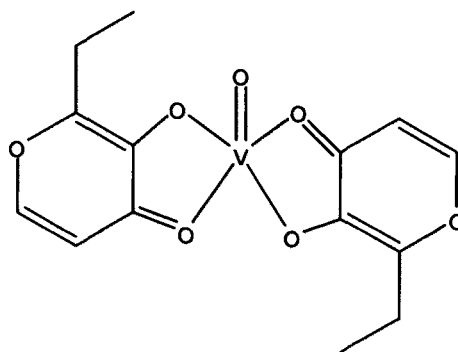


Figure 1.3. Structure of bis(ethyl maltolato) oxovanadium IV [18].

Common toxic effects of inorganic vanadium compounds were not observed and the anti-diabetic potency of BMOV, a BEOM derivate, was two to three times that of inorganic vanadium compounds [19]. This potency increase was observed in both oral and intraperitoneal administration which suggests that the difference in potency is not solely due to increased gastrointestinal absorption.

A phase I human clinical trial of BEOV was carried out by Medeval Ltd. (Manchester U.K.) and supported by Kinetek Pharmaceuticals Inc [18]. Escalating single doses (10 mg to 90 mg) were orally administrated to forty healthy volunteers to confirm the safety and tolerability of BEOV. Approximately 30% of the oral doses were absorbed which is significantly larger than the absorption efficiency of inorganic vanadium compounds (lower than 10%). When this phase was completed it was concluded that there were no adverse health effects in any of the volunteers. A phase IIa clinical trial of BEOV was carried out by Akesis Pharaceuticals Inc. The aim was to

assess the safety and efficacy of a 20 mg daily dose over a 28 day treatment period followed by a 14 day non-treatment period in type 2 diabetes patients. The daily dose of 20 mg was chosen because it had previously been determined to have the highest absorption rate in human subjects [20].

Vanadium (V) has also shown insulin-enhancing properties *in vivo* [21]. An organic complex of Vanadium (V), $\text{VO}_2\text{dipic}^-$, was first synthesized in 1978 and is shown in Figure 1.4 [22]. This compound is a clinically useful hypoglycemic agent in cats with type 1 diabetes [23]. The organic environment around Vanadium (V) increases its bioavailability and reduces its high toxicity.

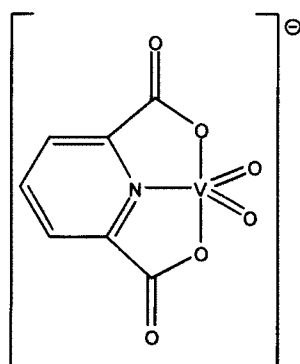


Figure 1.4. Structure of $\text{VO}_2\text{dipic}^-$ [23].

Diabetic Activities of Vanadium Compounds

The insulin-mimetic and the insulin-enhancing properties of vanadium have been extensively studied [4]. However, there are no conclusive results regarding the understanding of how vanadium compounds improve the health of diabetes patients. This is because the mechanism of diabetes at the molecular level is still unclear. Studies on the anti-diabetic actions of vanadium are separated into two categories, *in vivo* and

in vitro. *In vivo* studies have revealed that vanadium acts as the insulin enhancer and normalizes the blood-sugar level by enhancing glucose transport to cells, stimulating glycosynthesis, glycolysis and increasing their sensitivity to insulin. It is suggested that *in vitro* vanadium acts as an insulin-mimetic and *in vivo*, as an insulin enhancer [4, 19]. In order to understand the antidiabetic vanadium actions, the aquachemistry of vanadium IV and V must be fully understood.

Energy : Vanadium Redox Flow Battery

Development of renewable energy has become a hot topic due to the problems of climate change and imminent energy shortage [24]. In order to be competitive with current power sources (hydro and coal power plants), renewable energy must be cost-effective and reliable. Large scale energy storage is the technology to reach this goal. The vanadium redox flow battery (VRFB) has shown potential as an efficient large scale energy storage system for uninterruptible power supplies, stabilization of wind turbine output and hybrid photovoltaic cells [25, 26]. The major attraction of VRFB is that it stores energy in an electrolyte solution which can potentially result in a considerable increase in lifetime due to low discharge of the battery.

VRFB is an electrochemical system that interconverts between chemical and electrical energies [27]. There are two electrolyte tanks containing vanadium species in different valence states. The positive tank has vanadium IV and V and the negative tank has vanadium II and III redox couples. All of these vanadium species is dissolved in a sulphuric acid medium. During the charge-discharge process, active species are oxidized and reduced to force conversion between chemical and electric energies.

VRFB is unique because it consists of a single element, vanadium, thus eliminating the possibility of cross-contamination of electrolytes with different elements [27]. A battery with vanadium in both half-cells, also provides the following benefits: 1) easy electrolyte regeneration, 2) the electrochemical reversibility of vanadium redox couples allows high energy efficiency and 3) moderately abundant vanadium is an inexpensive metal.

The current challenges of the VRFB system is that Vanadium (V) in an electrolyte solution has poor stability at temperatures above 310K and at high concentrations (>2 M) [28]. The limiting factor of this issue is the not yet fully studied precipitation of Vanadium (V) from the electrolyte solution [29]. Understanding the aqueous chemistry of Vanadium (V) is an important step to the development of stabilizers or even new stable Vanadium (V) electrolyte solutions, which could increase the life cycle, energy density and reduce the operating cost of VRFBs.

Challenges of Instrumental Analysis of Aqueous Chemistry of Vanadium

The concentration of vanadium in natural water is very low, on the order of a few $\mu\text{g/L}$ which is below the detection limit of most conventional analytical tools [1]. However, vanadium is heavily emitted into the environment from oil refineries, and the iron, steel and chemical industries. This raises the concern of increased vanadium concentration in the environment [30]. The impact of vanadium on the environment and biological organisms is yet to be fully determined. Chromatographic methods often require time and cost consuming derivatization of the sample thus eliminating crucial structural information on the vanadium species present [31]. The solid-phase extraction

method is optimal for preconcentration of trace metals with minimal solvent waste generation. Solid phase extraction is a simple method where the sample is passed through a solid phase of packed metal chelates on microcrystalline naphthalene space [32]. The obvious disadvantage of this method is that the integrity or composition of the vanadium species is lost. Secondly, the result in the form of an ion gives very little information about the actual speciation of the original vanadium. The only structural information found was the valence state of the vanadium ions [31]. Unfortunately, this type of information is not enough to understand the chemical and biological role of vanadium in the environment or in biological systems. For this reason, one of the best methods to study vanadium speciation is computational chemistry.

The energy and dynamics of hydrated transition metals form the basis of many fundamental chemical and biological processes [33]. The progress of quantum theory and technological advancements has allowed computational chemistry to become a relatively inexpensive method for structure and reaction mechanism determination. Nordstrom has written an overview of both computational and analytical methods for trace metal speciation in natural waters [34]. There are three types of aqueous speciation: redox, metal-organic, and metal-inorganic. Redox speciation can only be determined analytically. Metal-organic speciation can be done by both methods but due to the complexity of organic systems in natural waters, analytical methods provide faster and more practical results. For metal inorganic speciation, analytical methods are very limited (due to the loss of structural information) hence computational speciation methods are preferred.

Computational methods allow a wide range of trace metal compositions to be studied [33]. Computational methods give a large qualitative picture of the chemistry of trace metal species in natural water. Some properties of a molecule, such as molecular bonding information, are easier to use theory to calculate than determine experimentally. However, computational models usually neglect thermodynamic and electrolyte properties of natural systems. This is necessary because of the complexity of natural systems. However, only computational methods enable are to calculate currently unattainable properties of low concentration hydrated vanadium species.

Part II: Computational Chemistry

Computational chemistry is a very broad field, which combines computer science with theoretical chemistry [33]. Theoretical chemistry consists of a large number of very different methods which can be divided into five main groups: *ab initio*, semi-empirical, molecular mechanics, chemical dynamics and molecular dynamics. The main focus of this research is *ab initio* methods and they will be discussed in greater detail. Semi-empirical methods use empirical data to approximate mathematical quantum results. Molecular mechanics uses classical mechanics to calculate the desired geometry and charge of a molecule. Dynamical methods use the time-dependent quantum equation to find the influence of time on the properties of molecules. There are also the hybrid methods of *ab initio* and molecular mechanics - *ab initio* molecular dynamics. This is mainly done in order to combine two complimentary methods.

Quantum Theory Basics: Schrödinger Equation

Quantum mechanics explains chemical systems at the atomic level where classical mechanics fails [35]. Classical mechanics cannot explain black body radiation and the decrease in the heat capacity of solids with decreasing temperature which resulted in the development of quantum mechanics. As the name of quantum mechanics suggests, it describes particle energy as a discrete quantized quantity. Quantum mechanics theory states that atoms and molecules exhibit the wave and particle properties, a phenomenon known as wave-particle duality.

The basis of quantum mechanics is the Schrödinger equation [36]. Schrödinger received the Nobel Prize for his work on this equation in 1933. The Schrödinger equation is written as:

$$H\psi(x, y, z) = E\psi(x, y, z) \quad 1.1$$

where H is the Hamiltonian operator, $\psi(x, y, z)$ is the wavefunction, which describes the system of interest, and E is the total energy. The total energy is the summation of the energies of the electrons and the nuclei. The wavefunction is the key term of quantum mechanics and it contains all the dynamical information about the system it describes. The Hamiltonian operator is an Hermitian operator and it is equal to:

$$H = -\frac{\hbar^2}{2m} \frac{d^2}{d(x^2, y^2, z^2)} + V(x, y, z) \quad 1.2$$

here \hbar equals $\frac{h}{2\pi}$, where h is Planck's constant, m is the mass of the particle in kg,

$\frac{d^2}{d(x^2, y^2, z^2)}$ is the Laplacian operator and $V(x, y, z)$ is the potential energy of the

particle at some point in space. The energy of a system is an eigenvalue of the Hamiltonian operator (1.2), where the wavefunction is the eigenfunction. An eigenfunction is a function with the following property – the function returns unchanged upon its operator action but scaled by a certain scalar value [33, 35]. The Schrödinger equation looks rather easy to solve. However, it can be solved only for a few simple systems; for example, a particle in a box, the harmonic oscillator, the rigid rotator and the hydrogen atom.

Solving the Schrödinger equation for more complex systems than the hydrogen atom requires some approximations [33, 35]. One of most popular is the Born-Oppenheimer approximation. The basis of this approximation is neglect of the coupling of the nuclei and electronic motion. Electrons are about two thousand times lighter than protons, which allow them to move almost instantaneously with respect to the nuclei. This allows the electronic part of the equation to be solved with nuclear positions as parameters. The Born-Oppenheimer assumption allows the nuclei to be treated as fixed or having zero kinetic energy. Therefore, the only contribution to the nuclear energy is the nuclear potential energy which significantly simplifies solving the Schrödinger equation.

Hartree-Fock Theory

Elaborate computational methods are required to solve and understand the dynamics of many-electron systems. Major conceptual and computational simplifications are needed to estimate properties of these complex systems [33, 35]. One of the simplest models is called the independent-particle model, where the motion of one electron is considered to be independent of the dynamics of all of the other electrons. In this model, the interactions between particles are approximated and all interactions are taken into account in an average fashion. The most popular method of this model is Hartree-Fock (HF) theory. In HF theory, each electron is described by an orbital and the total wavefunction is the product of these orbitals. The shape of a given molecular orbital describes the probability of finding an electron in that space. The method follows the Pauli exclusion principle in showing that the wavefunctions are

antisymmetric and includes a normalization constant to write the wavefunction as the Slater determinant:

$$\Psi(1,2,\dots,2N) = \frac{1}{\sqrt{(2N)!}} \begin{vmatrix} \psi_1\alpha(1) & \psi_1\beta(1) & \cdots & \psi_N\alpha(1) & \psi_N\beta(1) \\ \psi_1\alpha(2) & \psi_1\beta(2) & \cdots & \psi_N\alpha(2) & \psi_N\beta(2) \\ \vdots & \vdots & \ddots & \vdots & \vdots \\ \psi_1\alpha(2N) & \psi_1\beta(2N) & \cdots & \psi_N\alpha(2N) & \psi_N\beta(2N) \end{vmatrix} \quad 1.3$$

where $2N$ is number of electrons with α and β spins in the molecular orbital. The best set of orbitals is determined by the variational principle where any trial wavefunction will give energy greater than or equal to the ground state energy. Changing the coefficients of the trial wavefunction can be used to give the lowest possible value for it.

The Hartree-Fock energy is expressed by one and two-electron integrals, and can be written in the form:

$$E = 2 \sum_{j=1}^N H_j + \sum_{i=1}^N \sum_{j=1}^N (2J_{ij} - K_{ij}) \quad 1.4$$

where H_j is the core electron Hamiltonian and is represented by the one-electron integral:

$$H_j = \int dr_j \psi_j^*(r_j) \left(-\frac{1}{2} \nabla_j^2 - \frac{Z}{r_j} \right) \psi_j(r_j) \quad 1.5$$

J_{ij} is called the Coulomb integral and it represents the classical mechanics effects and repulsion between the two charge distributions:

$$J_{ij} = \int \int dr_i dr_j \psi_i^*(r_i) \psi_j^*(r_j) \frac{1}{r_{ij}} \psi_i(r_i) \psi_j(r_j) \quad 1.6$$

K_{ij} is the exchange integral and it represents the quantum effects of the anti-symmetry principle:

$$K_{ij} = \int \int dr_i dr_j \psi_i^*(r_i) \psi_j^*(r_j) \frac{1}{r_{ij}} \psi_i(r_j) \psi_j(r_i) \quad 1.7$$

The Hartree-Fock equations must be solved by an iterative process because of their antisymmetry [35]. This requirement makes the Hartree-Fock method known as the self-consistent field (SCF) method. Self-consistency is achieved by having orbitals no longer noticeably change with newly generated potentials.

Basis Sets

A basis set is a set of functions used to describe the shape of the orbitals in an atom [33]. Molecular orbitals and entire wavefunctions are created by taking linear combination of atomic orbitals (LCAO) or basis functions. A proper choice of basis set is required to obtain the desired accurate results. Ideally, one would like to use a complete basis set, which would contain an infinite number of functions. However, in practice there must be a finite number of basis functions in order to complete a calculation. A general rule is that the accuracy of the basis set is lower if fewer basis functions are used to describe the molecular orbitals.

The most basis sets are composed of either Slater-type orbitals (STO) or Gaussian-type orbitals (GTO) [33, 35]. These are typically expressed in spherical or Cartesian coordinates. Slater-type orbitals are represented as:

$$\phi_s(r, \theta, \phi) = Y_m^\ell(\theta, \phi) \left(\frac{\alpha}{\pi} \right)^{1/2} e^{-\alpha|r-\mathbf{R}_A|} \quad 1.8$$

where Y_m^ℓ is the spherical harmonic, and α and \mathbf{R}_A are normalization factors. Gaussian type orbitals have the following formula.

$$\phi_g(r, \theta, \phi) = Y_m^\ell(\theta, \phi) \left(\frac{2\alpha}{\pi} \right)^{3/4} e^{-\alpha|r-\mathbf{R}_A|^2} \quad 1.9$$

The major difference between STOs and GTOs is the behaviour of the orbital shape at the nucleus [33, 35]. An STO has the correct cusp at the nucleus and the decay expected of atomic orbitals. The existence of the cusp, however causes a discontinuity and it makes the STOs very difficult to use to calculations. On the other hand, a GTO does not have the cusp which makes it easier to use in calculations. The cusp is the correct representation of an atomic orbital at the nuclei, and to compensate for its absence several GTOs are used in a linear combination form to emulate the behaviour of one STO.

There are many different type of GTO modifiers [33, 35]. Split valence basis sets allow the size of orbitals to be modified. In order to change the shape of orbitals, the polarization functions can be added. These are labelled as “*”. The polarization functions add new orbitals with angular momentum beyond the required ground state to describe atoms. A diffuse function “+” can be added to allow s and p orbitals to occupy

larger space. This basis set is very useful for systems with lone pairs of electrons, anions and other systems with significant charge.

Post Hartree-Fock Methods

One of the biggest disadvantages of the HF method is that it completely neglects electron correlation or instantaneous electron-electron interactions [33, 35]. For example, electrons have the same Coulombic charge and they repel each other. This problem is accounted for in several methods known as the post Hartree-Fock methods.

Møller-Plesset is a post Hartree-Fock perturbation method. It makes the use of Rayleigh–Schrödinger perturbation theory [37]. The Hartree-Fock wavefunction is taken to be an unperturbed wave function and then the perturbation correction is applied to it. Second-order Møller-Plesset perturbation theory is a second-order correction to the Hartree-Fock wave function and is denoted as MP2. Perturbation theory involves a correction to the Hamiltonian as shown below:

$$H = H^{(0)} + \lambda H^{(1)} \tag{1.10}$$

where H is the unperturbed Hamiltonian, $H^{(0)}$ and $H^{(1)}$ are the perturbed and first-order correction to the Hamiltonian, respectively.

The second order Møller-Plesset MP2 is one of the most popular post Hartree-Fock methods [33, 35]. MP2 captures about 90% of the electron correlations and its correlation integrals usually are easy to calculate. However, Møller Plesset is not a true variational method. In fact, it is not uncommon to have MP2 calculations that give total

energies below the true energy. Other issues with MPn calculations are increasing the order of perturbation in a calculation makes it more expensive, and it does not always result in increased accuracy.

Density Functional Theory

A trend of last three decades has been the rise of density functional theory (DFT), another *ab initio* method [33, 35]. It has become the most commonly used quantum chemical calculation. It also provides the best balance of accuracy and computational cost. Several Canadian based chemists contributed heavily to the development of DFT, namely Walter Kohn, Axel Becke and Tom Ziegler [33, 35]. As the name DFT suggests, unlike the Hartree-Fock and Møller-Plesset theories, which are based on the wavefunctions of molecules, DFT is focused on the electron density. Electron density is a physically measurable quantity and is a function of only three spatial coordinates. It is clearly less computationally expensive in relation to a wavefunction which is not an observable quantity and is the function of 4N variables (three spatial and one spin) per electron. The ground state electronic energy of a molecule is a function of the electron density and the electron density is in turn a function of the position of electrons. A functional is a prescription for producing a number (the total estimated energy) from a function (the electron density), which in turn depends on variables (the positions of the electrons). The scientific duet of Hohenberg-Kohn developed the Hohenberg-Kohn theorem in 1964 [38]. This relationship can be expressed by the equation:

$$E = E[\rho] \qquad 1.11$$

where E is the ground state energy of the system and ρ is its electron density. The square bracket notation is used to illustrate the functional relationship. The intuitive proof of why density defines the electronic system was provided by E. B. Wilson who stated that: 1) the integral of the density determines the number of electrons, 2) the density cusps define the position of the nuclei 3) the heights of the cusp define the corresponding nuclear charge [39]. The second Hohenberg-Kohn theorem states that the ground state density is a variational quantity and can be represented as:

$$E_0 = E[\rho_0] \leq E[\rho] \tag{1.12}$$

where E_0 and ρ_0 are the true values and ρ is a trial electron density [40].

The major issue of DFT is the calculation of the exchange correlation functional [33, 35]. It acts as a catch-all for all the contributions to the energy that cannot be calculated exactly. There are four types of exchange-correlation energies: the exchange, the correlation, self-interaction energies and the kinetic energy correction [41]. The exchange energy is the classical electron-electron energy and it does not take into account the Pauli repulsion between electrons of the same spin. The correlation energy is the classical electron-electron energy that does not account for instantaneous Coulomb interactions between electrons. Self-interaction energy is the electron-electron energy which includes a contribution from each electron interacting with itself. The kinetic energy correction is the difference between kinetic energy of the reference system and real system. If the exchange-correlation functional could be computed exactly then the total energy of the system would be known. There are many exchange

correlation functionals being developed and B3LYP is one of the most popular DFT hybrid functional [33]. It uses the Becke 3 parameter functional (B3) which is responsible for the exchange potential and the Lee-Yang-Parr correlation energy [42 , 43].

Polarizable Continuum Model

The Polarizable Continuum Model (PCM) was developed by Tomasi and co-workers and it is one of the most frequently used continuum solvation models [44]. The PCM model describes the molecular free energy in solution as the sum of three energy terms:

$$G_{sol} = G_{es} + G_{gib} + G_{cav} \quad 1.13$$

where G_{es} represents the electrostatic component, G_{gib} is the contribution to the Gibbs energy and G_{cav} is the cavitation energy. The surface cavity used in the PCM is of the van der Waals type.

The PCM model of current interest is the Integral-Equation-Formalism PCM or IEFPCM and it was developed in 1997 by Cancès and Tomasi [45]. IEF was developed to solve the electrostatic solvation problem at the quantum mechanical level. IEF uses a novel integral approach to solve the Green functions (inhomogeneous differential equations), which is required to solve the electrostatic solvation of PCM. This model divides the system of interest into two subsystems, the molecule under the solute conditions and molecule under the environment conditions. A molecule under solute condition is assumed to be in a cavity in a form defined by its molecular shape itself

and dimension in the continuum. The environment condition is described by the dielectric permittivity of the chosen solvent. This method has been successfully used to compute solution geometries and many molecular properties, to simulate electronic, vibrational, and magnetic spectra, to study reaction mechanisms and to compute electronic excited states.

Natural Bond-Order Analysis

Natural bond order (NBO) analysis is a set of analysis techniques [33]. One of the techniques of interest is natural population analysis (NPA) which is used to obtaining electron occupancies and charges. It is considered a superior charge calculation technique compared to Mulliken charge analysis because of lesser dependence on the choice of basis set. NBO uses natural orbitals instead of molecular orbitals. Natural orbitals are the eigenfunctions of the first order reduced density matrix. The localization of natural orbitals allows the molecular orbitals to be centred on the atoms so that atomic charges on atoms can be obtained by performing an integration procedure on the localized natural orbitals.

Car-Parrinello Molecular Dynamics

Car-Parrinello Molecular Dynamics (CPMD) is a method that allows the quantum DFT method to be used to study the whole potential energy surface at finite temperature in a physically meaningful way [46]. In the past, *ab initio* molecular dynamics has not been physically feasible because of the high computational cost associated with including three more variables (velocities in x, y and z directions) to already complicated quantum mechanics equations. In CPMD, the core electrons are

described by pseudopotentials (also known as effective core potentials) and the wavefunction and valence electrons are described by a planewave basis set. Planewave basis sets describe whole systems, unlike GTOs which describe only orbitals. The planewave basis sets are very useful for simulations with periodic boundary conditions.

The main issue of previous *ab initio* molecular dynamics methods has been the requirement to have the wavefunction converge at each timestep of the simulation [35]. The CPMD breakthrough was that the wavefunction convergence was no longer necessary at each step of the simulation. The only requirement is that the first step of the simulation converges and then the wavefunction is allowed to evolve simultaneously with the nuclei and the electrons. This can be achieved using extended Lagrange functions to describe real particles and the wavefunction parameters.

Chapter II: Objective and Methods

The main objective of this thesis was to study aqueous Vanadium (V) compounds using *ab initio* computational methods. The target ions/molecules of this study are VO_2^+ , H_3VO_4 , and H_2VO_4^- . The hydration of these molecules was to be investigated using *ab initio* computational methods. The energetically favourable geometries at different levels of hydration were calculated. The methods employed were the Hartree-Fock, second order Moller Plesset (MP2) and B3LYP hybrid functional methods and they were used to calculate the wavefunction, energy, geometry and vibrational frequencies of the species studied. The following basis sets were chosen for the calculations: **6-31G***, **6-31+G*** and **cc-pVTZ**. The first principle molecular dynamics method CPMD was utilized to study the mechanism of conversion of H_2VO_4^- to VO_2^+ .

Hartree-Fock is a useful first calculation step to predict the appropriate geometry for higher level methods such as MP2 and B3LYP. The MP2 and B3LYP theory levels are capable of giving more reliable results because they take into account electron correlation. This is very important because transition metals have many valence electrons and correlating them is key in obtaining the correct structure and energy.

Gaussian software versions 2003/2009 were used for the *ab initio* calculations [47, 48]. Gaussian is a very powerful software package which uses Gaussian type orbitals (GTO) to approximate Slater type orbitals (STO). This approximation of the atomic orbitals provides a dramatic decrease in computing time. Linear combinations of

several GTOs can simulate a STO reasonably well. The Webmo interface for Gaussian 2009 was used for the charge and solvation studies. This software uses a very intuitive approach to set up calculations and possesses a very good system for submitting calculation jobs.

For the hydration study, each species of vanadium (V): VO_2^+ , H_3VO_4 , and H_2VO_4^- was studied with from one to six water molecules attached to the molecule of interest. Gradually increasing the number of bound water molecules helps one to predict the potential binding site of next water molecule. For VO_2^+ the study was completed when the absolute minima for the aqueous hexa coordinate VO_2^+ cation was found. The correct hydration of H_3VO_4 , and H_2VO_4^- was a more complicated task to solve because their optimized geometries contained multiple hydrogen bonded water molecules. A hydrogen bond is an attractive interaction between a hydrogen atom molecular fragment X-H, where X is more electronegative than H, and an atom or a group of atoms, in which there is evidence of bond formation [49]. There are many possible hydrogen bonding motifs in these species, for example the hydrogen of a water molecule can bond to the oxygen of vanadate or the oxygen of a water can bond to a hydrogen of the vanadate. This large number of possibilities meant that the potential energy surface had to be scanned thoroughly to find the global minima, which was a very time consuming part of this project.

In the Gaussian software input file, the starting geometries of the vanadium species can be specified by an internal coordinate system or z-matrix. The internal coordinate system is a very intuitive method for describing structures utilizing their

symmetries. The origin of this internal coordinate system is usually the central atom of a molecule oriented along with a principal symmetry axes. This approach allows the starting geometry to be described using the desired point group with a set of symmetries and minimal parameters.

If an optimized structure is a local or global minimum, then it will not have any imaginary or negative frequencies. For this reason, at each level of theory the frequency calculation option must be included in the calculation by adding “Freq” to the command line of input file. The existence of imaginary frequencies for a certain point group is an indication that the symmetry of the molecule under study should be lowered. In practice, a completely non-symmetrical initial guess could be chosen but it is considered to be poor practice, especially for large molecules because the computing time of a non-symmetrical structure are several times more longer than one utilizing a symmetrical point group.

Another advantage of including frequency calculations is that the calculated frequencies can be compared to experimental results. For vanadium ionic compounds experimental IR or Raman vibrational frequency are often available. Differences of $100\text{-}200\text{ cm}^{-1}$ are often observed because of substituent effects but comparison can still give a reasonably good judgment on the validity of calculated structures.

Imaginary frequencies are very important for studying the transition states in reaction mechanism calculations. An imaginary frequency is an indicator of a saddle point in the potential energy surface (PES). By definition, a structure which has n

imaginary frequencies is an n^{th} order saddle point [50]. Ordinary transition structures are usually characterized by the existence of one imaginary frequency *i.e.* a first-order saddle point. In the Gaussian program this can be achieved by adding the input “**Opt = (TS, CalcFC)**”. Reactive intermediates can be also could a part of the reaction mechanism. Reactive intermediates are short lived species and they are located at local minima on the PES. Such a structure usually resembles the transition state structure but does not have any imaginary frequencies.

The CPMD study is conducted on software CPMD 3.15.1. The Goedecker pseudopotential was chosen [51]. The Goedecker pseudopotential is considered to have less flexible core electrons which makes it ideal for metal applications. There are three steps of in a CPMD simulation: 1) first step is to have the wavefunction converge 2) optimize the geometry and wavefunction, 3) perform the simulation itself. The CPMD simulations were performed with the Nose-Hoover thermostat set at room temperature.

Equipment

This research was conducted using the Atlantic Computational Excellence Network (ACEnet) [52]. ACEnet is a pan-Atlantic network of High Performance Computing (HPC) clusters. ACEnet resources allow the researchers of Atlantic Canada to access first class resources such as high speed computing and large storage space. ACEnet currently operates as a partnership between ten Atlantic Canadian Universities. ACEnet possesses hardware with just over 3000 processing cores, terabytes of storage capacity, and hundreds of gigabytes of available memory. The Placentia and Mahone ACEnet clusters were utilized for this work. Placentia is the only cluster with the

Gaussian software package installed on it. CPMD is available for both the Placentia and Mahone clusters.

Chapter III: $\text{VO}_2(\text{H}_2\text{O})_4^+$

Introduction

$\text{VO}_2(\text{H}_2\text{O})_4^+$ exists as a yellowish aqueous solution in environments less than pH 3 [2,5,6]. It has very high proton content and it is the only known mononuclear Vanadium (V) compound in solution, even in the presence of strongly binding ligands. The accepted aqueous form of VO_2^+ is $\text{VO}_2(\text{H}_2\text{O})_4^+$ with terminal oxygens in the *cis* arrangement. It is documented that VO_2^+ is similar to other d^0 compounds that prefer the *cis*-conformation (bent) because it allows better oxygen $p\pi$ and metal $d\pi$ bonding than a linear arrangement would allow [2]. The detailed NBO B3LYP/6-31+G* calculated orbitals of the bent and linear VO_2^+ are shown in Figures A.1 and A.2.

Only the solid form of VO_2^+ can give structural and spectroscopic information. One VO_2^+ salt is $[(\text{VO}_2)_2(4,4\text{-bipy})_{0.5}(4,4'\text{-Hbipy})(\text{PO}_4)]\cdot\text{H}_2\text{O}$ [53]. The X-ray structure of this salt has a distorted trigonal bipyramidal geometry where the two equatorial positions are occupied by terminal oxygens. The VO_2^+ section of the salt has two identical short V=O bonds (*ca.* 1.62 Å), which is a characteristic feature of Vanadium (V). Vibrational studies of the $[(\text{VO}_2)_2(4,4\text{-bipy})_{0.5}(4,4'\text{-Hbipy})(\text{PO}_4)]\cdot\text{H}_2\text{O}$ complex yielded skeletal vibration information for VO_2^+ . The two expected VO_2^+ stretching vibrations occur at 919 and 943 cm^{-1} in the IR spectrum, and 905 and 939 cm^{-1} in the Raman spectrum. The weak Raman peak at 325 cm^{-1} was assigned as the VO_2^+ deformation mode.

A computational study of VO_2^+ using the Quantum Monte Carlo method showed that it belongs to the C_{2v} point group [54]. The calculated V=O bond length in VO_2^+

was 1.567 Å with an O-V=O angle of 105.8°. Later, Buhl and Parrinello studied VO_2^+ using CPMD and they found that in the gas phase $\text{VO}_2(\text{H}_2\text{O})_4^+$ breaks down to $\text{VO}_2(\text{H}_2\text{O})_3^+\cdot\text{H}_2\text{O}$ [55]. They employed DFT electronic structure methods such as BP86, BLYP and B3LYP and showed that $\text{VO}_2(\text{H}_2\text{O})_3^+\cdot\text{H}_2\text{O}$ was indeed more stable than octahedral $\text{VO}_2(\text{H}_2\text{O})_4^+$ in the gas phase. The authors suggested that in the bulk solution the fourth water ligand on vanadium is stabilized by inter- rather than intramolecular hydrogen bonds to form six coordinate $\text{VO}_2(\text{H}_2\text{O})_4^+$.

In this work, the binding pattern of water to VO_2^+ was studied by *ab initio* methods. Gradually increasing of the number of bound water molecules helped to explain the formation of $\text{VO}_2(\text{H}_2\text{O})_4^+$ in aqueous media. Hydration effects on the vanadium to oxygen bonds and vibrational frequencies were also investigated. Buhl and Parrinello's $\text{VO}_2(\text{H}_2\text{O})_3^+\cdot\text{H}_2\text{O}$ structure was studied by the aqueous PCM solvation method to verify its existence in an aqueous environment.

Results and Discussions

Geometries

The oxovanadyl cation VO_2^+ has C_{2v} point group. The linear VO_2^+ structure was considered as a possible alternative. Calculations using the highly sophisticated B3LYP/cc-pVTZ method showed that the linear analog had a much higher energy than the bent form. The energies of these optimized geometries were calculated using a single point method CCSD(T)/cc-pVTZ. The energy of linear VO_2^+ was significantly higher than its bent form by 375 kJ/mol. Also, the linear form produced a large

imaginary frequency (calculated by B3LYP/6-31+G*) for the deformation (bending) mode VO_2^+ . This means that linear VO_2^+ can exist only as a transition structure and hence VO_2^+ must have a bent structure with a point group symmetry of C_{2v} .

This local symmetry of VO_2^+ was preserved in most of the optimized structures. The optimized (stable) structures of the hydrated oxovanadyl cations at the B3LYP/6-31+G* theory level are shown in Figure 3.1.

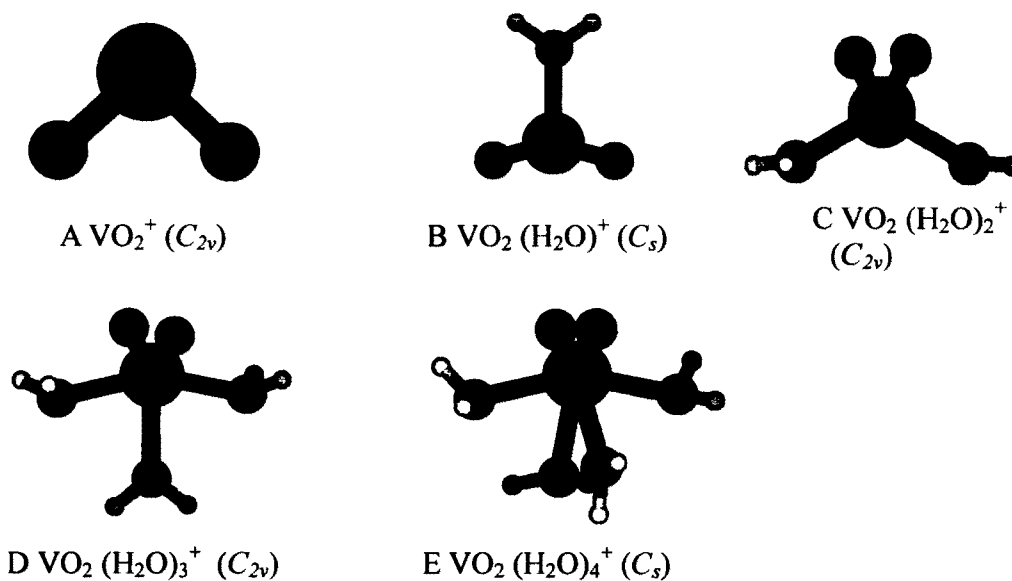


Figure 3.1. The B3LYP/6-31+G* optimized structures of oxovanadyl cation $\text{VO}_2(\text{H}_2\text{O})_n^+$, where $n=0-4$.

The PCM solvated geometry optimization can implicitly incorporate the effect of solvent on the shape, charge distribution and conformational preference of molecules of interest [35]. The PCM solvation water model in conjunction with the B3LYP/6-31+G* optimized structures was employed to study $\text{VO}_2(\text{H}_2\text{O})_n^+$, where $n=1-4$. The PCM optimized geometries are shown in Figure 3.2.

The PCM geometries of $\text{VO}_2(\text{H}_2\text{O})^+$ and $\text{VO}_2(\text{H}_2\text{O})_2^+$ are almost identical to the calculated gas phase geometries. However, the PCM optimization of $\text{VO}_2(\text{H}_2\text{O})_3^+$ and $\text{VO}_2(\text{H}_2\text{O})_4^+$ leads to a reduction of the symmetries of the gas phase geometries because of the natural out of plane bending tendency of the water molecules.

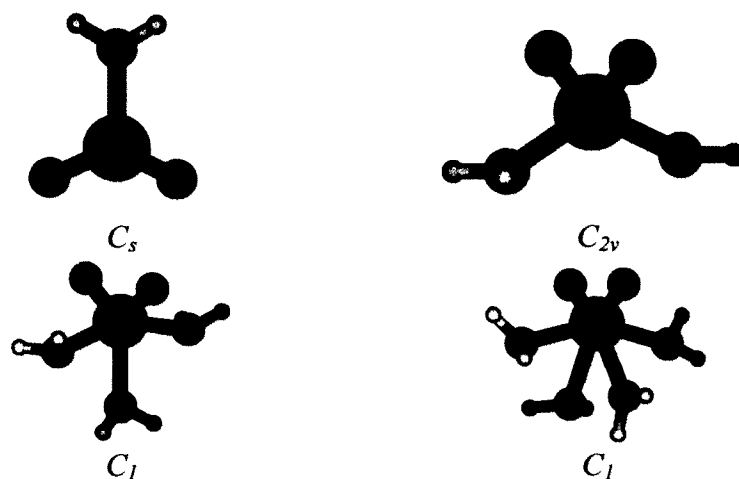


Figure 3.2 The PCM B3LYP/6-31+G* optimized $\text{VO}_2(\text{H}_2\text{O})_n^+$, where $n=1-4$.

Energies

The previously mentioned $\text{VO}_2(\text{H}_2\text{O})_3^+\cdot\text{H}_2\text{O}$ structure by Buhl and Parrinello was investigated by *ab initio* methods and the optimized structure is shown in Figure 3.3 [55]. The hydrogen bonded water molecule broken the C_{2v} symmetry of the $\text{VO}_2(\text{H}_2\text{O})_3^+$ ion.

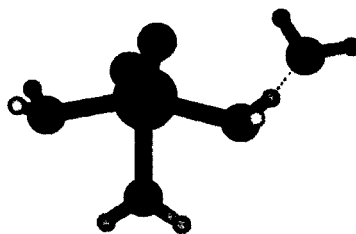


Figure 3.3. The B3LYP/6-31+G* Optimized Structure of $\text{VO}_2(\text{H}_2\text{O})_3^+ \cdot \text{H}_2\text{O}$.

The energy difference between $\text{VO}_2(\text{H}_2\text{O})_3^+ \cdot \text{H}_2\text{O}$ and $\text{VO}_2(\text{H}_2\text{O})_4^+$ was calculated and is shown in Table 3.1. The energy difference at the most *ab initio* levels show that indeed $\text{VO}_2(\text{H}_2\text{O})_3^+ \cdot \text{H}_2\text{O}$ had a lower energy than $\text{VO}_2(\text{H}_2\text{O})_4^+$ in both the gas phase and the PCM water environment.

Table 3.1. The relative energies of $\text{VO}_2(\text{H}_2\text{O})_4^+$ (A) and $\text{VO}_2(\text{H}_2\text{O})_3^+ \cdot \text{H}_2\text{O}$ (B) .

HF/6-31G*	9.5
MP2/6-31G*	-8.4
B3LYP/6-31+G*	17.3

Only at the MP2 levels, was $\text{VO}_2(\text{H}_2\text{O})_4^+$ found to have a lower energy than $\text{VO}_2(\text{H}_2\text{O})_3^+ \cdot \text{H}_2\text{O}$. However, upon closer inspection, it was also noticed that the MP2 level calculations produced a large number of unreasonably high vibrational frequencies for all species of VO_2^+ (see page 36-37). Since MP2 calculations did not produce frequencies close to the experimental values they were not applied for this species of Vanadium (V).

The effect of hydrogen bonded water molecules on the overall energies of $\text{VO}_2(\text{H}_2\text{O})_3^+$ and $\text{VO}_2(\text{H}_2\text{O})_4^+$ was studied and is shown in Table 3.2. This table shows the energy difference between $\text{VO}_2(\text{H}_2\text{O})_4^+$ with one or two hydrogen bonded water molecules and the corresponding $\text{VO}_2(\text{H}_2\text{O})_3^+$ isomers. The calculated PCM energy difference was found to be only 12 to 15 kJ/mol. This small energy gap suggests both complexes possibly exist in the aqueous environment. To fully resolve the question of which structure is the more stable structure, the second sphere of both $\text{VO}_2(\text{H}_2\text{O})_3^+$ and $\text{VO}_2(\text{H}_2\text{O})_4^+$ would have to be modelled and their static and dynamic stability in terms of energy compared.

Table 3.2. The PCM B3LYP/6-31+G* calculated energy of hydrogen bonded $\text{VO}_2(\text{H}_2\text{O})_3^+$ and $\text{VO}_2(\text{H}_2\text{O})_4^+$.

Complex Chemical Formula (A)	Complex Chemical Formula (B)	The Energy Difference (A)-(B), kJ/mol
$\text{VO}_2(\text{H}_2\text{O})_4^+ \cdot \text{H}_2\text{O}$	$\text{VO}_2(\text{H}_2\text{O})_3^+ \cdot 2\text{H}_2\text{O}$	14.7
$\text{VO}_2(\text{H}_2\text{O})_4^+ \cdot 2\text{H}_2\text{O}$	$\text{VO}_2(\text{H}_2\text{O})_3^+ \cdot 3\text{H}_2\text{O}$	11.8

As more water molecules are added to the oxovanadyl cation there is an overall stabilization of the structure. Usually, only one local minimum on the potential energy surface was found for each hydration level of the oxovanadyl cation. There have been published results on the formation of $\text{VO}_2(\text{H}_2\text{O})_4^+$ studied using analytical spectroscopic methods [56]. It was proposed that when VO_2^+ is in an aqueous solution it readily transforms to $\text{VO}_2(\text{H}_2\text{O})_4^+$, a hexa coordinate species. Cruywagen made the assumption that water and VO_2^+ react instantaneously to form the $\text{VO}_2(\text{H}_2\text{O})_4^+$ complex. The possibility of the existence of $\text{VO}_2(\text{H}_2\text{O})_n^+$, with $n=1-3$ was investigated in this project

by calculating the Gibbs energy of formation of the VO_2^+ complexes and the results are shown in Table 3.3 [57].

Table 3.3. The Gibbs energy of formation for the VO_2^+ complexes.

	B3LYP/6-31+G*	B3LYP/6-31+G*
	kJ/mol	kJ/mol
$\text{VO}_2^+ + \text{H}_2\text{O} \rightarrow \text{VO}_2(\text{H}_2\text{O})^+$	-216.05	-204.18
$\text{VO}_2(\text{H}_2\text{O})^+ + \text{H}_2\text{O} \rightarrow \text{VO}_2(\text{H}_2\text{O})_2^+$	-136.47	-124.20
$\text{VO}_2(\text{H}_2\text{O})_2^+ + \text{H}_2\text{O} \rightarrow \text{VO}_2(\text{H}_2\text{O})_3^+$	-67.67	-67.62
$\text{VO}_2(\text{H}_2\text{O})_3^+ + \text{H}_2\text{O} \rightarrow \text{VO}_2(\text{H}_2\text{O})_4^+$	-20.30	-20.25

The results in Table 3.3 indicate that the incremental Gibbs energy of formation between $\text{VO}_2(\text{H}_2\text{O})_3^+$ and $\text{VO}_2(\text{H}_2\text{O})_4^+$ is small (only 20 kJ/mol). This small difference in the energy of formation of $\text{VO}_2(\text{H}_2\text{O})_4^+$ suggests that the lower energy structure $\text{VO}_2(\text{H}_2\text{O})_3^+ \cdot \text{H}_2\text{O}$ was achieved by having a hydrogen bonded water molecule to $\text{VO}_2(\text{H}_2\text{O})_3^+$.

Bond Lengths

Bond length is another important property used to understand the bonding pattern of water ligands to Vanadium (V). Figures 3.4 and 3.5 show plots of vanadium-oxygen bond lengths for each of the optimized structures shown in Figure 3.1 at the HF/6-31+G* and the B3LYP/6-31+G*, respectively. There are two types of vanadium oxygen bonds in optimized VO_2^+ structures shown. The first type is the vanadium to oxygen double bond in the oxovanadyl ion itself (V=O bond), and the second type is the vanadium to oxygen single bond between the cation and the hydrating water molecules (V-O bond).

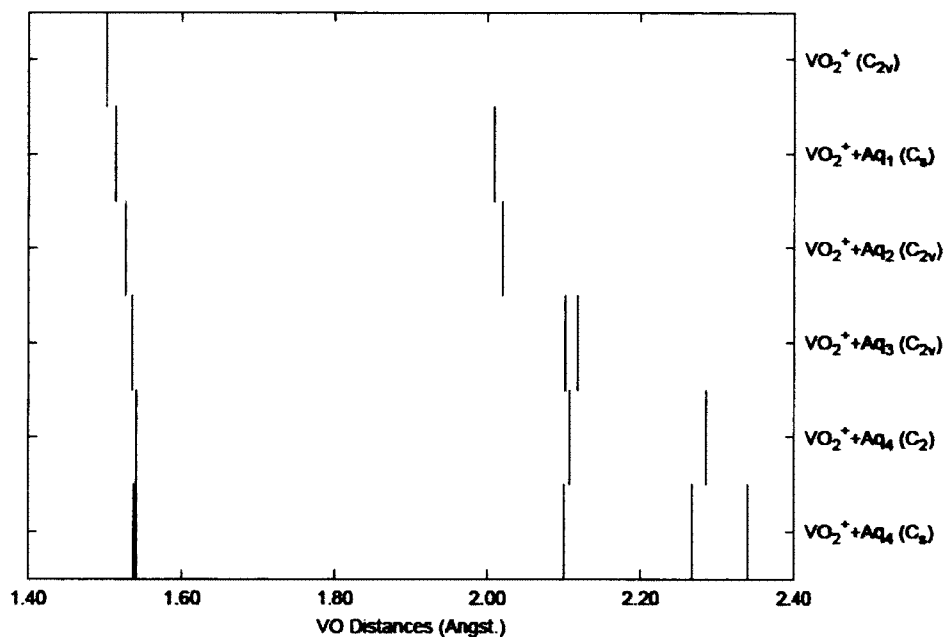


Figure 3.4. The V=O and V-O bond lengths calculated at the HF/6-31+G* level for $\text{VO}_2^+(\text{H}_2\text{O})_n^+$, with $n=0-4$.

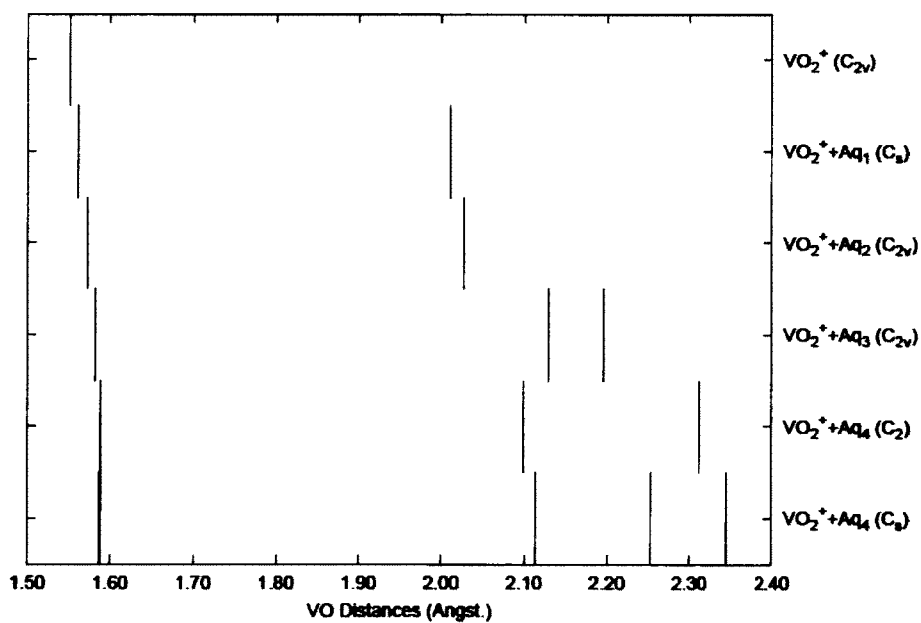


Figure 3.5. The V=O and V-O bond lengths calculated at the B3LYP/6-31+G* level for $\text{VO}_2^+(\text{H}_2\text{O})_n^+$, with $n=0-4$.

As expected, the V=O bond is much stronger than the V-O bond which results in shorter bond lengths of V=O (1.5-1.6 Å) than for V-O (2.0-2.3 Å). The HF/6-31+G* calculated V=O bond lengths were in the 1.50-1.55 Å range and the V-O bond lengths ranged from 2.0-2.35 Å. The B3LYP theory calculated V=O bond length ranged from 1.50-1.55 Å and V-O bond was in the range of 2.0-2.35 Å. The X-ray diffraction data for Baran's penta coordinate complex gives an average V=O bond length of 1.62 Å [53]. This is very close to the B3LYP calculated V=O bond lengths and can be used as a reference value. It is noticeable that at the HF level the V=O bond is underestimated by a larger margin than at the B3LYP level. The reason could be due to the absence of electron correlation [33, 35].

The calculations show a clear trend of the V=O and V-O bond lengths increasing as the hydration level rises. This is caused by steric effects and the repulsion of like atoms. As a result, each bond is weakened and its length is increased. This trend is consistent with the vibrational frequency trend where a frequency decrease is interpreted as bond weakening.

Vibrational Frequencies

Originally, this project intended to use only the MP2 and B3LYP calculated frequencies were going to be used in this project because electron correlation methods are more appropriate than HF for metals. However, MP2 calculated frequencies were consistently too high for VO₂⁺. The MP2 calculated frequency values were several times higher than those of measured experimentally for the oxovanadyl cation containing compounds. Several higher order MPn (n=2-4) methods, frequency

calculation techniques and basis sets were tested to pin point the issue. A summary of these tests is shown in Table 3.4.

Table 3.4. The summary tests of MPn (n= 2-4) vibrational frequency for VO₂⁺ [53].

Methods	Deformation Mode, cm ⁻¹	Symmetric Stretch V=O, cm ⁻¹	Asymmetric Stretch V=O, cm ⁻¹
MP2/cc-pVTZ	450	2089	4753
MP3/cc-pVTZ	491	1300	1513
MP4/cc-pVTZ	540	4085	13595
TD-DFT/6-311+G*	325	995	995

The higher order Møller-Plesset methods (MP3 and MP4) did not correct the incorrect MP2 frequencies. However, MP3 did show some promise as it had much lower frequency errors when compared to the MP2 results. Interestingly, the last method, MP4, performed worst as it overestimated the symmetrical V=O stretching frequencies three fold and the asymmetrical V=O stretches 13 fold! The basis set dependence of the MP2 method was verified using the larger basis sets 6-311+G* and cc-pVTZ. Both basis sets produced the same result as found for 6-31+G*. The default frequency calculation in the Gaussian software is an analytical method where the second derivatives of the energy are computed [47, 48]. An alternate method of frequency calculation is found in MP2/cc-pVTZ which uses a numerical frequency calculation. The second derivatives of the energy are computed numerically using analytically calculated first derivatives. The MP3 calculations with numerical frequency analysis were also carried out but no change in results was observed. The results of

these tests suggest that MPn methods fail at the theory level but due to a lack of time and the means to investigate deeper this issue remains unresolved.

HF/6-31+G* and B3LYP/6-31+G* frequencies were plotted in the Figure 3.6 and 3.7, respectively. The oxovanadyl cation has C_{2v} symmetry and the three vibrational modes have the irreducible representation $\Gamma_{\text{vib}} = 2A_1 + B_2$. As the number of water molecules grows, various new V=O modes appear in the vibrational spectra.

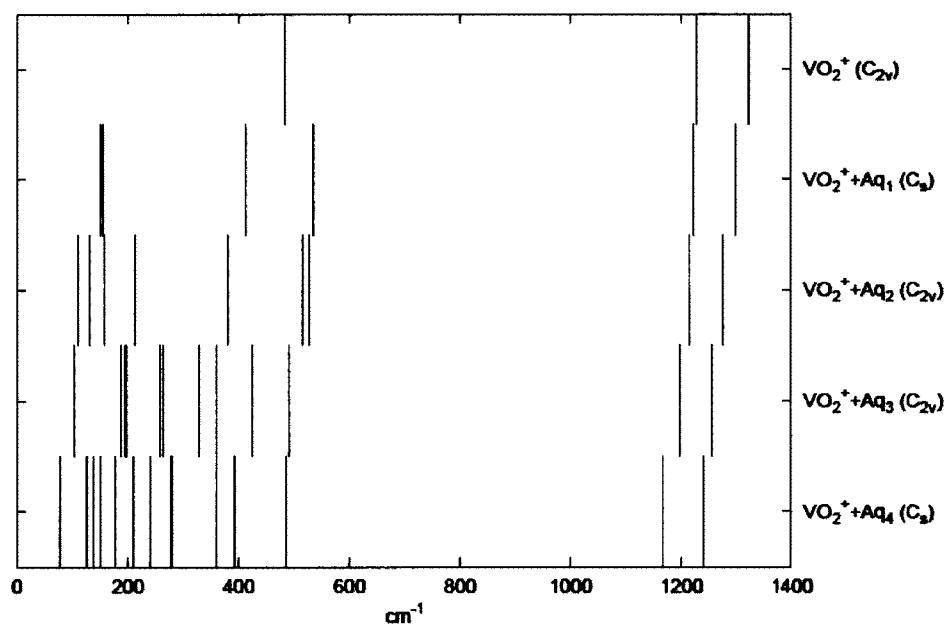


Figure 3.6. Vibrational frequencies calculated at the HF/6-31+G* level for $\text{VO}_2(\text{H}_2\text{O})_n^+$, with $n=0-4$.

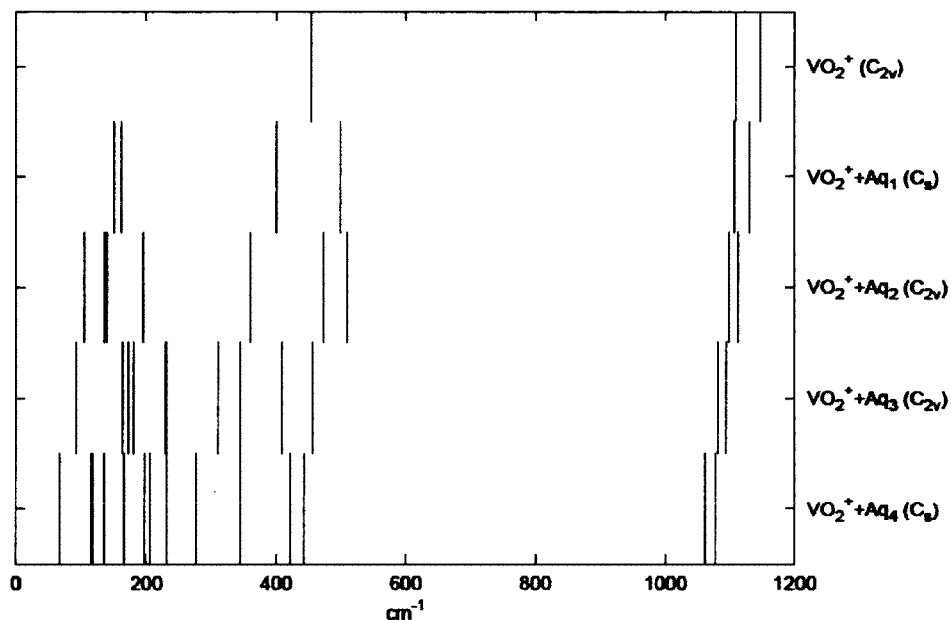


Figure 3.7. Vibrational frequencies calculated at the B3LYP/6-31+G* level for $\text{VO}_2(\text{H}_2\text{O})_n^+$, with $n=0-4$.

An initial observation of the calculated vibrational frequencies is that the frequencies decrease with increasing hydration of the cation. This is consistent at both the HF/6-31+G* and the B3LYP/6-31+G* levels. The HF/6-31+G* calculated frequencies are larger than those of B3LYP/6-31+G*, as expected, because Hartree-Fock neglects electron correlation. There is a widely used set of scale factors for the calculated frequencies to incorporate electron correlation and compensation for the use of a finite basis set. The scale factor used in the HF/6-31+G* calculations in this project was 0.8955 and for B3LYP/6-31+G* the scale factor used was 1.0062 [58]. Once the scale factors had been applied to the strong vibrational frequencies ($1000-1100 \text{ cm}^{-1}$) of VO_2^+ the disagreement between the two methods was only $\sim 30 \text{ cm}^{-1}$.

The calculated frequencies were compared to those in Baran's $[(VO_2)_2(4,4\text{-bipy})_{0.5}(4,4'\text{-Hbipy})(PO_4)]\cdot H_2O$ Vanadium (V) salt and the results are shown in Table 3.5 [53]. There is a large difference between the frequencies of the Baran complex and those of $VO_2(H_2O)_4^+$. $VO_2(H_2O)_4^+$ is the stable aqueous form of VO_2^+ hence it was used to compare with the Baran complex. It should be noted that the Baran complex is a solid salt which can lower the observed frequencies of the VO_2^+ ion.

Table 3.5. The B3LYP/6-31+G* calculated and experimental vibrational frequencies (cm^{-1}) of the oxovanadyl cation [53].

	Deformation, V=O, cm^{-1}	Symmetric Stretch V=O, cm^{-1}	Asymmetric Stretch V=O, cm^{-1}
Baran Complex	325	905	939
$VO_2(H_2O)_4^+$, gas	443	1104	1119
$VO_2(H_2O)_4^+$, PCM	439	1026	1066
$VO_2(H_2O)_4^+\cdot H_2O$, PCM	416	993	1046
$VO_2(H_2O)_4^+\cdot 2H_2O$, PCM	393	965	1007

The PCM frequencies are slightly closer to those of the Baran complex than the gas phase frequencies. There is a trend of the stretching frequency decreasing as the second hydration sphere at the cation is built up. In order to obtain calculated values even closer to the experimental values, more water molecules need to be added to complete the second hydration sphere of VO_2^+ and fully emulate the aqueous environment. However, this is a rather complicated task to perform because the number of possibilities increases exponentially in the global minima searches carried out with increasing numbers of water molecules.

Charges

All atomic charge calculations are arbitrary because this atomic property is not a quantum mechanical observable property [50]. Mulliken population analysis is a common method used to calculate charge [35]. It is a computationally inexpensive method, however, it is highly dependent on the choice of basis set and fails to converge with layer basis sets. Natural bond orbital (NBO) analysis is a more sophisticated method based on localized electron-pair “bonding” units [35]. Tests on charge convergence have proved that this method is independent of the basis set. Atomic charges are calculated as the difference between the nuclear charge and total natural population of electrons on the atoms.

The vanadium NBO charges were calculated for both the gas phase and the PCM optimized structures of $\text{VO}_2(\text{H}_2\text{O})_n^+$, where $n = 0-4$ using B3LYP/6-31+G* and are presented in Table 3.6.

Table 3.6. NBO vanadium charges in gas/PCM phase calculated at the B3LYP/6-31+G* level for $\text{VO}_2(\text{H}_2\text{O})_n^+$, with $n=0-4$.

Name of Complex	Gas Phase Charge on V	PCM Charge on V	Charge Difference (PCM- Gas Phase)
VO_2^+	1.540	1.981	0.441
$\text{VO}_2(\text{H}_2\text{O})^+$	1.585	1.815	0.230
$\text{VO}_2(\text{H}_2\text{O})_2^+$	1.510	1.627	0.117
$\text{VO}_2(\text{H}_2\text{O})_3^+$	1.547	1.559	0.012
$\text{VO}_2(\text{H}_2\text{O})_4^+$	1.467	1.503	0.036

Interestingly, only $\text{VO}_2(\text{H}_2\text{O})_3^+$ and $\text{VO}_2(\text{H}_2\text{O})_4^+$ have very small charge differences between the gas phase and PCM. The the rest of VO_2^+ species, especially VO_2^+ , have enormous change in the calculated charge. The two species of Vanadium

(V), $\text{VO}_2(\text{H}_2\text{O})_3^+$ and $\text{VO}_2(\text{H}_2\text{O})_4^+$, with the lowest charge difference are proposed to exist in either the gas and aqueous phases. However, this test does not provide a clear answer as to which vanadium species; $\text{VO}_2(\text{H}_2\text{O})_3^+$ or $\text{VO}_2(\text{H}_2\text{O})_4^+$, actually exists in aqueous solution. It does suggest that these two species will undergo the least amount of charge change in on going from the gas phase to the PCM environment.

Conclusion

The aqueous species of Vanadium (V) $\text{VO}_2(\text{H}_2\text{O})_n^+$ with $n = 0-4$ were studied by *ab initio* methods. The following trends were found with increased water molecule hydration. The V=O and V-O bond lengths were found to increase and the vibrational frequencies were found to decrease. This is because each water molecule contributed to an increase in the coordination number of VO_2^+ and as a result the bonds become weaker. $\text{VO}_2(\text{H}_2\text{O})_3^+ \cdot \text{H}_2\text{O}$ was found to be slightly more stable $\text{VO}_2(\text{H}_2\text{O})_4^+$ in both the gas phase and the PCM water solvation media with a median difference of ~ 15 kJ/mol. The possible existence of one of $\text{VO}_2(\text{H}_2\text{O})_3^+$ or $\text{VO}_2(\text{H}_2\text{O})_4^+$ in aqueous media was studied by solvation and NBO methods. In order to obtain conclusive results we need to complete the second hydration sphere around these species and compare their calculated energies.

Chapter IV: H_3VO_4

Introduction

H_3VO_4 (vanadic acid) is considered to be a minor component of aqueous Vanadium (V) speciation [2, 7]. There is no concrete experimental evidence to prove the existence of vanadic acid in aqueous solution. However, vanadic acid has been extracted into an organic solvent environment and its $\text{p}K_a$ value was determined to be 3.7 using a sensitive radiotracer method [59]. Schwarzenbach and Geier have suggested that not all neutral vanadic acid exists in the form of H_3VO_4 [60]. They propose that some of it exists as $\text{H}_3\text{VO}_4 \cdot \text{H}_2\text{O}$ which readily transforms into $\text{V}(\text{OH})_5$ because this form of the uncharged monomer is less acidic. However, this was never proven because the concentration of the putative aqueous H_3VO_4 was too low to be detected. Experimental work using a potentiometric method and a ^{51}V NMR study of vanadates in 1.25 mM solution did not find the uncharged monomer (H_3VO_4) [61]. However, the conclusion was that H_3VO_4 , if it exists, can never become the predominant aqueous species because its $\text{p}K_a$ is less than 3.1 while the $\text{p}K_a$ of VO_2^+ is greater than 3.9. Interestingly, various methods of the $\text{p}K_a$ determination of vanadic acid result in slightly different $\text{p}K_a$ and the range of $\text{p}K_a$ varies from 3.1-3.9 [59-61]. As it was mentioned before and shown in Figure 1.1 VO_2^+ is the predominant species of Vanadium (V) at low pH and concentration.

A computational study at the Hartree-Fock level on H_3VO_4 showed that it belongs to the C_{3v} point group with bond lengths for V-O(H) of 1.745 Å and V=O of 1.527 Å [62]. However, using local MP2 theory, the symmetry of H_3VO_4 was found to

be C_s (a slightly distorted C_{3v} structure) and having two V-O(H) bond lengths of 1.823 Å and one of 1.819 Å; the V=O bond length was found to be 1.639 Å.

The primary objective of this research was to find the stable structures of $H_3VO_4 \cdot nH_2O$, where $n=0-6$. The effects of hydration on the bond lengths and frequencies were also investigated. The possible existence of $V(OH)_5$ was verified in the gas phase and the aqueous PCM conditions.

Results and Discussions

Geometries

The initial guesses for the hydrated vanadic acid species were computed by the MP2 and B3LYP methods. The agreement between MP2 and B3LYP was total as they predicted the same global minima structures. The geometries of the optimized global minima of $H_3VO_4 \cdot nH_2O$ structures as determined by B3LYP/6-31+G*, where $n = 0-6$ are shown in Figure 4.1. Numerous local minima structures were calculated and they are shown in Figure B of the Appendix section.

Optimized H_3VO_4 has the point group symmetry C_{3v} . This structure was the most stable conformation of vanadic acid at all levels studied (HF, MP2 and B3LYP). However, the local symmetry (C_{3v}) was not preserved in the hydrated species. The preferred hydrated structure of vanadic acid was similar to the structure of the monohydrate where one of OH^- ligands points directly towards the oxygen of the water to more efficiently act as a hydrogen bond donor (see the structure **B**). The global minimum for $H_3VO_4 \cdot H_2O$ belonged to the C_s point group. All other optimized

structures for $\text{H}_3\text{VO}_4 \cdot n\text{H}_2\text{O}$ $n=2-6$, have no symmetry beyond C_1 because of the multiple hydrogen bonds formed among water molecules.

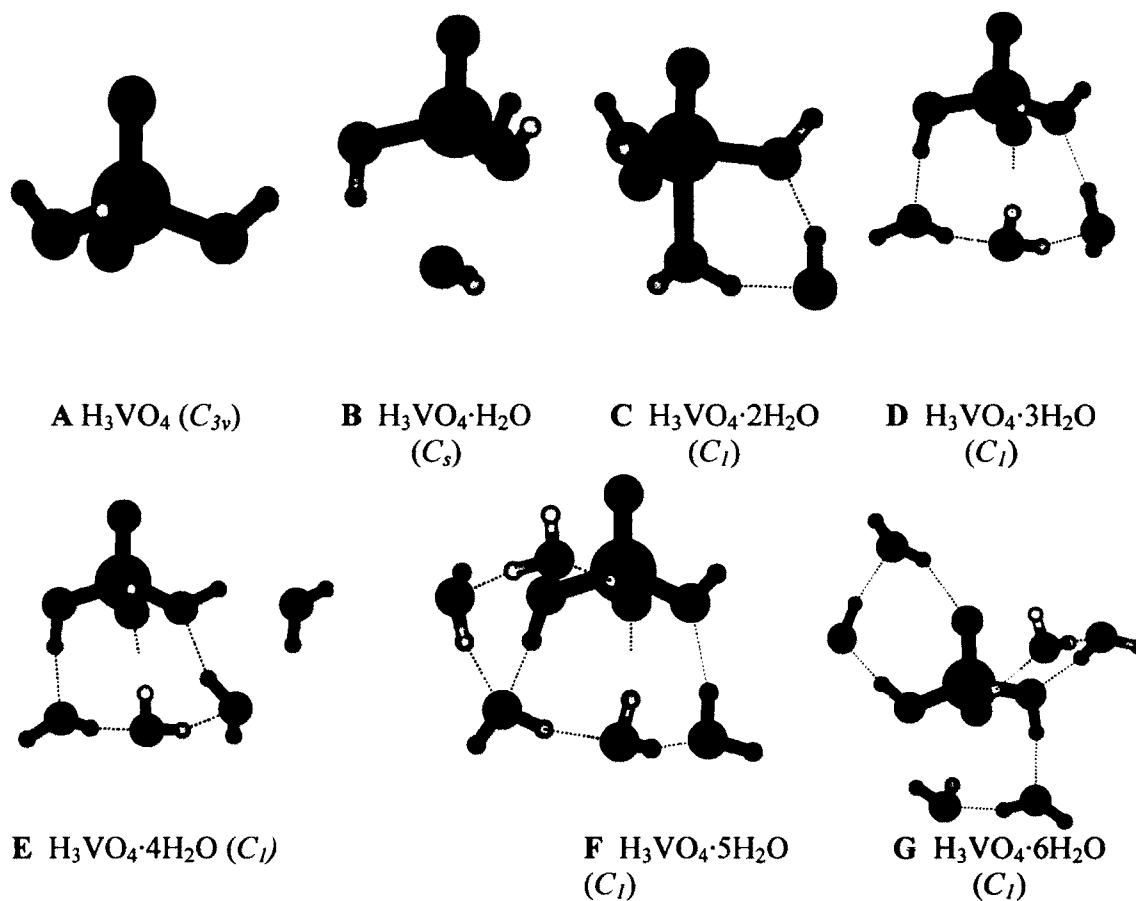


Figure 4.1. The B3LYP/6-31+G* optimized structures of $\text{H}_3\text{VO}_4 \cdot n\text{H}_2\text{O}$, where $n=0-6$.

As seen in Figure 4.1, Structures **B** and **C** show that vanadic acid can exist as a penta coordinate species. However, the newly formed bond is very weak, as it is broken when more water molecules are added. It is clear that when more than three water molecules are present, we start to see a small water cluster begins to form as seen in the

E, F and G structures. For some reason, Molden, the visualization software, did not recognize several apparent hydrogen bonds for the E and G structures.

Energies

The optimized structures of F ($\text{H}_3\text{VO}_4 \cdot 5\text{H}_2\text{O}$) and G ($\text{H}_3\text{VO}_4 \cdot 6\text{H}_2\text{O}$) from Figure 4.1 are not the calculated global minima. The global minima of these two structures did not satisfy our definition of hydration, in which the hydrated structure has to have each water molecule interacting with the vanadic acid. The global minima for $\text{H}_3\text{VO}_4 \cdot 5\text{H}_2\text{O}$ and $\text{H}_3\text{VO}_4 \cdot 6\text{H}_2\text{O}$ are shown in Figure 4.2 as the each complex has a water molecule (the hollow oxygen atom) that does not interact with the vanadic acid. This non-fully hydrated structure of $\text{H}_3\text{VO}_4 \cdot 6\text{H}_2\text{O}$ is 11.6 kJ/mol more stable than Structure G at the B3LYP/6-31+G* level of theory. This small difference in energy indicates that water cluster formation is slightly more favourable than forming a hydrogen bond directly with vanadic acid.

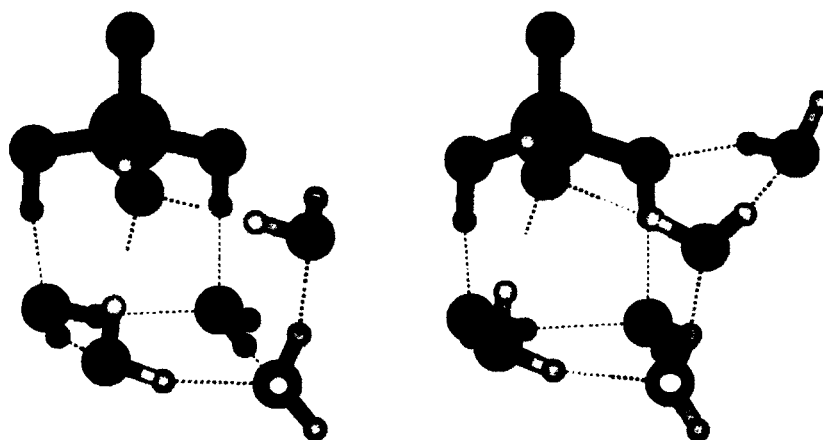


Figure 4.2. The B3LYP/6-31+G* optimized global minima of the $\text{H}_3\text{VO}_4 \cdot 5\text{H}_2\text{O}$ and $\text{H}_3\text{VO}_4 \cdot 6\text{H}_2\text{O}$ structures.

The incremental Gibbs energies of hydration for the hydrated forms of vanadic acid are shown in Table 4.1. In this case, the incremental Gibbs energy is used to describe the effect of water on vanadic acid as it forms various hydrogen bonds. Interestingly, the calculations of the MP2/6-31+G* theory level suggests that there is almost no change in the incremental Gibbs energy when two or more water molecules form a hydrogen bond with vanadic acid. This means that hydrogen bond formation does not contribute to the overall stabilization of the complex for the $\text{H}_3\text{VO}_4 \cdot n\text{H}_2\text{O}$ $n=2-6$ complexes. In the case of going from $\text{H}_3\text{VO}_4 \cdot 3\text{H}_2\text{O}$ to $\text{H}_3\text{VO}_4 \cdot 4\text{H}_2\text{O}$, the incremental Gibbs energy of hydration is slightly unfavourable but the overall difference is so small that very high accuracy methods need to be utilized to verify these results.

Table 4.1. The Incremental Gibbs energy of hydration for hydrated vanadic acid $\text{H}_3\text{VO}_4 \cdot n\text{H}_2\text{O}$ $n=1-6$.

	MP2/6-31+G*, kJ/mol	B3LYP/6-31+G*, kJ/mol
$\text{H}_3\text{VO}_4 \cdot \text{H}_2\text{O} \rightarrow \text{H}_3\text{VO}_4 \cdot 2\text{H}_2\text{O}$	-0.22	-48.92
$\text{H}_3\text{VO}_4 \cdot 3\text{H}_2\text{O} \rightarrow \text{H}_3\text{VO}_4 \cdot 4\text{H}_2\text{O}$	2.94	-46.23
$\text{H}_3\text{VO}_4 \cdot 5\text{H}_2\text{O} \rightarrow \text{H}_3\text{VO}_4 \cdot 6\text{H}_2\text{O}$	-7.17	-54.07

On the other hand, calculations carried out at the B3LYP/6-31+G* level of theory for incremental Gibbs energy showed that each new water molecule stabilizes the vanadic acid complex on average by 40-45 kJ/mol. Each water molecule forms a hydrogen bond with vanadic acid and most likely these hydrogen bonds are the major contributors to the stability energies. The formation of $\text{H}_3\text{VO}_4 \cdot 5\text{H}_2\text{O}$ and $\text{H}_3\text{VO}_4 \cdot 6\text{H}_2\text{O}$ have slightly higher Gibbs energies (50-70 kJ/mol) because there are now enough water

molecules present for hydrogen bonds to form between water molecules. It would be expected with a complete hydration sphere around the vanadic acid that the incremental Gibbs energy would fully converge to a value while representing the water-water hydrogen bond energy exclusively.

Schwarzenbach and Geier suggested that vanadic acid can react with a water molecule to form a new penta coordinate neutral species of Vanadium (V) $V(OH)_5$ [60]. The B3LYP/cc-pVTZ optimized structure of $V(OH)_5$ is shown in Figure 4.3. The energy of $V(OH)_5$ was compared to its stoichiometric equivalent, $H_3VO_4 \cdot H_2O$.

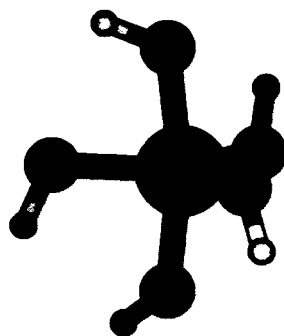


Figure 4.3. The B3LYP/cc-pVTZ optimized structure of $V(OH)_5$.

The geometries of both structures were optimized at the B3LYP/cc-pVTZ theory levels followed by a single point energy calculation using the CCSD(T)/cc-pVTZ method. Both structures are the penta coordinate species with some minor structural differences. $H_3VO_4 \cdot H_2O$ was found to be significantly more stable than $V(OH)_5$, by ~ 120 kJ/mol. The influence of solvating water was also studied; both structures were optimized under the aqueous PCM condition using B3LYP/cc-pVTZ. The CCSD(T)/cc-pVTZ calculations on the PCM optimized structures also showed that $H_3VO_4 \cdot H_2O$ was more

stable than $V(OH)_5$, this time by an even larger amount, ~ 146 kJ/mol. Based on these large differences in energies, it seems that $V(OH)_5$ is very unlikely to exist in either the gas or aqueous phase.

Bond Lengths

One of the most important properties used to measure the effects of hydration on a molecule is bond length. In the vanadic acid case, the water molecules prefer to form hydrogen bonds with the coordinated hydroxo groups rather than bond to the vanadium atom itself. Interestingly, the oxo group prefers not to have the any interactions with water. Figures 4.4 and 4.5 show the effect of hydration on the $V=O$ (oxo group) and the $V-O$ (hydroxo group) bond lengths in the hydrated H_3VO_4 .

Calculations at the B3LYP/6-31+G* level of theory indicate that the average $V=O$ bond length is slightly less than 1.6 Å, whereas for MP2/6-31+G* level of calculations is in the range of 1.60-1.65 Å. The effect of hydration on the $V=O$ bond is non-existent as mentioned above, because it does not participate in hydrogen bonding with any of the water molecules. On other hand, the $V-O$ bond length is heavily influenced by hydration. The MP2/6-31+G* range for its bond length is 1.75-1.90 Å and the B3LYP/6-31+G* range is between 1.73-1.85 Å. Both theories show a clear trend with overall a slight bond length decrease observed with increasing hydration. This $V-O$ bond length decrease is most likely a result of the cooperative effect caused by the water molecules and the hydrogen bonds formed. In order to observe a trend in the $V=O$ bond length, it seems that the vanadic acid would have to be solvated since our current results suggest that the oxo region of the hydration shell will be the last

completed. Such computations are very complicated because of the global minima search problem and increasing the number of water molecules also increases the number of possible bonding arrangements.

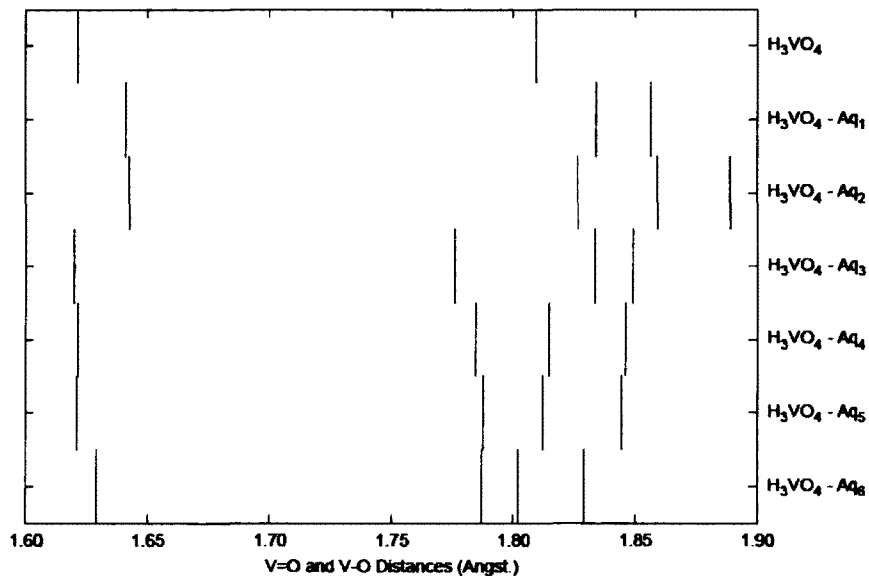


Figure 4.4. The V=O and V-O bond lengths calculated at the MP2/6-31+G* level for $\text{H}_3\text{VO}_4 \cdot n\text{H}_2\text{O}$, with $n=0-6$.

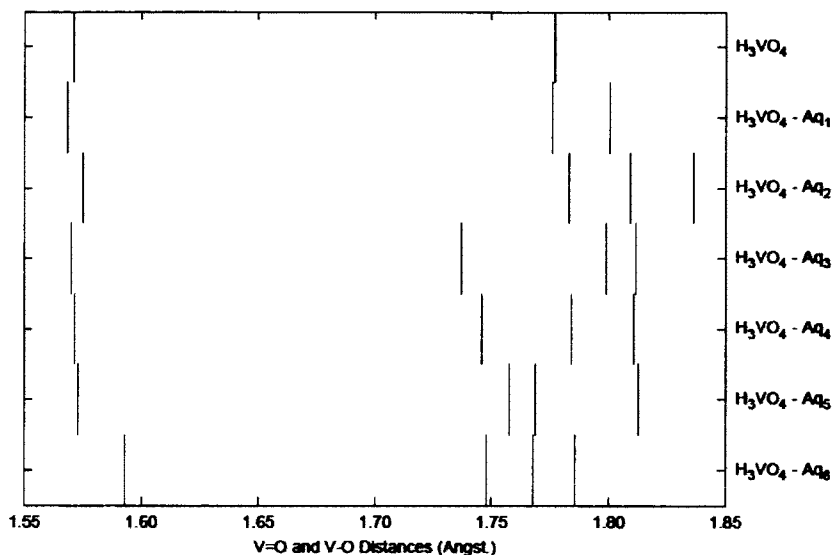


Figure 4.5. The V=O and V-O bond lengths calculated at the B3LYP/6-31+G* level for $\text{H}_3\text{VO}_4 \cdot n\text{H}_2\text{O}$, with $n=0-6$.

Another important measurable property is the distance between vanadium and the oxygen atoms of the hydrating water molecules (V--O). This distance provides an estimate of the radius of the complete hydration sphere. It was measured at the MP2/6-31+G* and B3LYP/6-31+G* levels of theories shown in as Figures 4.6 and 4.7. For the cases of one and two water molecules, one of the water molecules tends to act as a ligand which results in extremely short V--O distances in the range of 2.20-2.40 Å and 2.20-2.80 Å for the MP2 and B3LYP calculations, respectively. These figures show that as the vanadic acid becomes more hydrated, water molecules tend to hydrogen bond to the complex rather than to act as a ligand and bond directly to the vanadium. The vast majority of the V--O distances are in the range of 3.5-4.0 Å (for MP2/6-31+G*) and (3.6-4.1 Å for B3LYP/6-31+G*). If a complete hydration shell could be measured, it is suggested that its radius would be in the range of 3.5-4.1 Å.

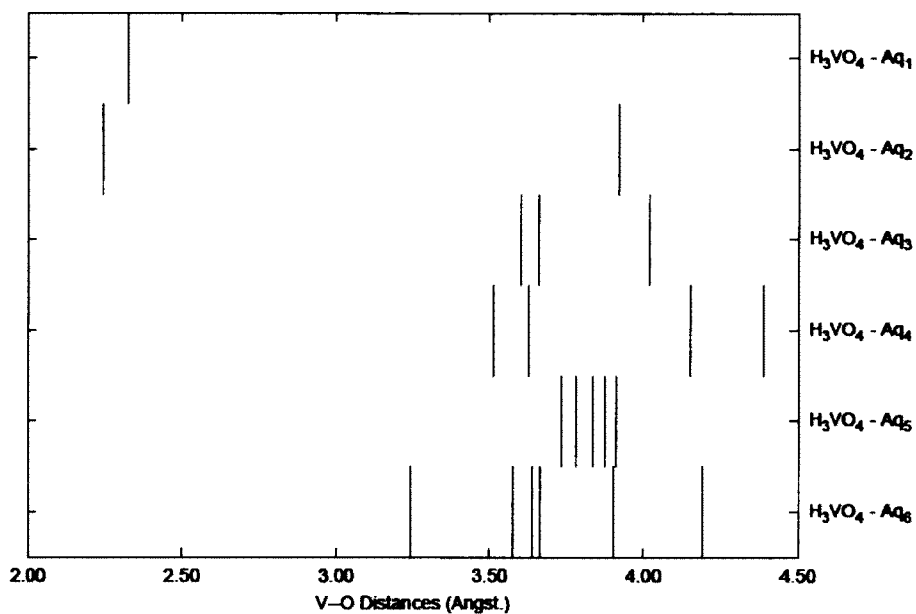


Figure 4.6. The V--O distances calculated at the MP2/6-31+G* level for $\text{H}_3\text{VO}_4 \cdot n\text{H}_2\text{O}$, with $n=0-6$.

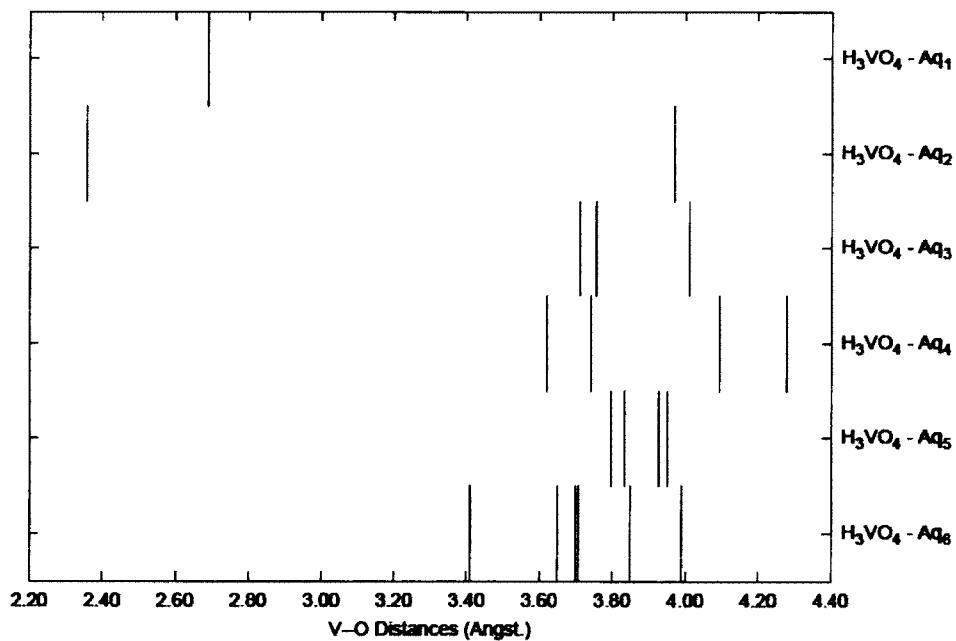


Figure 4.7. The V--O distances calculated at the B3LYP/6-31+G* level for $\text{H}_3\text{VO}_4 \cdot n\text{H}_2\text{O}$, with $n=0-6$.

Vibrational Frequencies

As previously mentioned, vanadic acid has never been directly observed in aqueous solution [7]. However, it is considered to be as a minor component in Vanadium (V) speciation because of the structural similarities between vanadates and phosphates. It is possible that vibrational properties of this minor component might never be measured experimentally. In consequence, it was decided to predict the vibrational spectra of vanadic acid. The electron correlation methods, MP2 and B3LYP, were used to calculate the vibrational spectra of vanadic acid. These calculated frequencies are shown in Figures 4.8 and 4.9 for the MP2/6-31+G* and B3LYP/6-31+G* levels, respectively. As expected, no clear trend was observed for the V=O stretching mode (1000-1100 cm^{-1}) because of its lack of interaction with the water molecules. In the deformation modes, 180-400 cm^{-1} (MP2/6-31+G*) and 150-350 cm^{-1} (B3LYP/6-31+G*) a clear trend of increasing frequency with increasing hydration was observed. A similar trend was observed for the stretching modes of V-O, with MP2/6-31+G* giving a range of 550-800 cm^{-1} and B3LYP/6-31+G* in the region of 650-850 cm^{-1} . These frequency increases are caused by the hydrogen bonding of the water molecules to the hydroxo groups of the vanadic acid. It was not possible to conclude which theory better estimated the vibrational spectra of vanadic acid because of the lack of experimental data available for comparison.

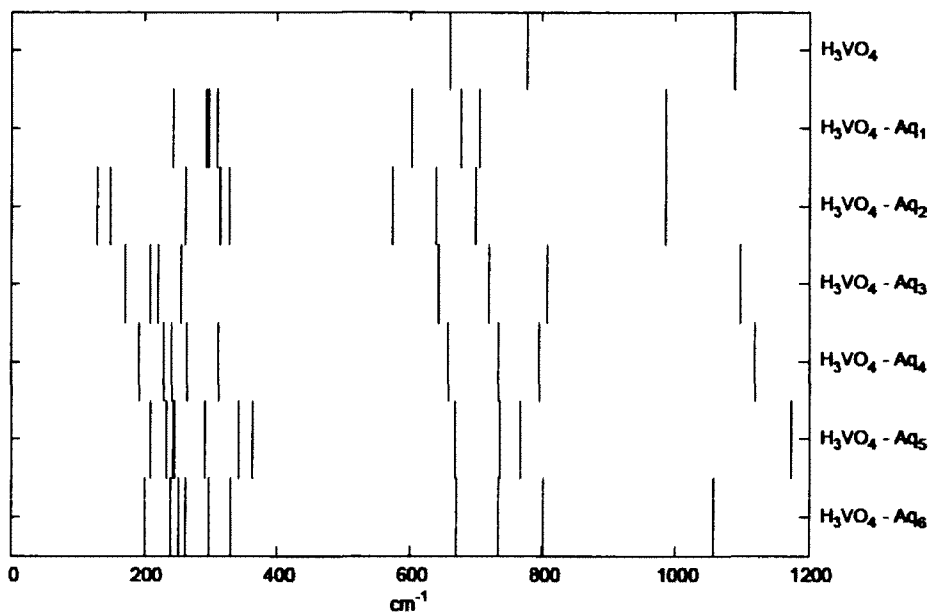


Figure 4.8. Vibrational Frequencies calculated at the MP2/6-31+G* level for $\text{H}_3\text{VO}_4 \cdot n\text{H}_2\text{O}$, with $n=0-6$.

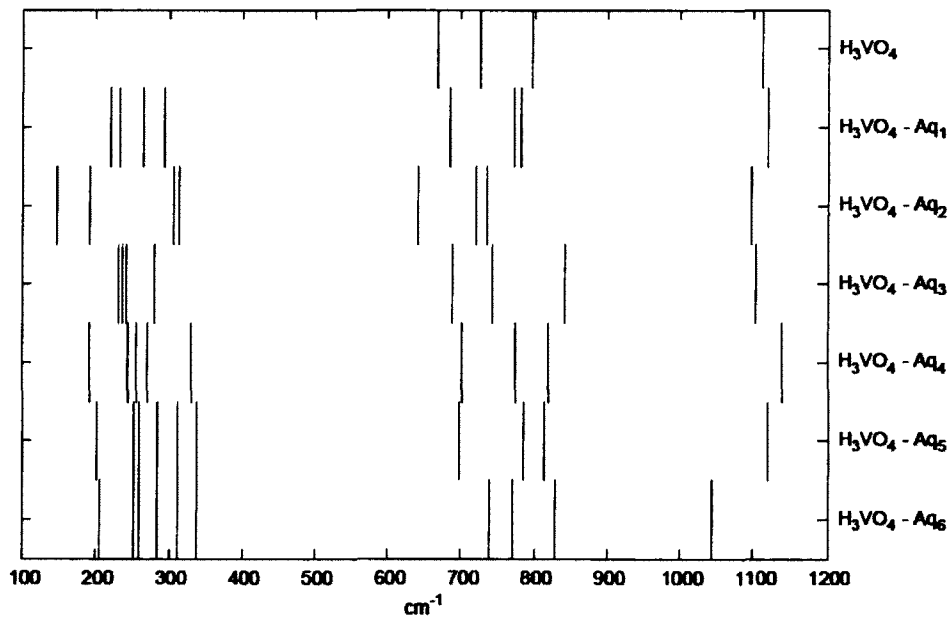


Figure 4.9. Vibrational Frequencies calculated at the B3LYP/6-31+G* level for $\text{H}_3\text{VO}_4 \cdot n\text{H}_2\text{O}$, with $n=0-6$.

Charges

NBO calculations using B3LYP/6-31+G* were performed for $\text{H}_3\text{VO}_4 \cdot n\text{H}_2\text{O}$, with $n=0-6$ in the gas phase and in the aqueous PCM mode. The NBO charge calculation in the PCM model can help to better understand the effects of water on the vanadium atom. The results are summarized in Table 4.2. Table 4.2 shows that the calculated charges

Table 4.2. NBO vanadium charges in gas/PCM phase calculated at the B3LYP/6-31+G* level for $\text{H}_3\text{VO}_4 \cdot n\text{H}_2\text{O}$, $n=0-6$.

Name of Complex	Gas Phase Charge	PCM Charge	The Charge Difference (PCM-Gas Phase)
H_3VO_4	1.591	1.622	0.031
$\text{H}_3\text{VO}_4 \cdot \text{H}_2\text{O}$	1.586	1.607	0.021
$\text{H}_3\text{VO}_4 \cdot 2\text{H}_2\text{O}$	1.613	1.626	0.013
$\text{H}_3\text{VO}_4 \cdot 3\text{H}_2\text{O}$	1.595	1.630	0.035
$\text{H}_3\text{VO}_4 \cdot 4\text{H}_2\text{O}$	1.599	1.635	0.036
$\text{H}_3\text{VO}_4 \cdot 5\text{H}_2\text{O}$	1.596	1.630	0.033
$\text{H}_3\text{VO}_4 \cdot 6\text{H}_2\text{O}$	1.592	1.635	0.043

have converged for all vanadic acid species for both the gas phase and the PCM calculations. Overall, the gas phase charges on vanadium show a very small fluctuation of only 0.027 of the charge. The PCM charges also have a very small range of 0.028. The computed charge difference between the two methods is also small and relatively constant. Interestingly, the charge difference for all tetra coordinate vanadium species (H_3VO_4 , $\text{H}_3\text{VO}_4 \cdot 3\text{H}_2\text{O}$, $\text{H}_3\text{VO}_4 \cdot 4\text{H}_2\text{O}$, $\text{H}_3\text{VO}_4 \cdot 5\text{H}_2\text{O}$ and $\text{H}_3\text{VO}_4 \cdot 6\text{H}_2\text{O}$) is small and constant and ranges from 0.030-0.035. The vanadic acid species with water molecules directly bonded to vanadium (the penta coordinate vanadic acid), have slightly lower

charge differences (PCM – gas phase) measuring 0.013 for $\text{H}_3\text{VO}_4 \cdot 2\text{H}_2\text{O}$ and 0.021 for $\text{H}_3\text{VO}_4 \cdot \text{H}_2\text{O}$. However, the charge differences are too small to declare any trends other than the fact that vanadic acid is a very stable structure and that hydration has not affect the vanadium charge.

Conclusion

The hydrated species of vanadic acid $\text{H}_3\text{VO}_4 \cdot n\text{H}_2\text{O}$ $n = 0 - 6$ were studied using *ab initio* methods. The effects of hydration on bond lengths, atomic distances, vibrational frequencies and vanadium charge were investigated. The water molecules tend to hydrogen bond to the hydroxo groups of the vanadic acid which leads to the V-O bond length decreasing and concurrent increases of its vibrational frequencies, both the deformation modes ($150\text{-}350\text{ cm}^{-1}$) and the stretching modes ($600\text{-}800\text{ cm}^{-1}$). The oxo group of the optimized structures did not interact with the water molecules and hence no trends in bond lengths or vibrational frequencies were found for $\text{V}=\text{O}$. The vanadium to water molecule distance for all water molecules were found to be in the range of 3.5 to 4.2 Å. The NBO charge study showed that the water molecules do not influence the charge on vanadium and it is independent of method, as the gas phase and the PCM calculations produced the same results – the vanadium charge is almost constant in all complexes. For completeness, vanadic acid needs to be studied with a complete hydration sphere. Only in this way can the hydration effects on the $\text{V}=\text{O}$ bond strength and vibrational frequency be determined. Also, a V- -O distance could then reveal the actual hydration sphere radius. However, building the complete hydration

shell is a very complicated task because of the multiple minima issue and it was not carried out in this work.

Chapter V: H_2VO_4^-

Introduction

Dihydrogen vanadate, H_2VO_4^- , exists in an aqueous environment in the pH range 3-8 in a colorless form [2, 7]. A simple protonation of hydrogen vanadate (HVO_4^{2-}) yields the anion H_2VO_4^- [63]. Dihydrogen vanadate is known to exist in very dilute solution with concentrations somewhere below 2×10^{-5} M [2] or 4×10^{-4} M. At concentrations above 4×10^{-4} M, dihydrogen vanadate undergoes various polymerization reactions [2, 7, 63]. The nature of these polymerization reactions is one of the most important unsolved problems remaining in aqueous Vanadium (V) speciation [64]. Studying these reactions has not provided conclusive results as to what kind of vanadate polymers form when the concentration of dihydrogen vanadate is increased to trigger the polymerization. Some researchers have suggested that, in the pH range 6.5 - 8.2 the polymeric species formed is the trimer $\text{V}_3\text{O}_9^{3-}$ [65]. On the other hand, some concrete results have shown showed that the main product of the polymerization reaction is the tetramer $\text{V}_4\text{O}_{12}^{4-}$ [66]. The research conducted by Brito on the acidic nature of dihydrogen vanadate revealed that the product of the polymerization reactions was an equilibrium mixture of trimers $\text{V}_3\text{O}_9^{3-}$ and tetramers $\text{V}_4\text{O}_{12}^{4-}$ [67].

H_2VO_4^- has traditionally been considered as a tetra coordinate species [2, 7, 62, 63]. However, the work by Harnung strongly suggests that dihydrogen vanadate is a penta coordinate species with the molecular formula H_4VO_5^- (the result of a water molecule binding to H_2VO_4^-) in the pH range of 7-8 [68]. His work showed that only a penta coordinate structure for dihydrogen vanadate was able to account for the observed

experimental results. Also, he made the assumption that H_4VO_5^- does not exist in the form of $\text{VO}(\text{OH})_4^-$ (the structural analog of H_4PO_5^-) but instead exists as $\text{VO}_2(\text{OH})_2(\text{H}_2\text{O})^-$.

A computational study conducted by Buhl and Parrinello on H_2VO_4^- , optimized dihydrogen vanadate as a tetra coordinate species with C_2 symmetry [55]. They began from C_2 and C_s geometries for dihydrogen vanadate and put these conformations into CPMD simulations. In a simulation box, each molecule was surrounded by 30 water molecules for a short, 2 ps, simulation. The C_2 symmetry for H_2VO_4^- allowed better fluxionality and was better attenuated by the water solvent. Another researcher, Ribeiro-Claro, performed several calculations using the *ab initio* effective core potential (ECP) method with various basis sets [69]. His work showed that if one considers dihydrogen vanadate as a tetra coordinate species, the traditional C_2 symmetry for the H_2VO_4^- ion was indeed the preferred geometry. However, in the case of the possibility of a penta coordinate species H_4VO_5^- , his calculations indicated that $\text{VO}(\text{OH})_4^-$ was slightly (by 15 kJ/mol) more stable than $\text{VO}_2(\text{OH})_2(\text{H}_2\text{O})^-$; the energy difference margin was too small to give a conclusive result. He also calculated the vibrational spectra for H_2VO_4^- and the V-O stretches to be in the range of 650-700 cm^{-1} and the V=O stretches to be in the 1000-1050 cm^{-1} region.

In this work, the primary research objective was to investigate the hydration properties of dihydrogen vanadate. The hydrated $\text{H}_2\text{VO}_4^- \cdot n\text{H}_2\text{O}$, ($n=0-6$), structures were optimized using the *ab initio* computational methods, MP2 and B3LYP. The effect of hydration on the bond lengths and vibrational frequencies of H_2VO_4^- will be

discussed in this section. The possible existence of the $\text{VO}(\text{OH})_4^-$ had been investigated and will also be discussed.

Results and Discussions

Geometries and Energies

The symmetry point group for dihydrogen vanadate has traditionally been assumed to be C_2 [55]. Alternatively, a symmetry point group of C_s has been proposed for H_2VO_4^- [69]. These conformations of dihydrogen vanadate were optimized at the B3LYP/6-31+G* theory level and the structures are shown in Figure 5.1.

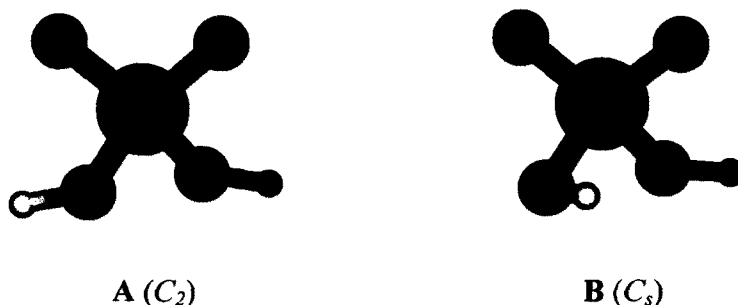


Figure 5.1 Two possible orientations of dihydrogen vanadate: **A** (C_2) and **B** (C_s) orientations.

The structure **A** is only about 1.5 kJ/mol lower in energy than **B** when calculated using B3LYP and MP2 with the 6-31+G* basis set. Previous work by Pye on a very similar compound, dihydrogen phosphate, showed that the C_2 structure was more stable than that with C_s symmetry for all the studied hydration levels, up to a maximum of six water molecules [70]. A molecular dynamics simulation on dihydrogen vanadate showed that **A** and **B** interconvert during the equilibration step [55]. On average eight

water molecules interact with the dihydrogen vanadate. Two water molecules act as donors and acceptors for the two OH⁻ groups of H₂VO₄⁻ and the other six act as hydrogen bond donors to all oxygens of dihydrogen vanadate (two oxo groups which accept two hydrogen bonds each). The A form allowed a better hydrogen bonding arrangement with less steric bulk strain than the form B. Based on this evidence, all hydrated structures of H₂VO₄⁻ were modelled with the C₂ symmetry for the starting geometry. H₂VO₄⁻·nH₂O, (n=0-6) structures were optimized using both MP2 and B3LYP methods. Only the optimized global minimum for each level of hydration is shown Figure 5.2. All the other local minima structures are shown in Figure C of the Appendix section.

Harnung's proposed penta coordinate dihydrogen vanadate, VO₂(OH)₂(H₂O)⁻, was found to be highly unstable; it decomposed to H₂VO₄⁻·H₂O in the gas phase optimization [68]. The hydrated H₂VO₄⁻·H₂O (B3LYP only), and H₂VO₄⁻·4H₂O (all levels) structures adopt to the low symmetry geometries of point group C₂. In the case of H₂VO₄⁻·H₂O, unlike hydrated vanadic acid, the water molecule actually prefers to interact with the oxo group instead of a hydroxo group. A similar hydrogen bonding pattern is observed in the B3LYP/6-31+G* optimized version of H₂VO₄⁻·2H₂O. Once there are three or more water molecules present, water cluster formation is observed. Interestingly, the optimized structure of H₂VO₄⁻·4H₂O was unexpectedly found to retain C₂ symmetry. This structure is unique because every single possible bond site of the dihydrogen vanadate interacts with the hydrating water molecules. The H₂VO₄⁻·5H₂O

and $\text{H}_2\text{VO}_4^- \cdot 6\text{H}_2\text{O}$ structures preserve the bonding pattern of $\text{H}_2\text{VO}_4^- \cdot 4\text{H}_2\text{O}$ with the additional water molecules acting as hydrogen bond donors to oxo groups.

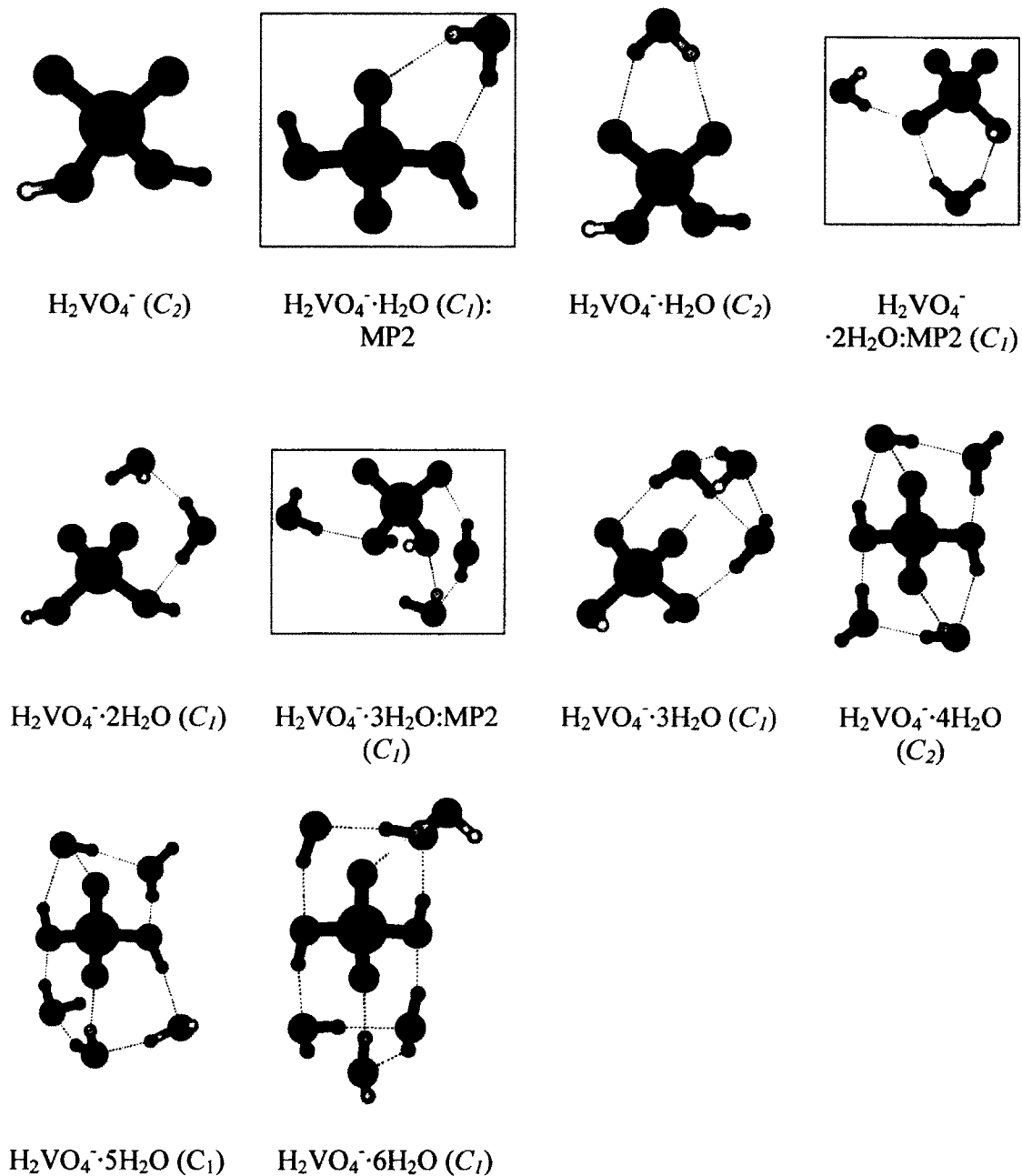


Figure 5.2. The optimized structures of $\text{H}_2\text{VO}_4^- \cdot n\text{H}_2\text{O}$, ($n=0-6$), calculated by B3LYP/6-31+G*. Solid boxes denote the MP2/6-31+G* global minima.

Only the $\text{H}_2\text{VO}_4^- \cdot \text{H}_2\text{O}$, $\text{H}_2\text{VO}_4^- \cdot 2\text{H}_2\text{O}$ and $\text{H}_2\text{VO}_4^- \cdot 3\text{H}_2\text{O}$ structures produced different global minima using the MP2/6-31+G* and the B3LYP/6-31+G* methods. The energy differences of these global minima are summarized in Table 5.1.

Table 5.1. The energy differences of the MP2 and B3LYP global minima for $\text{H}_2\text{VO}_4^- \cdot n\text{H}_2\text{O}$ structures, where $n=1-3$.

Hydration level	MP2 Global Minimum	MP2 Energy of B3LYP Global Minimum, kJ/mol	B3LYP Global Minimum	B3LYP Energy of MP2 Global Minimum, kJ/mol
$\text{H}_2\text{VO}_4^- \cdot \text{H}_2\text{O}$	-	+9	-	+9.5
$\text{H}_2\text{VO}_4^- \cdot 2\text{H}_2\text{O}$	-	+11	-	+3.3
$\text{H}_2\text{VO}_4^- \cdot 3\text{H}_2\text{O}$	-	+2.3	-	+14

These energy differences are so negligible that both geometries, at each hydration level, were considered to be global minima.

An important property calculated for the hydrated dihydrogen vanadate is the Gibbs energy of hydration. The Gibbs energy of hydration shows the energy effects of the hydrogen bonded water molecules on the overall energy. Table 5.2 includes the incremental Gibbs energies for $\text{H}_2\text{VO}_4^- \cdot n\text{H}_2\text{O}$, $n=0-6$.

Table 5.2. The incremental Gibbs energy of hydration of $\text{H}_2\text{VO}_4^- \cdot n\text{H}_2\text{O}$, where $n=0-6$.

	MP2/6-31+G*, kJ/mol	B3LYP/6-31+G*, kJ/mol
$\text{H}_2\text{VO}_4^- \cdot \text{H}_2\text{O} \rightarrow \text{H}_2\text{VO}_4^- \cdot 2\text{H}_2\text{O}$	-23.6	-8.3
$\text{H}_2\text{VO}_4^- \cdot 2\text{H}_2\text{O} \rightarrow \text{H}_2\text{VO}_4^- \cdot 3\text{H}_2\text{O}$	-11.6	-12.1
$\text{H}_2\text{VO}_4^- \cdot 3\text{H}_2\text{O} \rightarrow \text{H}_2\text{VO}_4^- \cdot 4\text{H}_2\text{O}$	-5.0	-1.1
$\text{H}_2\text{VO}_4^- \cdot 4\text{H}_2\text{O} \rightarrow \text{H}_2\text{VO}_4^- \cdot 5\text{H}_2\text{O}$	-13.0	-13.2
$\text{H}_2\text{VO}_4^- \cdot 5\text{H}_2\text{O} \rightarrow \text{H}_2\text{VO}_4^- \cdot 6\text{H}_2\text{O}$	-0.8	-5.1

Calculations at the MP2 level of theory show that as the number of water molecules increase, there is an overall stabilization of the incremental Gibbs energy. This energy seems to increase from -30 kJ/mol to a low in the range of -5 to -0.8 kJ/mol. The greatest energy stabilization occurs in the step where a water molecule hydrogen bonds to the naked dihydrogen vanadate. The hydration effect on the dihydrogen vanadate energy diminishes as more water molecules are added to the system. The B3LYP calculated incremental Gibbs energies fluctuate in a “saw tooth” pattern. However, it is clear that the largest energy stabilization is again obtained when the first water molecule forms hydrogen bonds with to the dihydrogen vanadate. The general trend is as the number of water molecules increases, the Gibbs energy decreases but in a non-uniform fashion.

Both $\text{VO}(\text{OH})_4^-$ and $\text{VO}_2(\text{OH})_2(\text{H}_2\text{O})^-$ have been suggested as possible conformations for dihydrogen vanadate when it interacts with one water molecule [68]. The gas phase calculation for $\text{VO}_2(\text{OH})_2(\text{H}_2\text{O})^-$ showed that this structure tends to break into the $\text{H}_2\text{VO}_4^- \cdot \text{H}_2\text{O}$. This strongly suggests that the water molecule prefers to form hydrogen bonds with dihydrogen vanadate rather to coordinate directly to vanadium and act as ligand. The preliminary calculations for $\text{VO}(\text{OH})_4^-$ confirm that this structure is viable structure. The optimized structure of $\text{VO}(\text{OH})_4^-$ calculated by B3LYP/cc-pVTZ is shown in Figure 5.3.

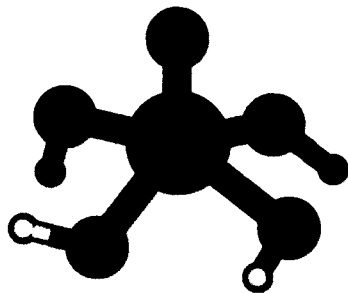


Figure 5.3. The B3LYP/cc-pVTZ Optimized Structure of $\text{VO}(\text{OH})_4^-$.

When the energy of $\text{VO}(\text{OH})_4^-$ was compared to that of $\text{H}_2\text{VO}_4^- \cdot \text{H}_2\text{O}$ (both energies were calculated by CCSD(T)/cc-pVTZ on the B3LYP/cc-pVTZ optimized structures) it was found to be 136 kJ/mol higher. This energy gap becomes even larger (146 kJ/mol) when the CCSD(T) energies are calculated under the aqueous PCM conditions. This large energy difference suggests that in an aqueous environment $\text{H}_2\text{VO}_4^- \cdot \text{H}_2\text{O}$ is more likely to exist than $\text{VO}(\text{OH})_4^-$.

Bond Lengths

One of the most significant properties that can be measured to quantify the effects of the hydration on a molecule is to determine changes in its bond lengths. In the dihydrogen vanadate case, water molecules prefer to form hydrogen bonds with the ligands rather than directly bond to the vanadium atom itself. Generally, the hydrogen bonds formed by the water molecules are evenly distributed between the oxo and the hydroxo groups of H_2VO_4^- . Figures 5.4 and 5.5 illustrate the effects of hydration on the $\text{V}=\text{O}$ (oxo ligand) and the $\text{V}-\text{O}$ (the hydroxo ligand) bond lengths, calculated using the MP2 and B3LYP methods, respectively. It should be noted that these two figures were

plotted with different $\text{H}_2\text{VO}_4^- \cdot \text{H}_2\text{O}$, $\text{H}_2\text{VO}_4^- \cdot 2\text{H}_2\text{O}$ and $\text{H}_2\text{VO}_4^- \cdot 3\text{H}_2\text{O}$ conformations as the two methods give different global minima.

When calculated at the B3LYP/6-31+G* theory, the average V=O bond length is slightly less than 1.65 Å, whereas at MP2/6-31+G* level is in the range of 1.65-1.70 Å. It is clear that the V-O bond length is more heavily influenced by hydration, which causes the bond length to change significantly. The MP2/6-31+G* is 1.80-1.95 Å and the B3LYP/6-31+G* range is between 1.80-1.90 Å. Both theories show a clear trend for the V-O bond length to decrease with increasing hydration. This shortening of the V-O bond is most likely a cooperative effect caused by coordination of the water molecules and the resulting hydrogen bond they form. The end result is also the weakening of the V=O bond. Figures 5.4 and 5.5 clearly show a trend for V=O bond length to increase with increasing hydration. This increase cannot be accounted for the hydrogen bonded water molecules as the expected trend would be a consistent bond shortening. Therefore, this increase most likely indicates that the hydroxo groups of dihydrogen vanadate participate in more, and are more influenced by hydrogen bonding than are the oxo groups.

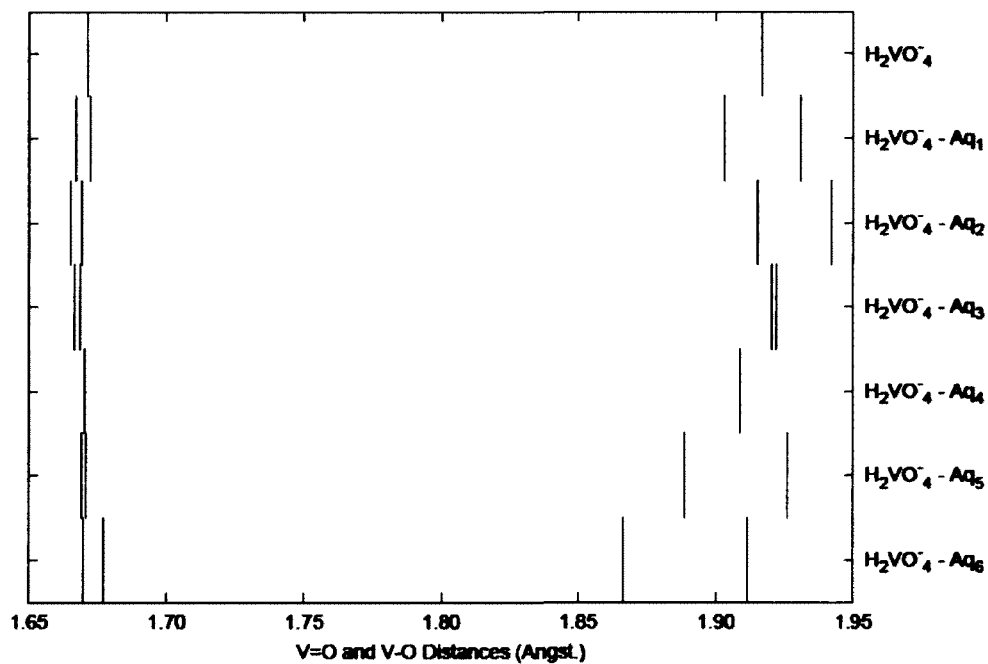


Figure 5.4. The V=O and V-O bond lengths calculated at the MP2/6-31+G* level for $\text{H}_2\text{VO}_4^- \cdot n\text{H}_2\text{O}$, with $n=0-6$.

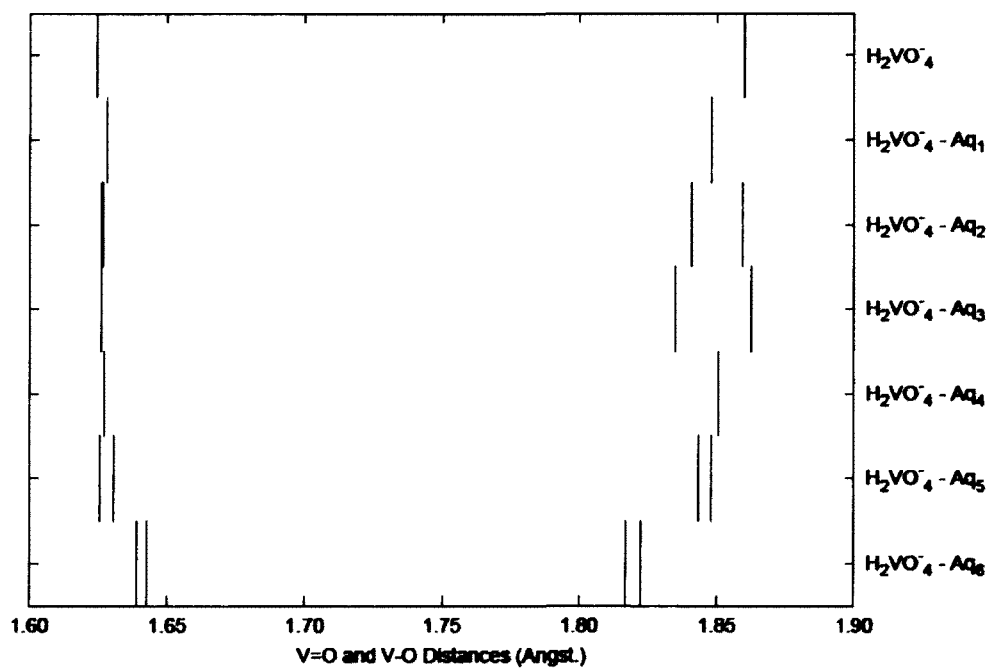


Figure 5.5. The V=O and V-O bond lengths calculated at the B3LYP/6-31+G* level for $\text{H}_2\text{VO}_4^- \cdot n\text{H}_2\text{O}$, with $n=0-6$.

Another important property of the system is the distance between the vanadium atom and the hydrating water molecules (V--O). This distance provides a raw estimate of the radius of a complete hydration sphere around H_2VO_4^- . This distance was calculated for the MP2/6-31+G* and B3LYP/6-31+G* optimized structures and is shown in Figures 5.6 and 5.7, respectively. The figures indicate that there are two V--O distance ranges observed independent of the choice of the calculation method. At the MP2/6-31+G* level (Figure 5.6), there is a series of V--O distances in 3.40-3.45 Å range and they can be assigned to the hydrating water molecules forming two hydrogen bonds with dihydrogen vanadate. The second cluster of the V--O distances has a much wider range, 3.60-3.90 Å. These water molecules make only be one hydrogen bond with dihydrogen vanadate. It can be seen in Figure 5.7, the B3LYP/6-31+G* calculations show that the water molecules with two hydrogen bonds to dihydrogen vanadate have the V--O distances in the range of 3.35-3.45 Å. The water molecules with one hydrogen bond belong to a second range of 3.65-3.95 Å. The real hydration sphere would not have any water molecules making two hydrogen bonds to dihydrogen vanadate because of the preference for water molecules to bond with each other. In summary, the calculations indicate that, the first hydration sphere radius will be in the range of 3.60-3.90 Å or 3.65-3.95 Å judging from the MP2/6-31+G* and the B3LYP/6-31+G* methods, respectively.

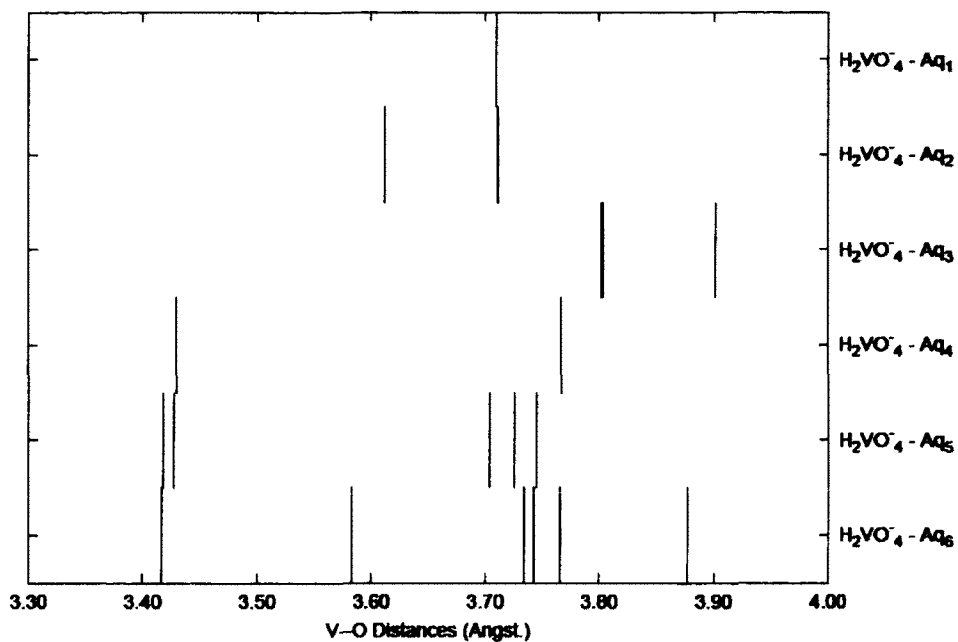


Figure 5.6. The V--O distances calculated at the MP2/6-31+G* level for $\text{H}_2\text{VO}_4^- \cdot n\text{H}_2\text{O}$, with $n=0-6$.

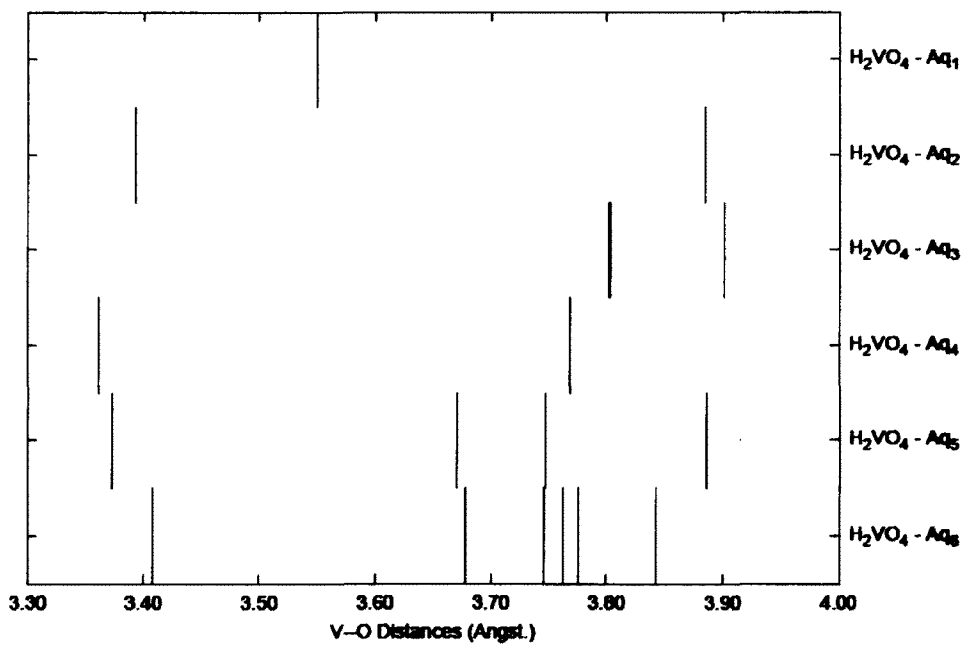


Figure 5.7. The V--O distances calculated at the B3LYP/6-31+G* level for $\text{H}_2\text{VO}_4^- \cdot n\text{H}_2\text{O}$, with $n=0-6$.

Vibrational Frequencies

Dihydrogen vanadate is a major mononuclear species of aqueous Vanadium (V) [7]. However, because of its aqueous nature and existence only at low concentrations it has not yet been possible to obtain any experimental vibrational spectra. The majority of the vanadate compounds that have been studied by spectroscopic methods are vanadate salts [71]. However, most of these salts have only anion part of vanadate and do not display the V-O bond stretching of dihydrogen vanadate. The electron correlation methods, MP2 and B3LYP were used to calculate the vibrational spectra of dihydrogen vanadate. As discussed before, using the MP2 and B3LYP methods predicted different global minima for the structures of $\text{H}_2\text{VO}_4^- \cdot \text{H}_2\text{O}$, $\text{H}_2\text{VO}_4^- \cdot 2\text{H}_2\text{O}$ and $\text{H}_2\text{VO}_4^- \cdot 3\text{H}_2\text{O}$. Since these global minima had very small energy differences, it was decided to use all minima for plotting the frequencies. These calculated frequencies are shown in Figures 5.8 and 5.9 for the MP2/6-31+G* and B3LYP/6-31+G* levels, respectively.

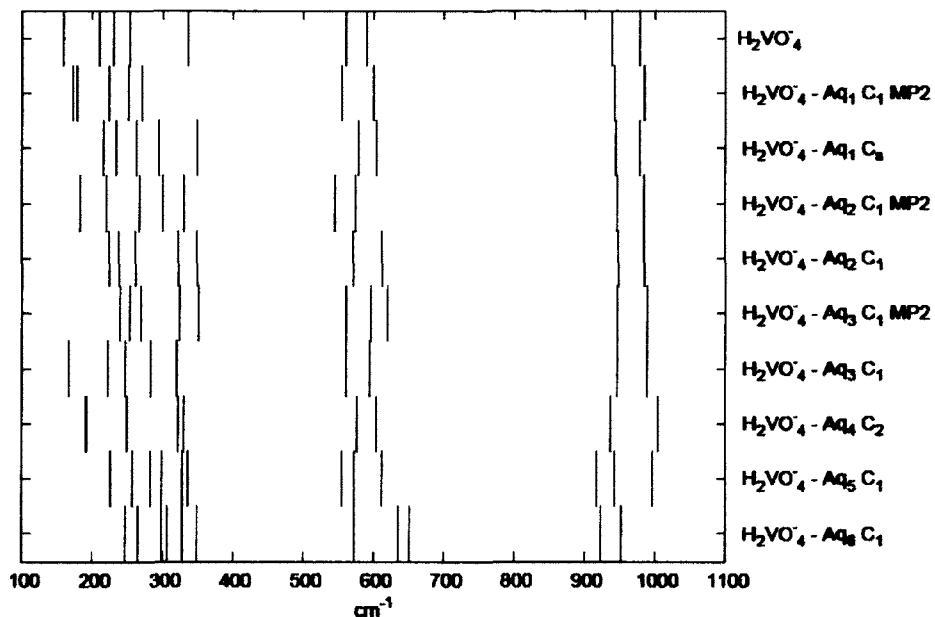


Figure 5.8. Vibrational frequencies calculated at the MP2/6-31+G* level for $\text{H}_2\text{VO}_4^- \cdot n\text{H}_2\text{O}$, with $n=0-6$.

There are three different visible frequency groups in these Figures (in increasing order of wavenumber, one deformation mode and two stretching (V-O and V=O) modes. The deformation mode ranges from 150-350 cm^{-1} or 170-400 cm^{-1} for the MP2 and B3LYP calculations, respectively. The V-O stretching mode lies in the range of 650-750 cm^{-1} or 550-700 cm^{-1} for MP2 and B3LYP respectively. The deformation and V-O stretching modes both show a clear trend of increasing frequency as the number of water molecules increases. This finding is consistent with the V-O bond length trend, discussed earlier, and confirms that upon hydration the V-O bond is strengthened. The V=O stretching modes range from 900-1000 cm^{-1} or 950-1050 cm^{-1} for the MP2 and B3LYP theory levels, respectively. The MP2 results show a small V=O frequency decrease as the number of water molecules increases, whereas, at the B3LYP level this trend is less obvious because the stretching modes are split by the presence of the water

molecules. However, close inspection shows that there actually is a slight decrease in wavenumber.

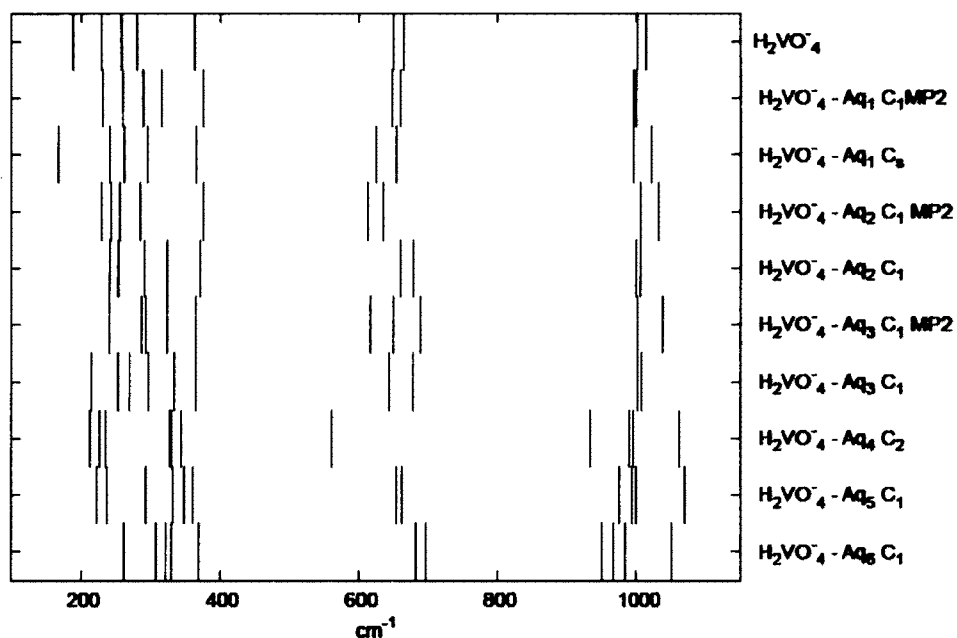


Figure 5.9. Vibrational frequencies calculated at the B3LYP/6-31+G* level for $\text{H}_2\text{VO}_4^- \cdot n\text{H}_2\text{O}$, with $n=0-6$.

Charges

NBO calculations using B3LYP/6-31+G* were performed for $\text{H}_2\text{VO}_4^- \cdot n\text{H}_2\text{O}$, with $n=0-6$ in both the gas phase and in the aqueous PCM model. The NBO charge calculation in the PCM model helps to give a better understanding of the effect of hydration on the vanadium electron density. These results are summarized in Table 5.3

Table 5.3. NBO vanadium charges in gas/PCM phase calculated at the B3LYP/6-31+G* level for $\text{H}_2\text{VO}_4^- \cdot n\text{H}_2\text{O}$, with $n= 0-6$.

Name of Complex	Gas Phase Charge	PCM Charge	The Charge Difference (PCM-Gas Phase)
H_2VO_4^-	1.515	1.524	0.009
$\text{H}_2\text{VO}_4^- \cdot \text{H}_2\text{O}$	1.529	1.542	0.012
$\text{H}_2\text{VO}_4^- \cdot 2\text{H}_2\text{O}$	1.524	1.549	0.025
$\text{H}_2\text{VO}_4^- \cdot 3\text{H}_2\text{O}$	1.536	1.561	0.025
$\text{H}_2\text{VO}_4^- \cdot 4\text{H}_2\text{O}$	1.531	1.532	0.001
$\text{H}_2\text{VO}_4^- \cdot 5\text{H}_2\text{O}$	1.540	1.547	0.007
$\text{H}_2\text{VO}_4^- \cdot 6\text{H}_2\text{O}$	1.557	1.566	0.009

Table 5.3 shows that the calculated charges have converged for all the dihydrogen vanadates in both the gas phase and in the PCM calculations. The gas phase charges fluctuate over a very small range of 0.032; the PCM charges also show very small variation, 0.042. The computed charge difference of these methods is so negligible and relatively constant that no trend could be drawn except that dihydrogen vanadates are very stable species. Hydration of dihydrogen vanadate does not influence the electron density of the vanadium atom.

Conclusion

The hydrated species of vanadic acid $\text{H}_2\text{VO}_4^- \cdot n\text{H}_2\text{O}$, with $n= 0-6$ were studied by *ab initio* methods. The effects of hydration on bond lengths, atomic distances, vibrational frequencies and vanadium charge were investigated. Water molecules tend to form hydrogen bonds to the both ligands (hydroxo and oxo) of dihydrogen vanadate in a uniform fashion. This leads to significant V-O bond strengthening and increase of its vibrational frequencies. The deformation modes are observed at $150-400 \text{ cm}^{-1}$ and

the stretching modes from 500-800 cm^{-1} . As the hydration level was increased, the strengthening of the V-O bond also forced the V=O bond to become slightly weaker.

The vanadium to oxygen of water molecules distance calculations indicated that all water molecules tend to be in the range of 3.4 to 3.9 Å from vanadium. Therefore, the proposed hydration sphere radius of a tetra coordinate dihydrogen vanadate would be in the range of 3.4-3.9 Å. The NBO charge study showed that the water molecules do not influence the charge on vanadium. The charge is independent of method as both the gas phase and the PCM calculations produced the same results; the vanadium charge was almost constant in all complexes.

To complete this work, dihydrogen vanadate should be studied with a complete hydration sphere. Completing the hydration shell will affect the V-O and V=O lengths and their vibrational frequencies. Also, the V--O distance study would then reveal the true hydration sphere radius. However, building the complete hydration shell is a very complicated task because of the multiple minima issue.

Chapter VI: The H_2VO_4^- to VO_2^+ Conversion

Introduction

The low concentration mononuclear vanadate species present in aqueous solution go through various pH-dependent conversion reactions [1, 2, 5]. Most of these reactions are simple protonation reactions of the various anionic vanadates to form more neutral species. The protonation steps from vanadate to dihydrogen vanadate are well known and have very trivial mechanisms. However, the protonation of dihydrogen vanadate is not well understood because the nature of the aqueous chemistry of dihydrogen vanadate is ambiguous. Most of the experimental works that have been done on the vanadate reaction has been based on electrochemical methods which can only provide pK_a values with no structural information [62-65].

Some researchers think that the coordination of vanadium in dihydrogen vanadate is five rather than the conventionally accepted four once the pH is lowered from the 12-13 range to 7-8 [68]. Harnung has suggested that the penta coordinate dihydrogen vanadate would then be the form of $\text{VO}_2(\text{OH})_2\text{H}_2\text{O}^-$ and it would have been formed as the result of a water ligand binding to the conventional H_2VO_4^- . His experimental results of ^{51}V NMR on dihydrogen vanadate-based organic molecules indicated that H_4VO_5^- is the stable aqueous form of dihydrogen vanadate. Harnung has suggested also that coordination of an additional water ligand weakens the strength of the oxo acids of transition metals [72]. Based on this theory, he stated that the observed acidity constant of aqueous dihydrogen vanadate should be closer to that of the H_4VO_5^- value than below the H_2VO_4^- value [68].

The oxovanadyl cation, VO_2^+ , is traditionally considered to be hexa coordinate in aqueous media, existing in the form of $\text{VO}_2(\text{H}_2\text{O})_4^+$ [2, 5]. However, a recent *ab initio* molecular dynamics study of $\text{VO}_2(\text{H}_2\text{O})_4^+$ has shown that this structure tends to lose one of its water ligands to form a penta coordinate oxovanadyl cation with a hydrogen bonded water molecule $\text{VO}_2(\text{H}_2\text{O})_3^+\cdot\text{H}_2\text{O}$ as shown in Figure 3.3 on page 32 [55]. The energies calculated using DFT at the levels BP86/I, BLYP/I, B3LYP/I+ showed that the $\text{VO}_2(\text{H}_2\text{O})_3^+\cdot\text{H}_2\text{O}$ energy was constantly lower than $\text{VO}_2(\text{H}_2\text{O})_4^+$ by 4.0 to 4.8 kcal/mol. Another research group performed a CPMD simulation (300K) on $\text{VO}_2(\text{H}_2\text{O})_4^+$ with 28 included water molecules [6]. The simulation confirmed that VO_2^+ prefers to have a coordination of five rather than the conventional six. By the end of the simulation, at the 11 ps mark, the oxovanadyl cation had been converted to the dihydrogen vanadate anion. Interestingly, the authors did not attempt to simulate the reverse of the studied reaction to see if VO_2^+ can be obtained from H_2VO_4^- . Another research group using a DFT method (B3LYP/QZ4P) showed that the $\text{VO}_2(\text{H}_2\text{O})_3^+$ structure was not stable at high temperatures and rapidly decomposed to vanadic acid H_3VO_4 [29].

The objective of the current research was to discover the exact mechanism of the conversion of dihydrogen vanadate to the oxovanadyl cation. Special attention was paid to changes of the coordination chemistry of the vanadium species. As stated before, dihydrogen vanadate is considered to have a tetra or penta coordinate chemistry and the oxovanadyl cation to be five or six coordinate [2, 5, 55, 67]. The main electronic structure method used in this part of the project was the B3LYP DFT method.

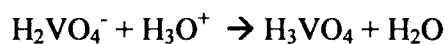
This theory provides reasonable electron correlation at relatively inexpensive computational cost [33, 36]. The aqueous PCM solvation model was used to simulate the implicit water effect on the solvates.

Mechanistic studies are the best carried out using molecular simulations as it allows the reactions to be studied in “real time” and gives information about the dynamic stability of compounds [33, 35]. However due to a lack of expertise in this field only very simple systems could be studied by CPMD simulations as reported herein. The functional and pseudopotential chosen for this project were respectively, BLYP and Goedecker. BLYP is a DFT functional and it is fairly well integrated into the CPMD conditions. A pseudopotential file for each element represents its electron core, motion-related properties [73]. This simplification allows the program to focus on the valence electrons during the molecular simulations. The Goedecker pseudopotential is commonly used for metals because unlike other pseudopotentials, it does not produce any “ghost” states [51]. A microcanonical simulation was performed using CPMD. The microcanonical or the NVE ensemble has the following fixed parameters: the number of atoms (N), the volume of the simulation cell (V) and the total energy of the system (E) [33, 35].

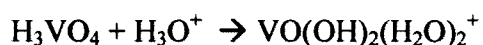
Results and Discussions

The VO_2^+ cation can be obtained from dihydrogen vanadate, H_2VO_4^- , via least two different mechanisms. The first proposed mechanism suggests that vanadic acid is involved in the reaction. This is slightly problematic in that vanadic acid is a proposed

minor component in the aqueous chemistry of Vanadium (V). The outline of the first mechanism consists of the following steps:

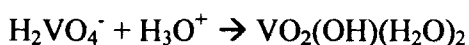


followed by a second protonation, and coordination of water

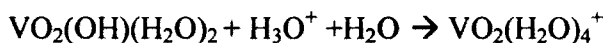
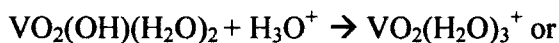


Hydrogen transfer occurs between the two hydroxo ligands of the vanadic acid cation, $\text{VO}(\text{OH})_2(\text{H}_2\text{O})_2^+$, to form $\text{VO}_2(\text{H}_2\text{O})_3^+$. A water molecule might possibly also bind to $\text{VO}_2(\text{H}_2\text{O})_3^+$ to form the hexa coordinate cation $\text{VO}_2(\text{H}_2\text{O})_4^+$.

The second proposed mechanism bypasses the formation of vanadic acid, suggesting that the formation of the oxovanadyl cation, VO_2^+ , occurs by double protonation of dihydrogen vanadate. The outline of the second proposed mechanism has the following protonation steps:



followed by,



DFT computational methods were utilized to study these mechanisms to try and determine which (if either) is the more probable.

Mechanism I: Vanadic Acid Cation

The first proposed mechanism assumes that vanadic acid is the predominant product of the protonation of dihydrogen vanadate. This assumption shifts the focus to a smaller scale issue – the conversion of H_3VO_4 to $\text{VO}_2(\text{H}_2\text{O})_3^+$. It was established in Chapter III, that the $\text{VO}_2(\text{H}_2\text{O})_3^+\cdot\text{H}_2\text{O}$ is more stable than $\text{VO}_2(\text{H}_2\text{O})_4^+$. Hence, $\text{VO}_2(\text{H}_2\text{O})_3^+$ was chosen as the more likely reaction product. The proposed reaction pathway is shown in Figure 6.1. The geometries of all the reactants and products were optimized at the B3LYP/cc-pVTZ theory level.

To explain the low abundance of aqueous vanadic acid, it must instantaneously be converted to other vanadate species. The first step of this reaction would be the protonation of vanadic acid to form the vanadic acid cation, $\text{VO}(\text{OH})_2(\text{H}_2\text{O})_2^+$, (shown as *(A)* in the Figure 6.1). This species was proposed because of the unique increasing coordination behaviour of vanadic acid and with increasing numbers of water molecules (true for mono and dihydrates) as observed in Chapter IV. The calculation at the B3LYP/cc-pVTZ level indicates that the formation of *(A)* is highly energetically favourable by ~340 kJ/mol.

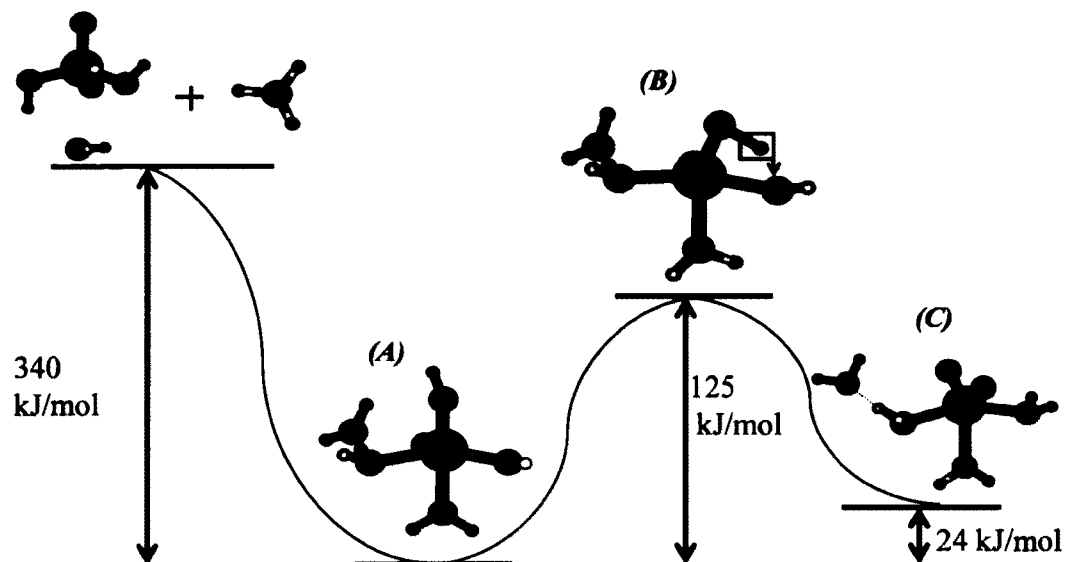


Figure 6.1. The proposed reaction pathway (mechanism I) for the formation of the oxovanadyl cation by protonation of vanadic acid.

The next step after the formation of (A) is its transformation to $\text{VO}_2(\text{H}_2\text{O})_3^+$ (structure (C) in Figure 6.1). For this conversion to occur a hydrogen atom must be transferred from one hydroxo group to the other hydroxo group forming a water ligand. It is highly unlikely that this transformation occurs in a single step, without formation of a transition structure. The optimized geometry of the proposed transition structure is shown as (B) in Figure 6.1. This transition state (B) is a first degree saddle point where one hydrogen atom of a hydroxo group wants to transfer to an oxygen atom of the second hydroxo group. The hydrogen transfer objective of (B) is represented by the boxed hydrogen atom which is about to be transferred to its neighbouring oxygen atom to form a water ligand. Vibrational analysis of (B) showed the presence of an intense imaginary frequency at -1600 cm^{-1} which represents the intention of the boxed

hydrogen to migrate to the closest oxygen. Upon the successful hydrogen transfer, the structure **(B)** transforms $\text{VO}_2(\text{H}_2\text{O})_3^+$ (the **(C)** structure).

An energy study of this reaction showed that this proposed mechanism is not energetically favourable. The energies of the three structures (**(A)**), **(B)** and **(C)**) were calculated at the B3LYP/cc-pVTZ theory level which gives highly accurate energies. The gas phase energy differences are included in Figure 6.1. The activation energy of the reaction was calculated to be ~125 kJ/mol. The overall enthalpy of reaction ΔH is +24 kJ/mol making it endothermic. However, in reality this reaction takes place in aqueous media and it is known to be dependent only on the pH of the solution. To emulate the aqueous environment, the reaction energetics were recalculated at the B3LYP/cc-pVTZ level under the aqueous PCM conditions to study hydration effects. The activation energy of the reaction decreased to 108 kJ/mol and the overall enthalpy of the reaction decreased to only +10 kJ/mol suggesting that the reaction is more likely to proceed in the aqueous environment.

The proposed reaction route for mechanism I involves the formation of a very stable intermediate product in the form of $\text{VO}(\text{OH})_2(\text{H}_2\text{O})_2^+$. The energy calculation indicates that this cationic structure is likely to be formed as the product of the protonation of vanadic acid. However, no aqueous structures similar to this vanadic acid cation have been reported before. This proposed mechanism thus has no experimental evidence to support it. The biggest flaw of this mechanism was making the assumption that vanadic acid exists in aqueous solution [7]. Its presence has never been directly observed in an aqueous environment even if it is considered a minor

component in the aqueous speciation of Vanadium (V). pK_a studies have revealed that the pK_a value of vanadic acid (3.1-3.7 depending on the source) is lower than that of the more acidic oxovanadyl cation (3.8) [58-60]. These pK_a values strongly suggest that the protonation of dihydrogen vanadate bypasses the formation of vanadic acid.

Mechanism II : Direct Double Protonation of Dihydrogen Vanadate

The formation of the oxovanadyl cation directly from dihydrogen vanadate can be achieved by two consecutive protonations of the hydroxo ligands and hydration of dihydrogen vanadate. The reaction pathway of this proposed mechanism is shown in Figure 6.2. The results from Chapter V indicate that gas phase hydrated dihydrogen vanadate compounds are always tetra coordinate species. This means that an increase of the coordination number of vanadium would take place during/after each protonation step. The product of the first protonation step would form the penta coordinate structure, $VO_2(OH)(H_2O)_2$ (shown as {A} structure in Figure 6.2):



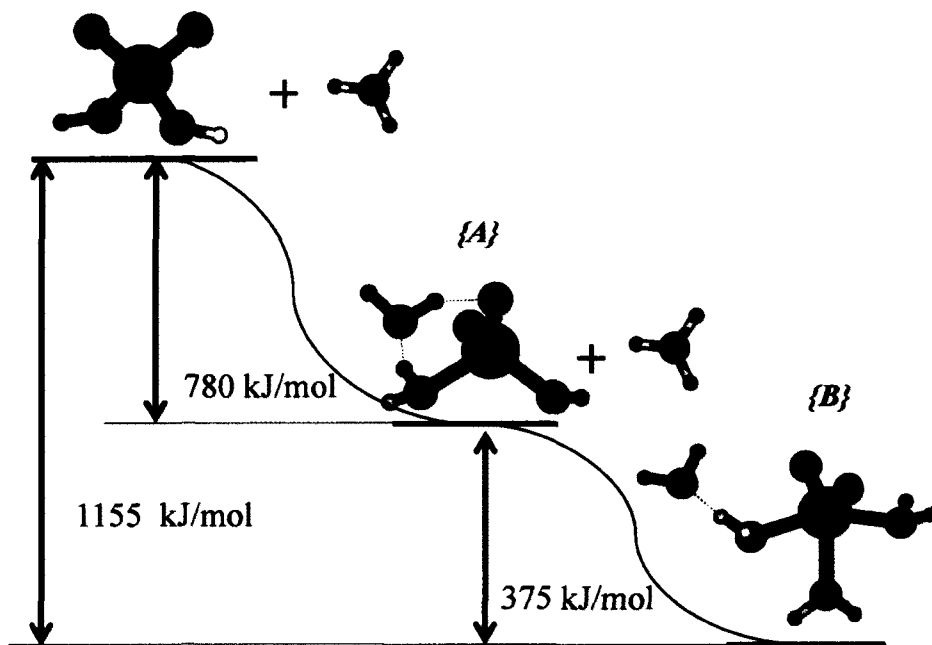


Figure 6.2. The proposed reaction pathway mechanism II for the formation of the oxovanadyl cation by the double protonations of dihydrogen vanadate.

{A} structure is significantly lower than its reactants, dihydrogen vanadate and the hydronium ion. The calculated enthalpy of the reaction is -780 kJ/mol at the B3LYP/cc-pVTZ theory level. The second protonation step, for the neutral species $\text{VO}_2(\text{OH})(\text{H}_2\text{O})_2$, leads to the formation of $\text{VO}_2(\text{H}_2\text{O})_3^+\cdot\text{H}_2\text{O}$ (*{B}*) in Figure 6.2). The calculated enthalpy of the second protonation step again indicates that the product is energetically favoured (-375 kJ/mol). The overall energetic of the complete reaction is -1150 kJ/mol. Interestingly, the energy of the neutral structure *{A}* is 60 kJ/mol higher than its stoichiometric equivalent, the vanadic acid monohydrate, $\text{H}_3\text{VO}_4\cdot\text{H}_2\text{O}$. This energy difference suggests that in the gas phase the protonation of dihydrogen vanadate will form the vanadic acid monohydrate $\text{H}_3\text{VO}_4\cdot\text{H}_2\text{O}$.

Mechanism II: The CPMD Attempt

A study of the conversion of dihydrogen vanadate to the oxovanadyl cation using CPMD was attempted. The gas phase CPMD simulation was set to room temperature using the Nose-Hover thermostat. First, vanadic acid was formed by introducing a single hydronium ion to dihydrogen vanadate. It was found that if the hydronium ion closely approached to the hydroxo ligand on the complex it would transfer a hydrogen atom to that ligand forming a coordinated water ligand. However this $\text{VO}_2(\text{OH})(\text{H}_2\text{O})$ intermediate quickly evolved to the traditional vanadic acid structure with a water molecule hydrogen bonded to one of its hydroxo ligands. Once a second hydronium ion comes to contact with the vanadic acid it forms the tetra coordinated species $\text{VO}(\text{OH})_2(\text{H}_2\text{O})$, with two hydrogen bonded water molecules. In the CPMD simulation carried out in this work, a water molecule was observed to form a hydrogen bond to a ligand instead of binding directly to the vanadium atom. This CPMD result is similar to the proposed mechanism I, as both methods predict the formation of a highly stable vanadic cation. The BLYP calculations with the Goedecker pseudopotential show the preference for vanadic acid to exist as the tetra coordinate species.

The Solvation Effect

The aqueous PCM results, just discussed, suggest that the enthalpy change of a reaction can be narrowed by adding water molecules explicitly. The issue then becomes that it is relatively easy to build a large hydrated dihydrogen vanadate complex but it is extremely difficult to find its global minimum. Due to the time constraints, it was

decided that the best approach would be to find a hydrated local minimum for dihydrogen vanadate and then observe the protonation reaction in under these conditions. The starting point was the optimized six water hydrated dihydrogen vanadate structure $\text{H}_2\text{VO}_4^- \cdot 6\text{H}_2\text{O}$ shown in Figure 5.2 on page 61. The hydration level was enlarged by adding three or four water molecules at a time and the resulting assembly was optimized using, a trivial theory level, HF/3-21G. Upon completion of each phase more water molecules were added and the process was repeated. Once the number of water molecules exceeded twenty, an unusual transformation was observed to occur to dihydrogen vanadate – **a water molecule became a ligand (and giving), a penta coordinate species.** The B3LYP/6-31+G* optimized assembly of the penta coordinate dihydrogen vanadate with 24 waters, $\text{H}_4\text{VO}_5^- \cdot 24\text{H}_2\text{O}$ <A> is shown in Figure 6.3. The distance of the oxygen in the water ligand to vanadium is 2.385 Å which is close to the related distance in the hydrated oxovanadyl cation to its water ligands. This penta coordinate species of dihydrogen vanadate was first proposed by Harnung where it was used to better explain his experimental results [68].

Another important question that needed to be addressed was how stable is this penta coordinate structure in comparison with tetra coordinated dihydrogen vanadate? As the first step, the hydration effect was studied by removing all the water molecules from the complex and leaving only the naked penta coordinate H_4VO_5^- . Interestingly, when this naked structure was optimized using the B3LYP/6-31+G* theory level, the water ligand dissociated and formed two hydrogen bonds with oxo groups. The final structure obtained was identical to the $\text{H}_2\text{VO}_4^- \cdot \text{H}_2\text{O}$ structure reported in Chapter V.

Therefore to keep the molecule intact, single point calculations of the naked H_4VO_5^- and $\text{H}_2\text{VO}_4^- \cdot \text{H}_2\text{O}$ were performed using the B3LYP/ccpVTZ method to compare their energies. The energy difference between these complexes showed that $\text{H}_2\text{VO}_4^- \cdot \text{H}_2\text{O}$ is significantly more stable, by 124 kJ/mol, than the naked H_4VO_5^- . In addition, the results indicate that implicit PCM solvation decreases the energy gap to 73 kJ/mol.

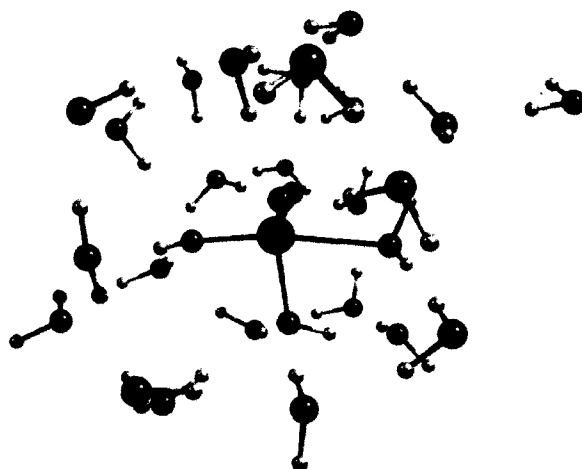


Figure 6.3. The B3LYP/6-31+G* optimized structure of $\text{H}_4\text{VO}_5^- \cdot 24\text{H}_2\text{O}$ <A> .

A first principle molecular dynamics method CPMD calculated for structure <A> was performed with a periodic boundary box condition, to emulate an aqueous solution, using BLYP theory level with the Goedecker pseudopotentials. The goal was to observe the stability of structure <A> is in a dynamic aqueous environment. As soon as the simulation started, the water ligand dissociated and became part of the water cluster, which led to the formation of the traditional tetra coordinate dihydrogen vanadate. However, difficulties were occurred when the water molecules began to behave in a very odd fashion - they preferred to form water walls and to leave parts of

the dihydrogen vanadate unhydrated. It was almost as if water molecules were trying to escape the dihydrogen vanadate. Due to the lack of expertise with the CPMD software, this issue could not be resolved and physically meaningful simulations of the explicitly hydrated dihydrogen vanadate were never obtained.

An explicitly hydrated tetra coordinate dihydrogen vanadate structure was still needed to compare its energy with that of $\langle A \rangle$. Structure $\langle B \rangle$ similar to $\langle A \rangle$ was built by pulling the water ligand of $\langle A \rangle$ away from the vanadium atom. Structure $\langle B \rangle$ was optimized using B3LYP/6-31+G* and shown in is Figure 6.4. The vanadium oxygen distance for the “pulled” water molecule distance was 2.95 Å. This large distance ensured that the bond had been broken.

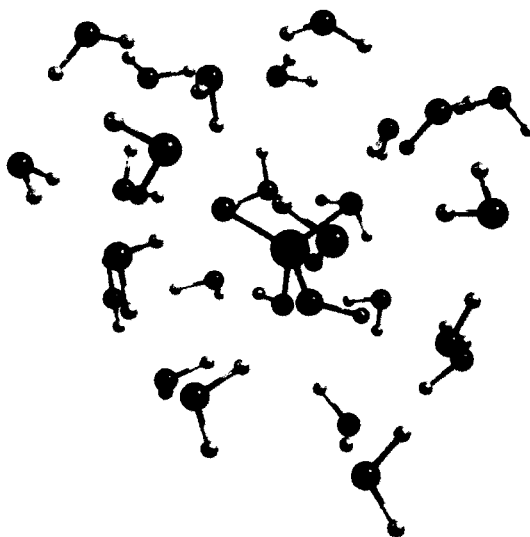


Figure 6.4. The B3LYP/6-31+G* Optimized Structure of $\text{H}_2\text{VO}_4^{2-} \cdot 25\text{H}_2\text{O}$ $\langle B \rangle$.

When the energy difference between $\langle A \rangle$ and $\langle B \rangle$ was compared, it was found that $\langle B \rangle$ was only ~30 kJ/mol more stable than $\langle A \rangle$. The aqueous PCM condition did

not change this energy gap much (~26 kJ/mol) because the explicitly added hydration sphere molecules have created a complete aqueous continuum. To increase the level of solvation models of tetra and penta coordinate dihydrogen vanadate with 34 water molecules were built and optimized by B3LYP/6-31+G*. The structures of these complexes are shown in Figure D of Appendix. The energy gap of the two showed that the new tetra coordinate H_2VO_4^- was more stable than its penta coordinate analog by only 3.3 kJ/mol. However, in the aqueous PCM condition this energy gap becomes larger (to ~32 kJ/mol). It should be noted that, the energy gaps calculated were between **two local minima** (not necessarily two global minima), hence these energy values should not be considered as being very accurate. It would be more interesting to compare **the global minima** of these dihydrogen vanadate structures in a heavily solvated environment, to obtain the quantitative results. However, it is still clear that the energy gap between these two isomers of dihydrogen vanadate is very small and that both of these structures could exist in aqueous solution. There is a clear trend that the overall energy gap decreases of for both the four and five coordinate dihydrogen vanadate species as more water molecules are added to solvate them.

The protonation of dihydrogen vanadate forms a short-lived neutral species which quickly transforms into the oxovanadyl cation. There are four possible sites on dihydrogen vanadate which could be attacked by the hydronium ion. Two of these sites are the oxo ligands and the other two are oxygen atoms of hydroxo ligands. The site of the initial protonation is most likely to be highly electronegative. The NBO charges using the B3LYP/cc-pVTZ method were calculated on the tetra and penta coordinate

dihydrogen vanadates. The NBO results are shown in Figure 6.5. The calculated charges on the oxygen atoms of the hydroxo groups were more negative than those of the oxo by ~ 0.27 for both the tetra and penta dihydrovanadates. This means that the more electronegative oxygen atoms of the hydroxo ligands are the most likely to be targeted by the hydronium ion. The energy study of the mechanism II showed that vanadic acid monohydrate is the energetically favourable product than structure $\{A\}$ (Figure 6.2). However, the NBO calculations suggest that the first protonation is likely to occur at a hydroxo ligand to form the $\{A\}$ structure. In the gas phase, $\{A\}$ likely rearranges to the give vanadic acid monohydrate. In aqueous solution, this hydrogen rearrangement is less to occur because of the multiple hydrogen bonds formed around the dihydrogen vanadate species. The hydrogen bonded network possibly restricts the hydrogen transfer and leave the oxo ligands intact.

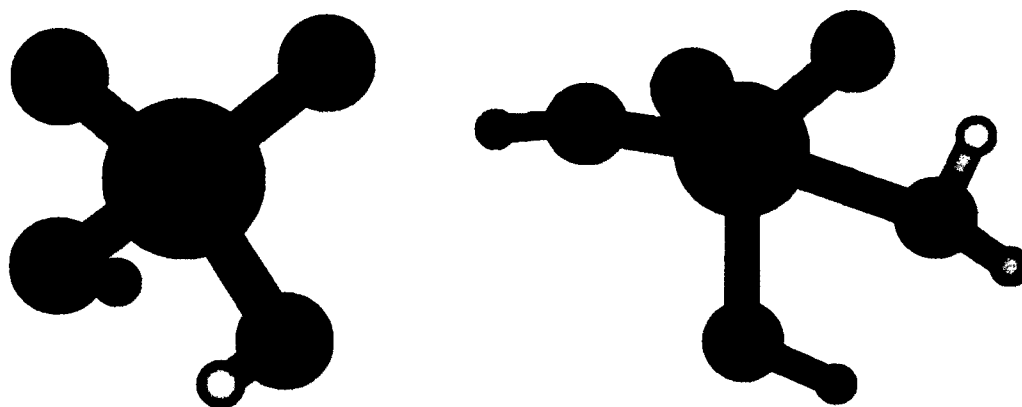


Figure 6.5. The NBO charges of the vanadium atom and oxygens of H_2VO_4^- and H_4VO_5^- .

The existence of five coordinate dihydrogen vanadate better explains the lack of experimental evidence of the existence of aqueous vanadic acid. Although there is practically no evidence for the neutral aqueous mononuclear Vanadium (V) species, the question is to which hydroxo ligand will the hydronium cation bind to form a neutral $\text{VO}_2\text{OH}(\text{H}_2\text{O})_2$ $\langle C \rangle$ (Figure 6.2). The order is important because each new water ligand will affect the geometry of the neutral species before forming the oxovanadyl cation VO_2^+ . There are only two possible binding sites to form $\langle C \rangle$ axial ($\langle C1 \rangle$ in Figure 6.6) or equatorial ($\langle C2 \rangle$ Figure 6.6). The newly formed water ligands are boxed in Figure 6.6.

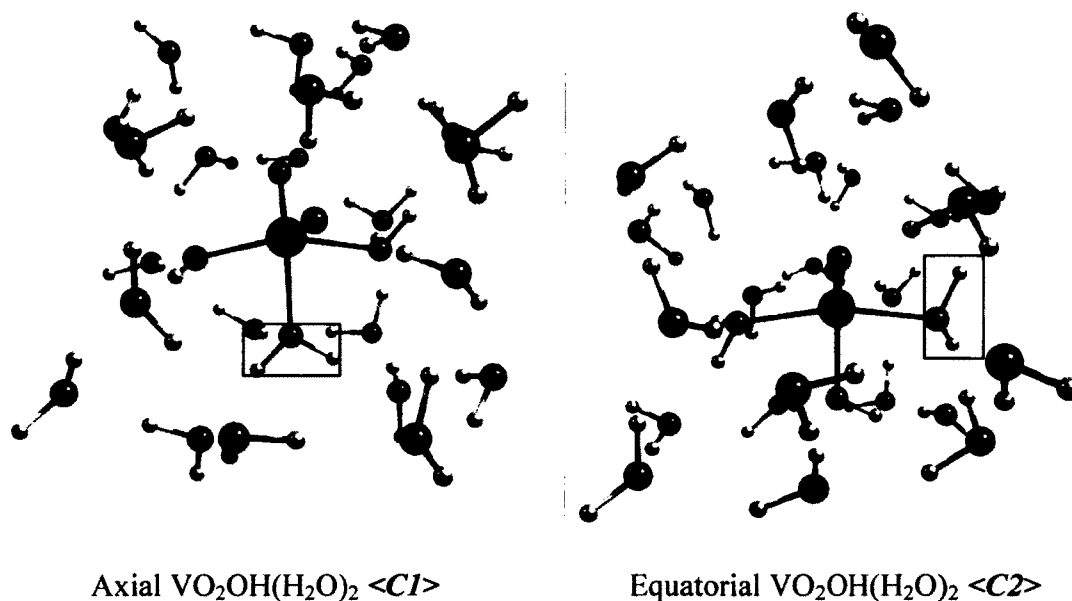


Figure 6.6. The B3LYP/6-31+G* optimized structures of two possible hydrated $\text{VO}_2\text{OH}(\text{H}_2\text{O})_2$ conformations in $\text{H}_5\text{VO}_5 \cdot 24\text{H}_2\text{O}$.

Molecular modeling could be used to calculate the formation energies of these two isomers. The addition of H^+ to $\langle A \rangle$ increases the overall energy of the complex,

but the added H^+ ion by itself does not have any associated energy as it has no electrons. The protonation step energy calculation should involve an energy comparison between $\langle A \rangle$ and H_3O^+ and their neutral product. However, due to time constraints this calculation was never carried out.

The energy difference between the $\langle C1 \rangle$ and $\langle C2 \rangle$ structures was only 22 kJ/mol in favour of $\langle C1 \rangle$. The PCM calculated energy difference of these structures was almost the same as that calculated in the gas phase and it was 26 kJ/mol in favour of $\langle C1 \rangle$. The NBO charge study of the “naked” penta coordinate dihydrogen vanadate results indicates that the axial oxygen is slightly more electronegative than the equatorial. Therefore, $\langle C1 \rangle$ is slightly more likely to be the intermediate to the formation of VO_2^+ . However, due to the small energy differences between these two structures $\langle C2 \rangle$ cannot be excluded as a viable intermediate structure.

The $\langle C1 \rangle$ structure has one unusual property – its newly formed water ligand is slightly distorted from its axial position. Once all of the water molecules of $\langle C1 \rangle$ were manually removed, the structure of the penta coordinate species H_5VO_5 became easier to study. The image of this structure is shown in Figure 6.7.

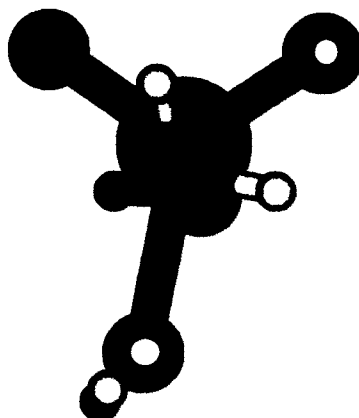


Figure 6.7. The structure of H_5VO_5 from $\langle C1 \rangle$ with all of the water molecules removed.

The angle O-V-O (the oxygens involved are circled in Figure 6.7) in naked H_5VO_5 was calculated to be 133° . A preliminary calculation of this intermediate surrounded by 33 water molecules showed this angle widening even further to 152° . This happens because the hydrogen atoms of the axially located water molecule are eager to form hydrogen bonds with water molecules of the first hydration sphere. This hydration effect leads to the possibility that the coordination of H_5VO_5 could increase from five to six. Widening this angle creates the space for water molecule to approach close enough to become the sixth ligand.

The last step of the reaction sequence is trivial, protonation to form of VO_2^+ from $\langle C1 \rangle$ or $\langle C2 \rangle$. The protonation and addition of a water molecule to $\langle C1 \rangle$ will lead to the formation of hexa coordinate $VO_2(H_2O)_4^+$. Since calculation showed that $\langle C1 \rangle$ is only slightly more stable than $\langle C2 \rangle$, the existence of $\langle C2 \rangle$ cannot be ruled out. Based on the hydration effect on the axial water molecule of $\langle C1 \rangle$, it is predicted

that the protonation of $\langle C2 \rangle$ will form a short-lived species $\text{VO}_2(\text{H}_2\text{O})_3^+$. The new axial water ligand of the penta coordinate oxovanadyl cation will form hydrogen bonds with water molecules from the hydration shell. These newly formed hydrogen bonds will result in the water ligand tilting away from its axial position, similar to the $\langle C1 \rangle$ situation. This in turn, will create the room for another water molecule to come in to form hexa coordinate $\text{VO}_2(\text{H}_2\text{O})_4^+$. Therefore, the final structure obtained $\text{VO}_2(\text{H}_2\text{O})_4^+$, is independent of the nature of its intermediate. Since the neutral mononuclear vanadium species has never been observed experimentally, the protonation reactions must happen almost simultaneously. This is the only way one can explain why dihydrogen vanadate converts directly to VO_2^+ in acidic solution.

Conclusion

The mechanism for the conversion of H_2VO_4^- to VO_2^+ was studied using *ab initio* computational methods. Two mechanisms were proposed, I with vanadic acid as the intermediate and II without vanadic acid. Calculations showed that for the conversion to occur, the vanadic acid cation could be the intermediate. The energy of the cationic form of vanadic acid was found to be too stable to form VO_2^+ and there is no available experimental evidence. This energy conflict, along with the fact that vanadic acid is only a minor component of aqueous Vanadium (V) chemistry, and this indicates that the mechanism I to be highly improbable. The second mechanism proposed involved the double protonation of dihydrogen vanadate to form the oxovanadyl cation. Energetically, this reaction was found more likely to occur, with the only issue being that the energy of the neutral intermediate was in fact higher than that

of vanadic acid. A local minimum of dihydrogen vanadate hydrated with 25 water molecules was constructed and it led to the formation of a penta coordinate dihydrogen vanadate water complex. Once the existence of the penta coordinate dihydrogen vanadate had been proven it was trivial to show that it will go through two protonation steps to form $\text{VO}_2(\text{H}_2\text{O})_4^+$. The protonation sites are most likely be the hydroxo ligands because they are slightly more electronegative than the oxo coordinated ligands. Possible expansion of the coordination number of vanadium in the aqueous oxovanadyl cation, from five to six, was observed. Protonation of the axially located hydroxo ligand and its subsequent tilting due to hydrogen bonding are the key to the expansion of the coordination number of the aqueous oxovanadyl cation.

References

- [1] Rehder, D. *Inorg Chem Comm.* **2003**, *6*, 604.
- [2] Cotton, F. A.; Wilkinson, G.; Murillo, C.A.; and Bochmann, M. *Advanced Inorganic Chemistry 6-th edition*. Wiley: Toronto, Canada, 1999.
- [3] Pyrzynska, K.; Wierzbicki, T. *Talanta.* **2004**, *64*, 823.
- [4] Srivastava, A. K.; Mehdi, M. Z. *Diabetic Medicine.* **2004**, *22*, 2.
- [5] Richens, D. *The Chemistry of Aqua ions: Synthesis, Structure, and Reactivity: A Tour through the Periodic Table of the Elements*; Wiley: Chichester, U.K., 1997.
- [6] Sadoc, A.; Messaoudi, S.; Furet, E.; Gautier, R.; Le Fur, E; Polles, L. amd Pivan, J-Y. *Inorg. Chem.* **2007**, *46*, 4835.
- [7] Tracey, A. S; Willsky, G. R. and Takeuchi, E.S. *Vanadium: Chemistry, Biochemistry, Pharmacology, and Practical applications*. Taylor & Francis Group: New York 2007.
- [8] Clare, B. W.; Kepert, D.L. Watts, D.W. *J. Chem. Soc., Dalton Trans.* **1973**, 2479.
- [9] Crans, D.C. *J. Inorg Biochem.* **2000**, *80*, 123.
- [10] Henschen, F. *Med Hist.* **1969** April 3(2), 190.
- [11] World Health Organization. *Diabetes.* **2009**.
<http://www.who.int/mediacentre/factsheets/fs312/en/> retrieved March 27th 2011.
- [12] World Health Organization. *About Diabetes.* **1999**.
<http://www.who.int/diabetesactiononline/diabetes/basics/en/index4.html> retrieved March 28th 2010
- [13] Nogrady, T; Weaver, D.F. *Medicinal Chemistry: a Molecular and Biochemical Approach*. 3rd edition. Oxford University Press: NY, 2005.
- [14] Lyonnet B.; Martz X, Martin, E. *La Presse Med*, **1899**, 191.
- [15] Heyliger, C. E.; Tahiliani, A.G.; McNeill, J.H. *Science*, **1985**, *227*, 1474.
- [16] No author, *Alter. Med. Rev.* **2009**, *14* (2), 177.
- [17] Pocherertt P.; Velma, S.; Grynypas, M.D.; McNeill, J.H. *Mol and Cell Biochem.* **1998**, *188*, 73.
- [18] Thompson, K.H.; Orvig. C. *J. Inorg. Biochem.* **2006**, *100*, 1925.
- [19] Ou, H.; Yan, L., Mustafi, D. ; Makinen, M.W.; Brady, M.J. *J Biol Inorg Chem.* **2005**, *10*, 874.
- [20] Thompson, K.H.; Orgiv. C. *J. Inorg. Biochem.* **2006**, *100*, 1925.
- [21] Li, M.; Ding, W.; Smee, J.J.; Baruah, B., Willsky, G.R.; Crans, D.C. *Biometals*, **2009**, *22*, 895.
- [22] Wieghardt. K. *Inorg. Chem.*, **1978**, *17*, 57.
- [23] Crans. D.C. *J. Inorg. Biochem.* **2000**, *80*, 123.
- [24] Lund, H. *Energy*, **2005**, *30*, 2402.
- [25] Zhao, P.; Zhang, H.; Zhou, H.; Chen, J.; Gao, S.; Yi, B. *J. Power Sources.* **2006**, *162*, 1416.
- [26] Fabjan, C.; Garche, J.; Harrer, B.; Jorissen, L.; Kolbeck, C.; Phillippi, F.; Tomazic, G.; Wagner, F. *Electrochim. Acta.* **2001**, *47*, 825.

-
- [27] Li, X.; Zhang, H., Mai, Z.; Zhang, H., Vankelecom. *Energy Environ. Sci.*, **2011**, *4*, 1147.
- [28] Rahman, F.; Skyllas-Kazacos, M. *J. Power Sources*. **2009**. *189*, 1212.
- [29] Vijayakumar, M., Li, L., Graff, G., Liu, J., Zhang, H., Yang, Z., Hu, J. *J. Power Sources*. **2011**. *196*, 3669.
- [30] Abbasi, S. A. *Anal Letters*. **1987**, *20*, 1347.
- [31] de Beer, H.; Coetzee, P. P. Fresenius *J. Anal Chem*. **1994**, *348*, 806.
- [32] Wuilloud. R.G.; Wuilloud, J.C.; Olsina, R.A., Martinez, L.D. *Analyst*. **2001**, *126*, 715.
- [33] Young, D. *Computational Chemistry: a Practical Guide for Applying Techniques to Real World Problems*. Wiley-InterScience: Toronto, 2001.
- [34] Nordstrom. D. K. *Water, Air and Soil Pollution*. **1996**, *90*, 257
- [35] Jensen, F. *Introduction to Computational Chemistry: Second Edition*. Chichester, England: John Wiley and Sons. Toronto, 2007.
- [36] Schrödinger, E. *Phys Rev*. **1926**, *28(6)*, 1049.
- [37] Møller, C.; Plesset, M.S. *Phys. Rev.*, **1934**, *46*, 618-622.
- [38] Hohenberg, P; Kohn, W. *Phys. Rev*. **1964**. *136 (3B)*, B864.
- [39] Lowdin. P. O. *Int. J. Quant Chem*. **1986**. *S19*, 19.
- [40] Hohenberg, P; Kohn, W. *Phys. Rev*. **1965**. *140*, A1133.
- [41] Perdew, J.P.; Ruzsinsky, A.; Tao, J.; Staroverov, V. N.; Scuseria, G. E.; Csonka, G. I. *J. Chem. Phys*. **2005**. *123*, 062201.
- [42] Becke, A.D. *J. Chem. Phys*. **1993**. *98*, 5648.
- [43] Lee, C.; Yang, W.; Parr, R. G. *Phys. Rev. B*. **1988**. *37*, 785.
- [44] Miertus, S.; Scrocco, E.; Tomasi, J. *J. Chem. Phys*. **1981**. *55*, 117.
- [45] Cancès, E.; Mennucci, B.; Tomasi, J. *J. Chem. Phys*. **1997**. *107*, 3032.
- [46] Car, R.; Parrinello, M. *Phys. Rev. Lett*. **1985**. *55(22)*, 2471.
- [47] Gaussian 03, Revision C.02, Frisch, M. J.; Trucks, G. W.; Schlegel, H. B.; Scuseria, G. E.; Robb, M. A.; Cheeseman, J. R.; Montgomery, Jr., J. A.; Vreven, T.; Kudin, K. N.; Burant, J. C.; Millam, J. M.; Iyengar, S. S.; Tomasi, J.; Barone, V.; Mennucci, B.; Cossi, M.; Scalmani, G.; Rega, N.; Petersson, G. A.; Nakatsuji, H.; Hada, M.; Ehara, M.; Toyota, K.; Fukuda, R.; Hasegawa, J.; Ishida, M.; Nakajima, T.; Honda, Y.; Kitao, O.; Nakai, H.; Klene, M.; Li, X.; Knox, J. E.; Hratchian, H. P.; Cross, J. B.; Bakken, V.; Adamo, C.; Jaramillo, J.; Gomperts, R.; Stratmann, R. E.; Yazyev, O.; Austin, A. J.; Cammi, R.; Pomelli, C.; Ochterski, J. W.; Ayala, P. Y.; Morokuma, K.; Voth, G. A.; Salvador, P.; Dannenberg, J. J.; Zakrzewski, V. G.; Dapprich, S.; Daniels, A. D.; Strain, M. C.; Farkas, O.; Malick, D. K.; Rabuck, A. D.; Raghavachari, K.; Foresman, J. B.; Ortiz, J. V.; Cui, Q.; Baboul, A. G.; Clifford, S.; Cioslowski, J.; Stefanov, B. B.; Liu, G.; Liashenko, A.; Piskorz, P.; Komaromi, I.; Martin, R. L.; Fox, D. J.; Keith, T.; Al-Laham, M. A.; Peng, C. Y.; Nanayakkara, A.; Challacombe, M.; Gill, P. M. W.; Johnson, B.; Chen, W.; Wong, M. W.; Gonzalez, C.; and Pople, J. A.; Gaussian, Inc., Wallingford CT, 2004.
- [48] Gaussian 09, Revision A.1, Frisch, M. J.; Trucks, G. W.; Schlegel, H. B.; Scuseria, G. E.; Robb, M. A.; Cheeseman, J. R.; Scalmani, G.; Barone, V.; Mennucci, B.;

-
- Petersson, G. A.; Nakatsuji, H.; Caricato, M.; Li, X.; Hratchian, H. P.; Izmaylov, A. F.; Bloino, J.; Zheng, G.; Sonnenberg, J. L.; Hada, M.; Ehara, M.; Toyota, K.; Fukuda, R.; Hasegawa, J.; Ishida, M.; Nakajima, T.; Honda, Y.; Kitao, O.; Nakai, H.; Vreven, T.; Montgomery, Jr., J. A.; Peralta, J. E.; Ogliaro, F.; Bearpark, M.; Heyd, J. J.; Brothers, E.; Kudin, K. N.; Staroverov, V. N.; Kobayashi, R.; Normand, J.; Raghavachari, K.; Rendell, A.; Burant, J. C.; Iyengar, S. S.; Tomasi, J.; Cossi, M.; Rega, N.; Millam, N. J.; Klene, M.; Knox, J. E.; Cross, J. B.; Bakken, V.; Adamo, C.; Jaramillo, J.; Gomperts, R.; Stratmann, R. E.; Yazyev, O.; Austin, A. J.; Cammi, R.; Pomelli, C.; Ochterski, J. W.; Martin, R. L.; Morokuma, K.; Zakrzewski, V. G.; Voth, G. A.; Salvador, P.; Dannenberg, J. J.; Dapprich, S.; Daniels, A. D.; Farkas, Ö.; Foresman, J. B.; Ortiz, J. V.; Cioslowski, J.; Fox, D. J. *Gaussian, Inc., Wallingford CT, 2009.*
- [49] Arunan, E.; Desiraju, G. R.; Klein, R. A.; Sadlej, J.; Scheiner, S.; Alkorta, I.; Clary, D. C.; Crabtree, R. H.; Dannenberg, J. J.; Hobza, P.; Kjaergaard, H. G.; Legon, A. C.; Mennucci, B.; Nesbitt, D. J. *Pure Appl. Chem.* **2011**, *83(8)*, 1637.
- [50] . Foresman, J. B. *Exploring Chemistry With Electronic Structure Methods: A Guide to Using Gaussian, 2-nd edition.* Gaussian, USA, 1996.
- [51] Goedecker, S.; Teter, M.; Hutter, J. *Phys Rev. B.* **1996**, *54*, 1703.
- [52] Acenet
- [53] Baran, E.J.; Lii, K-H. *Naturforsch.*, **2003**, *58b*, 485.
- [54] Bande, A.; Luchow, A. *Phys. Chem. Chem. Phys.* **2008**, *10*, 3371.
- [55] Buhl, M.; Parrinello, M., *Chem. Eur.J.* **2001**, *7 (20)*, 4487.
- [56] Cruywagen, J. J.; Heyns, J. B.; and Westra, A.,N. *Inorg Chem.* **1996**, *35*, 1556.
- [57] Ochterski, J. *Thermochemistry in Gaussian*, 2000, Gaussian Inc.
- [58] Merrick, J. P.; Moran, D.; Radom, L. *J. Phys. Chem A.* **2007**, *111*, 11683.
- [59] Dyrseen, D.; Sekine, T., *Acta Chem. Scand.* **1961**, *15*, 1399.
- [60] Schwarzenbach, G.; Geier, H. *Helv. Chim. Acta.* **1963**, *46*, 906.
- [61] Petterson, L., Hedman, B., Nenner, A.-M., Andersson, I. *Acta Chem. Scand.* **1985**, *A39*, 499.
- [62] Gabuda, S. P.; Kozlova, S.G.; Pletnev, R. N.. *Doklady Chemistry.* **2007**, *413 (2)*, 86.
- [63] Schwarzenbach, G., *J. Inorg. Nuclear Chem.* **1958**, *8*, 302.
- [64] Pope, M. P.; Dale, B. W. *Q. Rev. Chem. Soc.* **1968**, *22*, 527.
- [65] Schiller, K.; Thilo, E., *Z. Anorg. Chem.* **1961**, *310*, 261.
- [66] Naumann, A.W.; Hallada, C.J., *Inorg. Chem.* **1964**, *3*, 70.
- [67] Brito, F.. *Anales. Real. Soc. Esp. Fis. Quim.*, **1966**, *62 B*, 123.
- [68] Harnung, S. E.; Larsen, E.; Pedersen, E. J. *Acta Chem. Scand.* **1993**, *47*, 674.
- [69] Ribeiro, P. J. A.; Amado, A. M.; Teixeira-Dias, J. J. C. *J Comput Chem.* **1996**, *17(10)*, 1183.
- [70] Pye, C.C.; Zhang, Y.; Michels, M. *Unpublished Results*, **2011**.
- [71] Hardcastle, F. D.; Wachs, I. E. *J. Phys. Chem.* **1991**, *95*, 5031.
- [72] Tytko, K-H. *Polyhedron.* **1986**, *5*, 497.
- [73] Marx, D.; Hutter, J. *Ab Initio Molecular Dynamics: Basic Theory and Advanced Methods.* Cambridge University Press. New York, USA. 2009.

The Appendix

Chapter III

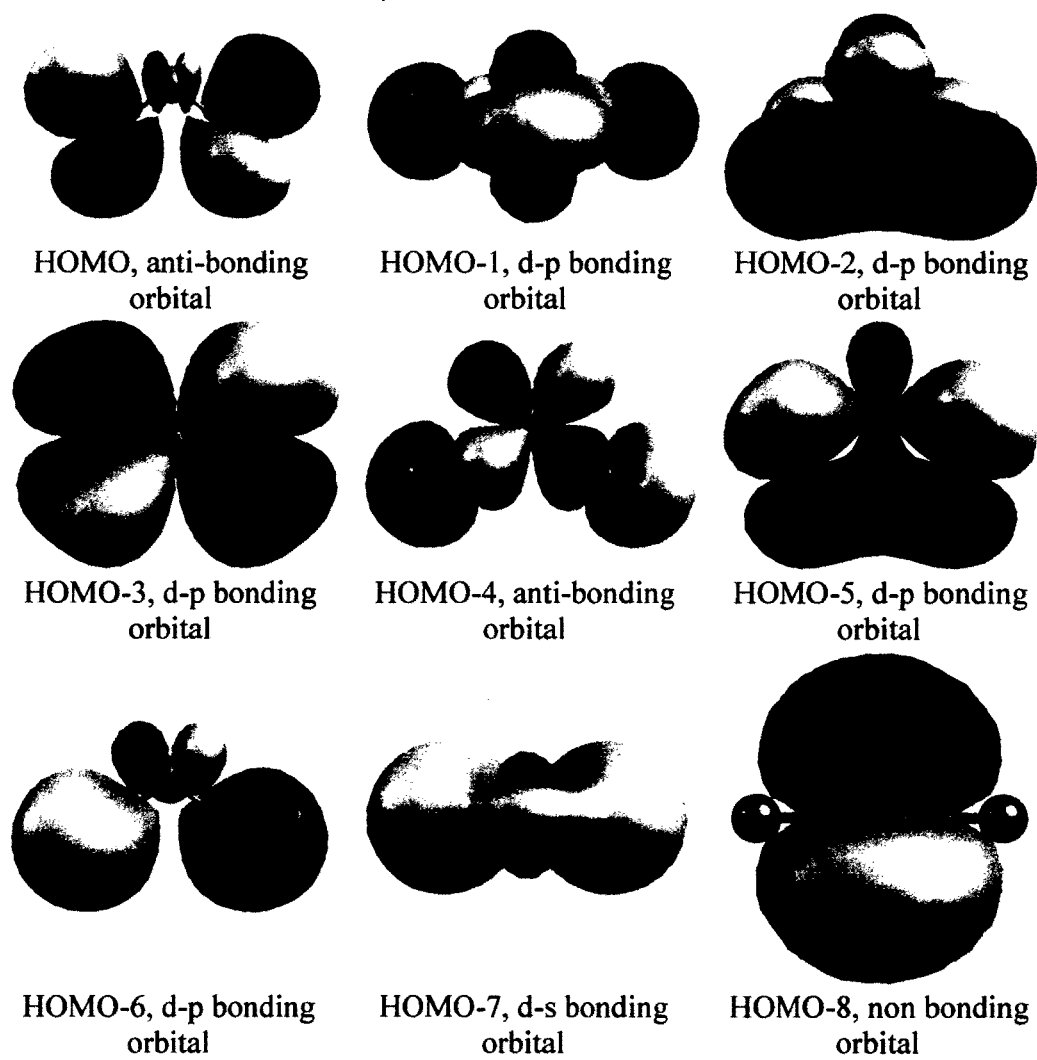


Figure A.1. The B3LYP/6-31+G* calculated NBO orbitals of the bent VO_2^+ .

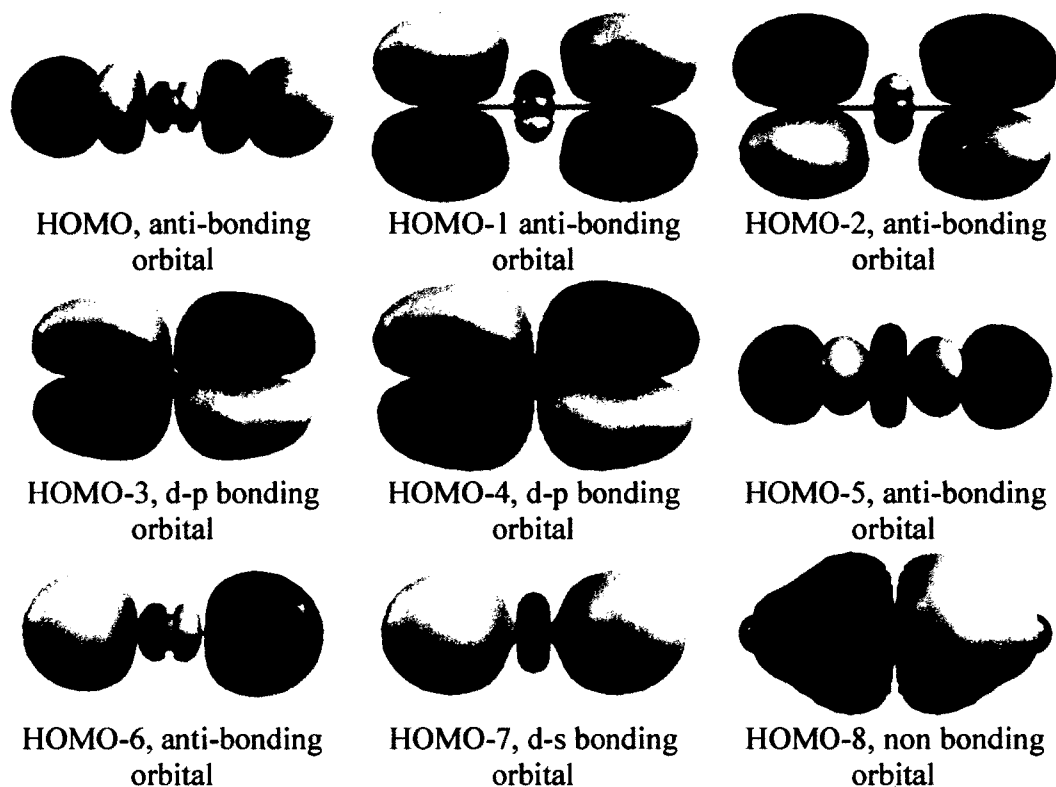


Figure A.2. The B3LYP/6-31+G* calculated NBO orbitals of the linear VO_2^+ .

A1. Energy for Comparison of Linear and Bent VO_2^+

Name of the Compound	Method/Basis Set	HF Energy/H
Bent VO_2^+	B3LYP/cc-pVTZ	-1094.23429565
Bent VO_2^+	CCSTD(T)/ cc-pVTZ	-1092.9561766
Linear VO_2^+	B3LYP/cc-pVTZ	-1094.08588723
Linear VO_2^+	CCSTD(T)/ cc-pVTZ	-1092.892459

A2. Vibrational frequencies of linear VO₂⁺ calculated at the B3LYP/cc-pVTZ theory level

Frequency wavenumber, cm ⁻¹	Mode
-1492.77	Π _u , bending
-1492.77	Π _u , bending
954.88	Σ _g , Sym stretch
1002.30	Σ _g , Asym stretch

A3. Calculated energies of naked bent VO₂⁺

Method/Basis set	Energy, H
HF/STO-3G	-1080.6242361
HF/3-21G	-1086.8170052
HF/6-31G*	-1092.0835190
HF/6-31+G*	-1092.0898790
MP2-FC/6-31*	-1092.8512672
MP2-FC/6-31+G*	-1092.8629216
B3LYP/6-31+G*	-1094.0892905

A4. Calculated energies of VO₂ (H₂O)⁺

Method/Basis set	Energy, H
HF/STO-3G	-1155.7590576
HF/3-21G	-1162.542542
HF/6-31G*	-1168.1974806
HF/6-31+G*	-1168.2071482
MP2-FC/6-31*	-1169.1353995
MP2-FC/6-31+G*	-1169.1579212
B3LYP/6-31+G*	-1170.6070005

A5. Calculated energies of naked bent VO₂ (H₂O)₂⁺

Method/Basis set	Energy, H
HF/STO-3G	-1230.8769486
HF/3-21G	-1238.2593119
HF/6-31G*	-1244.3017625
HF/6-31+G*	-1244.3149345
MP2-FC/6-31*	-1245.4195671
MP2-FC/6-31+G*	-1245.4509449
B3LYP/6-31+G*	-1247.1146575

A6. Calculated energies of VO₂ (H₂O)₃⁺

Method/Basis set	Energy, H
HF/STO-3G	-1305.9196271
HF/3-21G	-1313.9207335
HF/6-31G*	-1320.3632416
HF/6-31+G*	-1320.3792982
MP2-FC/6-31*	-1321.6707635
MP2-FC/6-31+G*	-1321.7111331
B3LYP/6-31+G*	-1323.5821441

A7. Calculated energies of naked bent C_2 $VO_2(H_2O)_4^+$

Method/Basis set	Energy, H
HF/STO-3G	-1380.9243314
HF/3-21G	-1389.5501698
HF/6-31G*	-1396.4006381
HF/6-31+G*	-1396.4213666
MP2-FC/6-31*	-1397.901812
MP2-FC/6-31+G*	-1397.9532602
B3LYP/6-31+G*	-1400.0293913

A8. Calculated energies of C_s $VO_2(H_2O)_4^+$

Method/Basis set	Energy, H
HF/STO-3G	-1380.9234255
HF/3-21G	-1389.5514133
HF/6-31G*	-1396.4015538
HF/6-31+G*	-1396.4223868
MP2-FC/6-31*	-1397.9033329
MP2-FC/6-31+G*	-1397.9555950
B3LYP/6-31+G*	-1400.0308058

A9. Aqueous PCM B3LYP/6-31+G* Calculated energies of $VO_2^+(H_2O)_n$, where n=1-4

Name of Complex	Energy, H
$VO_2^+(H_2O)$	-1170.76713893
$VO_2^+(H_2O)_2$	-1247.23525678
$VO_2^+(H_2O)_3$	-1323.68690504
$VO_2^+(H_2O)_4$	-1400.12928803

A 10. Energies of $VO_2(H_2O)_4^+$ and $VO_2(H_2O)_3^+ \cdot H_2O$

Method/Basis set	Energy of $VO_2(H_2O)_4^+$ (A), H	Energy of $VO_2(H_2O)_3^+ \cdot H_2O$, H
HF/6-31G*	-1396.4015538	-1396.405135
HF/6-31+G*	-1396.4223868	-1396.426238
MP2/6-31G*	-1397.9033329	-1397.9001603
MP2/6-31+G*	-1397.955595	-1397.9517204
B3LYP/6-31+G*	-1400.0308058	-1400.0373414
B3LYP/6-31+G* PCM	-1400.12928410	-1400.13433647

A11. The PCM/B3LYP/6-31+G* Energy Comparison of Hydrogen Bonded VO₂⁺

Chemical Formula of Complex	Energy, H	Chemical Formula of Complex	Energy, H
VO ₂ (H ₂ O) ₄ ⁺ ·H ₂ O	-1476.575888	VO ₂ (H ₂ O) ₃ ⁺ ·2H ₂ O	-1476.581491
VO ₂ (H ₂ O) ₄ ⁺ ·2H ₂ O	-1553.022090	VO ₂ (H ₂ O) ₃ ⁺ ·3H ₂ O	-1553.026606

A. 12. The V=O bond length of all VO₂⁺ species

Name of the Complex	V=O bond length, Å	
	HF/6-31+G*	B3LYP/6-31+G*
VO ₂ ⁺	1.5012	1.5506
VO ₂ (H ₂ O) ⁺	1.5142	1.5617
VO ₂ (H ₂ O) ₂ ⁺	1.5267	1.5728
VO ₂ (H ₂ O) ₃ ⁺	1.5359	1.5821
VO ₂ (H ₂ O) ₄ ⁺ C ₂	1.5411	1.5880
VO ₂ (H ₂ O) ₄ ⁺ C _s	1.5381	1.5865

A.13 V-O bond length of VO₂⁺ species

Name of Complex	V-O Bond Length, Å	
	HF/6-31+G*	B3LYP/6-31+G*
VO ₂ (H ₂ O) ⁺	2.0092	2.0114
VO ₂ (H ₂ O) ₂ ⁺	2.0200	2.0274
VO ₂ (H ₂ O) ₃ ⁺	2.1012	2.1291
	2.1173	2.1947
VO ₂ (H ₂ O) ₄ ⁺ C ₂	2.1070	2.0997
	2.2855	2.3103
VO ₂ (H ₂ O) ₄ ⁺ C _s	2.1029	2.1128
	2.2686	2.2527
	2.3406	2.3427

A.14 Calculated frequencies of $\text{VO}_2(\text{H}_2\text{O})_n^+$, $n=0-4$ at HF/6-31+G*

Name of the Complex			
	Wavenumber, cm^{-1}	Mode	
VO_2^+	483	A_1	sym. bend
	1228	A_2	asym stretch
	1319	B_2	sym stretch
$\text{VO}_2(\text{H}_2\text{O})^+$	150	A'	Deformation
	156	A''	Deformation
	413	A'	Deformation
	534	A'	stretch V-O
	1222	A''	asym stretch V=O
	1296	A'	sym stretch V=O
$\text{VO}_2(\text{H}_2\text{O})_2^+$	110	A_1	Deformation
	140	A_2	Deformation
	158	B_2	Deformation
	212	B_1	Deformation
	379	A_1	Deformation
	515	A_1	sym stretch V-O
	526	B_1	asym stretch V-O
	1214	B_2	asym stretch V=O
1275	A_1	sym stretch V=O	
$\text{VO}_2(\text{H}_2\text{O})_3^+$	102	B_1	Deformation
	187	A_1	Deformation
	194	B_1	Deformation
	197	B_2	Deformation
	258	B_2	Deformation
	263	A_1	Deformation
	327	A_1	asym stretch V--O
	360	B_2	sym stretch V-O
	426	A_1	asym stretch V-O
	489	B_1	Deformation
	1197	A_1	asym stretch V=O
	1254	B_2	sym stretch V=O

VO ₂ (H ₂ O) ₄ ⁺ C _s	78	A''	Deformation
	125	A'	Deformation
	136	A'	Deformation
	149	A'	Deformation
	176	A''	Deformation
	211	A''	Deformation
	240	A'	Deformation
	277	A''	asym stretch V-O
	280	A'	sym stretch V-O
	359	A'	asym stretch V-O
	393	A''	sym stretch V-O
	484	A'	Deformation
	1167	A'	asym stretch V=O
1240	A'	sym stretch V=O	

A.15 Calculated frequencies of VO₂(H₂O)_n⁺, n=0-4 at B3LYP/6-31+G*

Name of the Complex			
	Wavenumber cm ⁻¹	Mode	
VO ₂ ⁺	454	A ₁	Sym bending
	1108	A ₂	asym stretch
	1148	B ₂	sym stretch
VO ₂ (H ₂ O) ⁺	149	A'	Deformation
	161	A''	Deformation
	400	A'	Deformation
	499	A'	stretching V-O
	1105	A''	asym stretch V=O
	1132	A'	sym stretch V=O
VO ₂ (H ₂ O) ₂ ⁺	104	A ₁	Deformation
	136	A ₂	Deformation
	140	B ₂	Deformation
	194	B ₁	Deformation
	360	A ₁	Deformation
	474	A ₁	sym stretch V-O
	510	B ₁	asym stretch V-O
	1097	B ₂	asym stretch V=O
	1112	A ₁	sym stretch V=O

$\text{VO}_2(\text{H}_2\text{O})_3^+$	163	B_1	Deformation
	171	B_1	Deformation
	180	B_2	Deformation
	230	B_1	Deformation
	231	A_2	Deformation
	310	B_2	asym stretch V-O
	345	A_1	sym stretch V-O
	410	A_2	asym stretch V-O
	455	B_2	Deformation
	1080	A_1	asym stretch V=O
	1092	B_1	sym stretch V=O
$\text{VO}_2(\text{H}_2\text{O})_4^+ C_s$	67	A'	Deformation
	116	A''	Deformation
	118	A'	Deformation
	135	A'	Deformation
	165	A'	Deformation
	197	A'	Deformation
	205	A''	Deformation
	231	A'	asym stretch V-O
	276	A'	sym stretch V-O
	344	A'	asym stretch V-O
	421	A''	sym stretch V-O
	443	A'	Deformation
	1059	A'	asym stretch V=O
	1075	A'	sym stretch V=O

Chapter IV**B1. Calculated energies of C_{3v} H_3VO_4**

Method/Basis set	Energy, H
HF/3-21G	-1237.953228
HF/6-31G*	-1244.008800
HF/6-31+G*	-1244.031208
MP2-FC/6-31*	-1245.062319
MP2-FC/6-31+G*	-1245.109056
B3LYP/6-31+G*	-1246.830476

B2. Calculated energies of C_s $H_3VO_4 \cdot H_2O$

Method/Basis set	Energy, H
HF/3-21G	-1313.570953
HF/6-31G*	-1320.034756
HF/6-31+G*	-1320.061281
MP2-FC/6-31*	-1321.292331
MP2-FC/6-31+G*	-1321.346428
B3LYP/6-31+G*	-1323.266739

**B3. Calculated energies of C_1
 $H_3VO_4 \cdot 2H_2O$**

Method/Basis set	Energy, H
HF/6-31G*	-1396.579759
HF/6-31+G*	-1396.901951
MP2-FC/6-31*	-1397.509804
MP2-FC/6-31+G*	-1397.574952
B3LYP/6-31+G*	-1399.704512

**B4. Calculated energies of C_1
 $H_3VO_4 \cdot 3H_2O$**

Method/Basis set	Energy, H
HF/6-31G*	-1472.089424
HF/6-31+G*	-1472.126036
MP2-FC/6-31*	-1473.723650
MP2-FC/6-31+G*	-1473.800553
B3LYP/6-31+G*	-1476.151106

**B5. Calculated energies of C_1
 $H_3VO_4 \cdot 4H_2O$**

Method/Basis set	Energy, H
HF/6-31G*	-1548.113714
HF/6-31+G*	-1548.155841
MP2-FC/6-31*	-1549.940580
MP2-FC/6-31+G*	-1550.026987
B3LYP/6-31+G*	-1552.587855

**B6. Calculated energies of C_1
 $H_3VO_4 \cdot 5H_2O$**

Method/Basis set	Energy, H
HF/6-31G*	-1624.145252
HF/6-31+G*	-1624.191249
MP2-FC/6-31*	-1626.166036
MP2-FC/6-31+G*	-1626.262139
B3LYP/6-31+G*	-1629.033238

B7. Calculated energies of $C_1 H_3 VO_4 \cdot 6H_2O$

Method/Basis set	Energy, H
HF/6-31G*	-1700.173594
RHF/6-31+G*	-1700.224522
MP2 /6-31G*	-1702.404565
MP2 /6-31+G*	-1702.507803
B3LYP/6-31+G*	-1705.477400

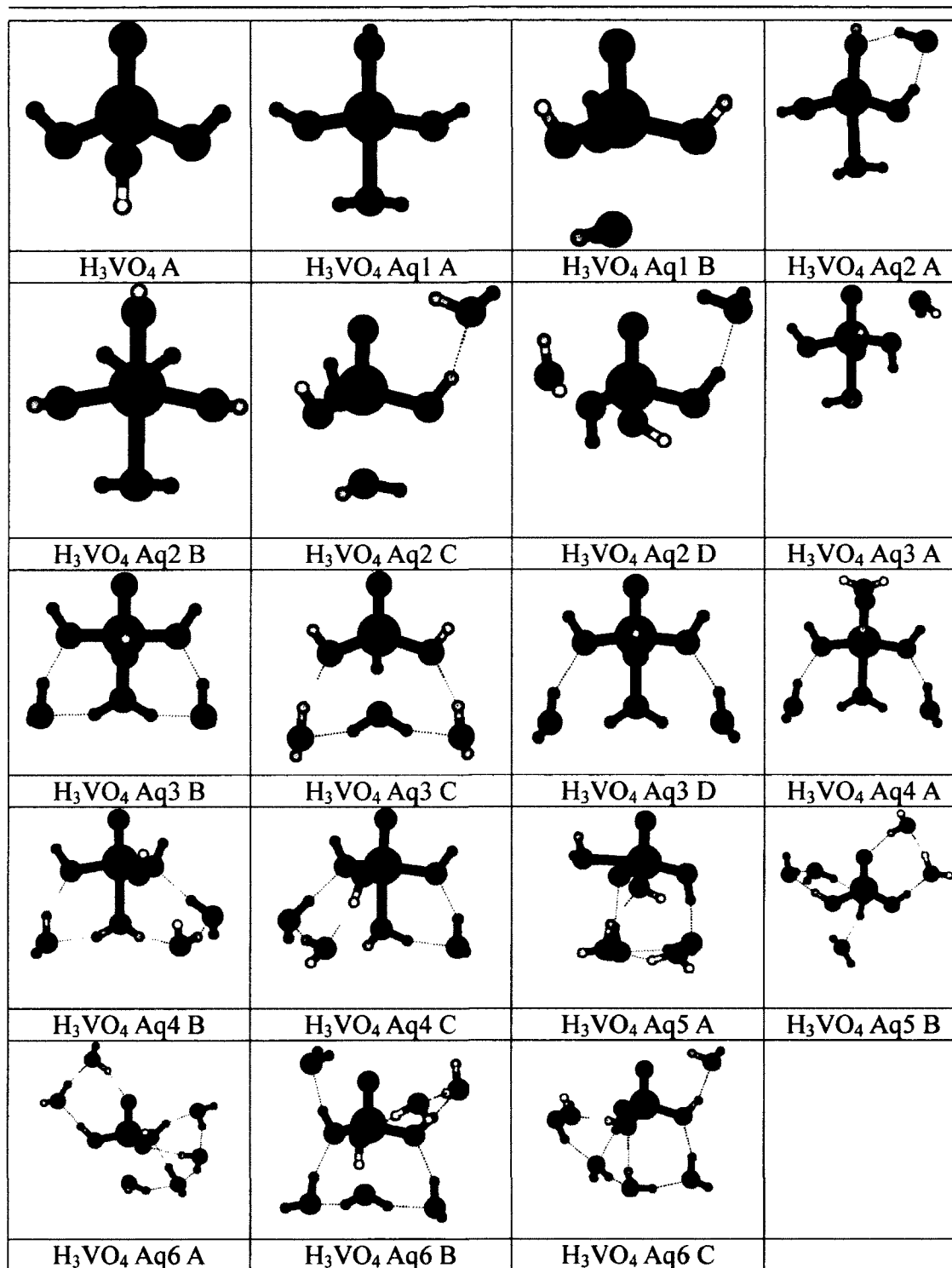


Figure B. The B3LYP/ 6-31+G* Optimized Local Minima of Vanadic Acid with $n\text{H}_2\text{O}$, $n=0-6$.

B8. Calculated energies of C_s H₃VO₄ A

Method/Basis set	Energy, H
HF/6-31G*	-1244.006483
HF/6-31+G*	-1244.028781
MP2-FC/6-31*	-1245.061013
MP2-FC/6-31+G*	-1245.107259
B3LYP/6-31+G*	-1246.827818

B10. Calculated energies of C_s H₃VO₄ Aq1 B

Method/Basis set	Energy, H
HF/6-31G*	-1320.019249
HF/6-31+G*	-1320.046524
MP2-FC/6-31*	-1321.271022
MP2-FC/6-31+G*	-1321.328039
B3LYP/6-31+G*	-1323.251885

B12. Calculated energies of C₁ H₃VO₄ Aq2 B

Method/Basis set	Energy, H
HF/6-31G*	-1396.043908
HF/6-31+G*	-1396.075128
MP2-FC/6-31*	-1397.497449
MP2-FC/6-31+G*	-1397.564176
B3LYP/6-31+G*	-1399.687587

B14. Calculated energies of C₁ H₃VO₄ Aq2 D

Method/Basis set	Energy, H
HF/6-31G*	-1396.044584
HF/6-31+G*	-1396.076224
MP2-FC/6-31*	-1397.480168
MP2-FC/6-31+G*	-1397.546420
B3LYP/6-31+G*	-1399.689678

B9. Calculated energies of C_s H₃VO₄ Aq1 A

Method/Basis set	Energy, H
HF/6-31G*	-1320.031054
HF/6-31+G*	-1320.058339
MP2-FC/6-31*	-1321.287473
MP2-FC/6-31+G*	-1321.342985
B3LYP/6-31+G*	-1323.263915

B11. Calculated energies of C₁ H₃VO₄ Aq2 A

Method/Basis set	Energy, H
HF/6-31G*	-1396.043636
HF/6-31+G*	-1396.078910
MP2-FC/6-31*	-1397.487897
MP2-FC/6-31+G*	-1397.554843
B3LYP/6-31+G*	-1399.691902

B13. Calculated energies of C₁ H₃VO₄ Aq2 C

Method/Basis set	Energy, H
HF/6-31G*	-1396.055195
HF/6-31+G*	-1396.087253
MP2-FC/6-31*	-1397.499473
MP2-FC/6-31+G*	-1397.565582
B3LYP/6-31+G*	-1399.700978

B15. Calculated energies of C_s H₃VO₄ Aq3 A

Method/Basis set	Energy, H
HF/6-31G*	-1472.081293
HF/6-31+G*	-1472.118742
MP2-FC/6-31*	-1473.727275
MP2-FC/6-31+G*	-1473.802757
B3LYP/6-31+G*	-1476.140973

B16. Calculated energies of $C_5 H_3 VO_4$
Aq3 B

Method/Basis set	Energy, H
HF/6-31G*	-1472.086588
HF/6-31+G*	-1472.123314
MP2-FC/6-31*	-1473.736326
MP2-FC/6-31+G*	-1473.810080
B3LYP/6-31+G*	-1476.146583

B17. Calculated energies of $C_5 H_3 VO_4$
Aq3 C

Method/Basis set	Energy, H
HF/6-31G*	-1472.081351
HF/6-31+G*	-1472.119089
MP2-FC/6-31*	-1473.726756
MP2-FC/6-31+G*	-1473.802302
B3LYP/6-31+G*	-1476.140440

B18. Calculated energies of $C_1 H_3 VO_4$
Aq4 A

Method/Basis set	Energy, H
HF/6-31G*	-1548.105285
HF/6-31+G*	-1548.147721
MP2-FC/6-31*	-1549.939103
MP2-FC/6-31+G*	-1550.026347
B3LYP/6-31+G*	-1552.577471

B19. Calculated energies of $C_1 H_3 VO_4$
Aq4 B

Method/Basis set	Energy, H
HF/6-31G*	-1548.111429
HF/6-31+G*	-1548.153556
MP2-FC/6-31*	-1549.952539
MP2-FC/6-31+G*	-1550.037212
B3LYP/6-31+G*	-1552.583823

B20. Calculated energies of $C_1 H_3 VO_4$
Aq4 C

Method/Basis set	Energy, H
HF/6-31G*	1548.111391
HF/6-31+G*	-1548.153421
MP2-FC/6-31*	-1549.953250
MP2-FC/6-31+G*	-1550.038803
B3LYP/6-31+G*	-1552.585003

B21. Calculated energies of $C_1 H_3 VO_4$
Aq5 A

Method/Basis set	Energy, H
HF/6-31G*	-1624.175020
HF/6-31+G*	-1626.157368
MP2-FC/6-31*	-1626.252411
MP2-FC/6-31+G*	-1629.015677
B3LYP/6-31+G*	-1624.175020

B22. Calculated energies of $C_1 H_3VO_4$
Aq5 B

Method/Basis set	Energy, H
HF/6-31G*	-1624.141271
HF/6-31+G*	-1624.188174
MP2-FC/6-31*	-1626.161455
MP2-FC/6-31+G*	-1626.259308
B3LYP/6-31+G*	-1629.029269

B23. Calculated energies of $C_1 H_3VO_4$
Aq6 A

Method/Basis set	Energy, H
HF/6-31G*	-1700.156398
HF/6-31+G*	-1700.209208
MP2-FC/6-31*	-1702.380534
MP2-FC/6-31+G*	-1702.488641
B3LYP/6-31+G*	-1705.462196

B24. Calculated energies of $C_1 H_3VO_4$
Aq6 B

Method/Basis set	Energy, H
HF/6-31G*	-1700.156398
HF/6-31+G*	-1700.209208
MP2-FC/6-31*	-1702.380534
MP2-FC/6-31+G*	-1702.488641
B3LYP/6-31+G*	-1705.462196

B25. Calculated energies of $C_1 H_3VO_4$
Aq6 C

Method/Basis set	Energy, H
HF/6-31+G*	-1700.222084
MP2-FC/6-31*	-1702.381596
MP2-FC/6-31+G*	-1702.487994
B3LYP/6-31+G*	-1705.472384

B26. Energies of $V(OH)_5$ and $H_3VO_4 \cdot H_2O$

Method/Basis set	Energy of $V(OH)_5$, H	Energy of $H_3VO_4 \cdot H_2O$, H
PCM B3LYP/cc-pVTZ	-1323.492823	-1323.53827412
CCSD(T)/cc-pVTZ	-1321.8588003	-1321.9102909
PCM CCSD(T)/cc-pVTZ	-1321.872901	-1321.9285481

B27. The calculated V=O bond Lengths of $H_3VO_4 \cdot nH_2O$, n =0-6.

Name of Complex	MP2 V=O, Å	B3LYP V=O, Å
H_3VO_4	1.621397	1.570869
$H_3VO_4 \cdot H_2O$	1.640868	1.568452
$H_3VO_4 \cdot 2H_2O$	1.642289	1.574897
$H_3VO_4 \cdot 3H_2O$	1.62021	1.56998
$H_3VO_4 \cdot 4H_2O$	1.621432	1.571297
$H_3VO_4 \cdot 5H_2O$	1.621012	1.572969
$H_3VO_4 \cdot 6H_2O$	1.629176	1.592963

B28. The calculated V-O bond lengths of $\text{H}_3\text{VO}_4 \cdot n\text{H}_2\text{O}$, $n = 0-6$.

Name of Complex	MP2 V=O Bond Length, Å	B3LYP V=O Bond Length, Å
H_3VO_4	1.809479	1.776765
$\text{H}_3\text{VO}_4 \cdot \text{H}_2\text{O}$	1.834116	1.776033
	1.856488	1.80045
	1.856488	1.80045
$\text{H}_3\text{VO}_4 \cdot 2\text{H}_2\text{O}$	1.859415	1.809016
	1.826643	1.783074
	1.88879	1.836648
$\text{H}_3\text{VO}_4 \cdot 3\text{H}_2\text{O}$	1.833821	1.798743
	1.775826	1.736896
	1.848691	1.811564
$\text{H}_3\text{VO}_4 \cdot 4\text{H}_2\text{O}$	1.84585	1.81067
	1.784195	1.745601
	1.814742	1.78409
$\text{H}_3\text{VO}_4 \cdot 5\text{H}_2\text{O}$	1.84585	1.768 33
	1.784195	1.812938
	1.814742	1.757235
$\text{H}_3\text{VO}_4 \cdot 6\text{H}_2\text{O}$	1.787176	1.767904
	1.829247	1.747511
	1.801932	1.785874

B29. The calculated V- -O bond lengths of $\text{H}_3\text{VO}_4 \cdot n\text{H}_2\text{O}$, $n = 0-6$.

Name of Complex	MP2 V- -O Bond Length, Å	B3LYP V- -O Bond Length, Å
$\text{H}_3\text{VO}_4 \cdot \text{H}_2\text{O}$	2.325689	2.689104
$\text{H}_3\text{VO}_4 \cdot 2\text{H}_2\text{O}$	2.24259	2.358257
	3.919636	3.971273
$\text{H}_3\text{VO}_4 \cdot 3\text{H}_2\text{O}$	3.660336	3.711871
	3.602265	3.754674
	4.021065	4.010767
$\text{H}_3\text{VO}_4 \cdot 4\text{H}_2\text{O}$	3.509234	3.619933
	3.62649	3.738589
	4.391664	4.279213
	4.151314	4.093296

H ₃ VO ₄ ·5H ₂ O	3.910814	3.926761
	3.77899	3.795622
	3.733645	3.797446
	3.875658	3.833292
	3.835639	3.95204
H ₃ VO ₄ ·6H ₂ O	3.253875	3.605478
	3.951212	3.972378
	4.729181	4.741449
	3.909335	3.847993
	3.84004	3.96221
	3.996527	4.050808

B30. The MP2/6-31+G* calculated vibrational frequencies of H₃VO₄·nH₂O, n =0-6.

Name of Complex	MP2 V=O Bond Length, Å		
	Wavenumber, cm ⁻¹	Mode	
H ₃ VO ₄	660	E	Sym Stretch V-O
	777	E	Asym Stretch V-O
	778	E	Asym Stretch V-O
	1070	A1	Stretch V=O
H ₃ VO ₄ ·H ₂ O	243	A'	Deformation
	293	A'	Deformation
	298	A''	Deformation
	310	A'	Deformation
	602	A'	Sym Stretch V-O
	677	A''	Asym Stretch V-O
	705	A'	Asym Stretch V-O
	986	A'	Stretch V=O
H ₃ VO ₄ ·2H ₂ O	130	A	Deformation
	149	A	Deformation
	261	A	Deformation
	313	A	Deformation
	328	A	Deformation
	574	A	Sym Stretch V-O
	640	A	Asym Stretch V-O
	699	A	Asym Stretch V-O
	986	A	Stretch V=O

H ₃ VO ₄ ·3H ₂ O	172	A	Deformation
	208	A	Deformation
	221	A	Deformation
	256	A	Deformation
	643	A	Sym Stretch V-O
	719	A	Asym Stretch V-O
	807	A	Asym Stretch V-O
	1098	A	Stretch V=O
H ₃ VO ₄ ·4H ₂ O	192	A	Deformation
	230	A	Deformation
	242	A	Deformation
	264	A	Deformation
	311	A	Deformation
	657	A	Sym Stretch V-O
	733	A	Asym Stretch V-O
	795	A	Asym Stretch V-O
	1121	A	Stretch V=O
H ₃ VO ₄ ·5H ₂ O	209	A	Deformation
	233	A	Deformation
	244	A	Deformation
	247	A	Deformation
	290	A	Deformation
	343	A	Deformation
	363	A	Deformation
	667	A	Sym Stretch V-O
	735	A	Asym Stretch V-O
	767	A	Asym Stretch V-O
1173	A	Stretch V=O	
H ₃ VO ₄ ·6H ₂ O	201	A	Deformation
	239	A	Deformation
	251	A	Deformation
	261	A	Deformation
	297	A	Deformation
	330	A	Deformation
	671	A	Sym Stretch V-O
	734	A	Asym Stretch V-O
	801	A	Asym Stretch V-O
	1057	A	Stretch V=O

B31. The B3LYP/6-31+G* calculated vibrational frequencies of $\text{H}_3\text{VO}_4 \cdot n\text{H}_2\text{O}$, $n = 0-6$.

Name of Complex	B3LYP V=O Bond Length, Å		
	Wavenumber, cm^{-1}	Mode	
H_3VO_4	668	E	Sym Stretch V-O
	725	E	Asym Stretch V-O
	798	E	Asym Stretch V-O
	1113	A1	Stretch V=O
$\text{H}_3\text{VO}_4 \cdot \text{H}_2\text{O}$	220	A'	Deformation
	233	A'	Deformation
	266	A''	Deformation
	294	A'	Deformation
	684	A'	Sym Stretch V-O
	772	A''	Asym Stretch V-O
	781	A'	Asym Stretch V-O
	1119	A'	Stretch V=O
$\text{H}_3\text{VO}_4 \cdot 2\text{H}_2\text{O}$	147	A	Deformation
	191	A	Deformation
	307	A	Deformation
	313	A	Deformation
	641	A	Sym Stretch V-O
	719	A	Asym Stretch V-O
	735	A	Asym Stretch V-O
	1098	A	Stretch V=O
$\text{H}_3\text{VO}_4 \cdot 3\text{H}_2\text{O}$	232	A	Deformation
	236	A	Deformation
	242	A	Deformation
	281	A	Deformation
	688	A	Sym Stretch V-O
	743	A	Asym Stretch V-O
	842	A	Asym Stretch V-O
	1104	A	Stretch V=O
$\text{H}_3\text{VO}_4 \cdot 4\text{H}_2\text{O}$	191	A	Deformation
	244	A	Deformation
	256	A	Deformation
	271	A	Deformation
	332	A	Deformation
	701	A	Sym Stretch V-O
	774	A	Asym Stretch V-O
	819	A	Asym Stretch V-O
	1139	A	Stretch V=O

H ₃ VO ₄ ·5H ₂ O	202	A	Deformation
	252	A	Deformation
	260	A	Deformation
	284	A	Deformation
	312	A	Deformation
	338	A	Deformation
	697	A	Sym Stretch V-O
	785	A	Asym Stretch V-O
	814	A	Asym Stretch V-O
	1120	A	Stretch V=O
H ₃ VO ₄ ·6H ₂ O	205	A	Deformation
	252	A	Deformation
	260	A	Deformation
	284	A	Deformation
	312	A	Deformation
	338	A	Deformation
	739	A	Sym Stretch V-O
	770	A	Asym Stretch V-O
	830	A	Asym Stretch V-O
	1043	A	Stretch V=O

Chapter V**C1. Calculated energies of C_s and C₂ symmetries of H₂VO₄⁻**

Method/Basis set	C _s Energy, H	C ₂ Energy, H
HF/6-31G*	1243.463241	-1243.463994
RHF/6-31+G*	-1243.494977	-1243.495625
MP2 /6-31G*	-1244.536234	-1244.537144
MP2 /6-31+G*	-1244.602651	-1244.603262
B3LYP/6-31+G*	-1246.305313	-1246.305875

**C2. Calculated energies of C₁ H₂VO₄⁻
H₂O MP2**

Method/Basis set	Energy, H
HF/6-31G*	-1319.499843
HF/6-31+G*	-1319.536155
MP2-FC/6-31*	-1320.764989
MP2-FC/6-31+G*	-1320.841163
B3LYP/6-31+G*	-1322.753412

C3. Calculated energies of C₂ H₂VO₄⁻H₂O

Method/Basis set	Energy, H
HF/6-31G*	-1319.500700
HF/6-31+G*	-1319.536376
MP2-FC/6-31*	-1320.763256
MP2-FC/6-31+G*	-1320.837681
B3LYP/6-31+G*	-1322.753574

**C4. Calculated energies of C₁ H₂VO₄⁻
2H₂O MP2**

Method/Basis set	Energy, H
HF/6-31G*	-1395.532492
HF/6-31+G*	-1395.573414
MP2-FC/6-31*	1396.992469
MP2-FC/6-31+G*	-1397.078162
B3LYP/6-31+G*	-1399.197508

**C5. Calculated energies of C₁ H₂VO₄⁻
2H₂O**

Method/Basis set	Energy, H
HF/6-31G*	-1395.531614
HF/6-31+G*	-1395.57169
MP2-FC/6-31*	-1396.986106
MP2-FC/6-31+G*	-1397.074026
B3LYP/6-31+G*	-1399.198787

C6. Calculated energies of $C_1 H_2 VO_4^- \cdot 3H_2O$ MP2

Method/Basis set	Energy, H
HF/6-31G*	-1471.566531
HF/6-31+G*	-1471.609497
MP2-FC/6-31*	-1473.221519
MP2-FC/6-31+G*	-1473.311743
B3LYP/6-31+G*	-1475.642556

C7. Calculated energies of $C_1 H_2 VO_4^- \cdot 3H_2O$

Method/Basis set	Energy, H
HF/6-31G*	-1471.564964
HF/6-31+G*	-1471.610470
MP2-FC/6-31*	-1473.221557
MP2-FC/6-31+G*	-1473.310837
B3LYP/6-31+G*	-1475.647752

C8. Calculated energies of $C_2 H_2 VO_4^- \cdot 4H_2O$

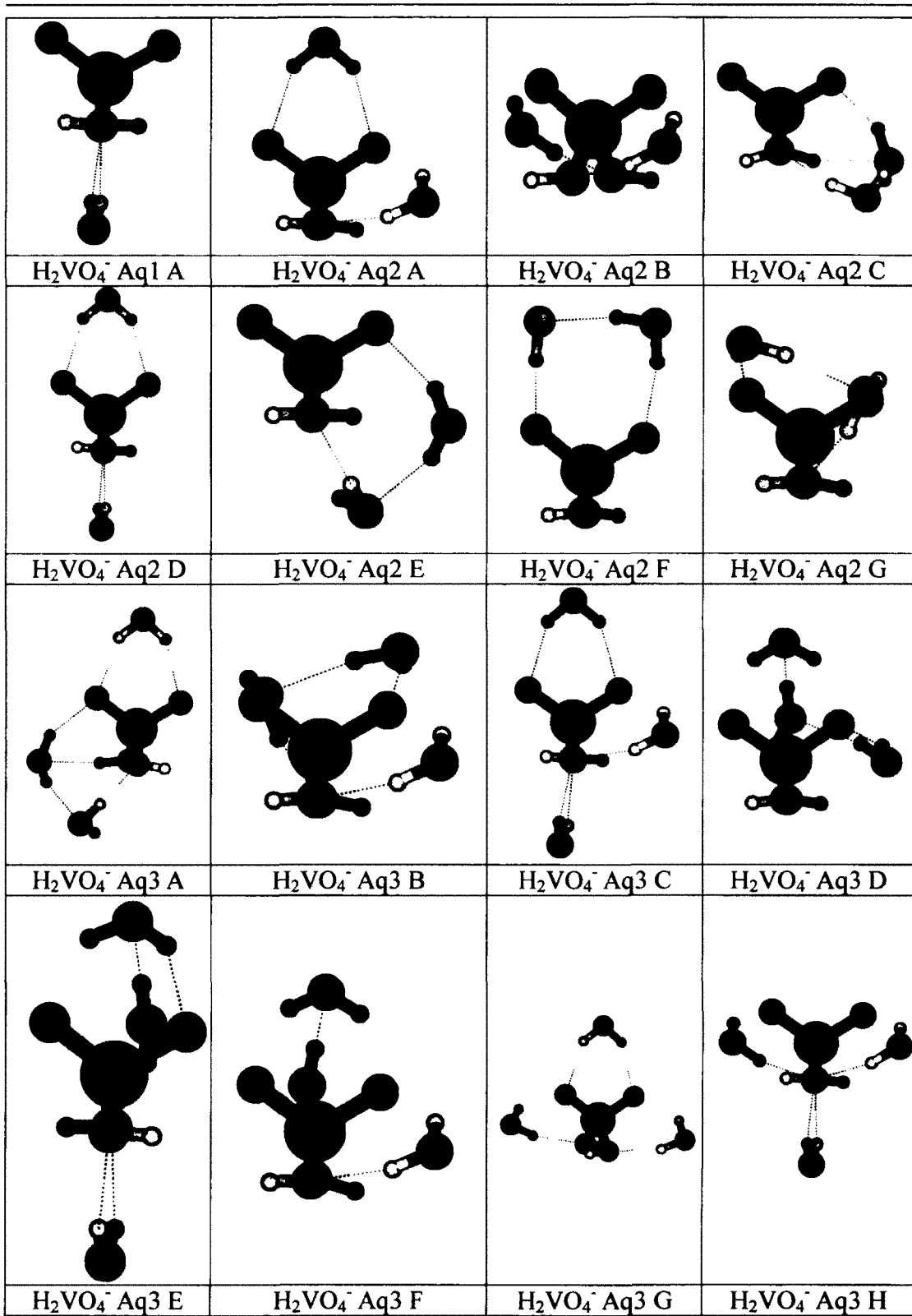
Method/Basis set	Energy, H
HF/6-31G*	-1547.601087
HF/6-31+G*	-1547.646337
MP2-FC/6-31*	-1549.446315
MP2-FC/6-31+G*	-1549.545385
B3LYP/6-31+G*	-1552.089415

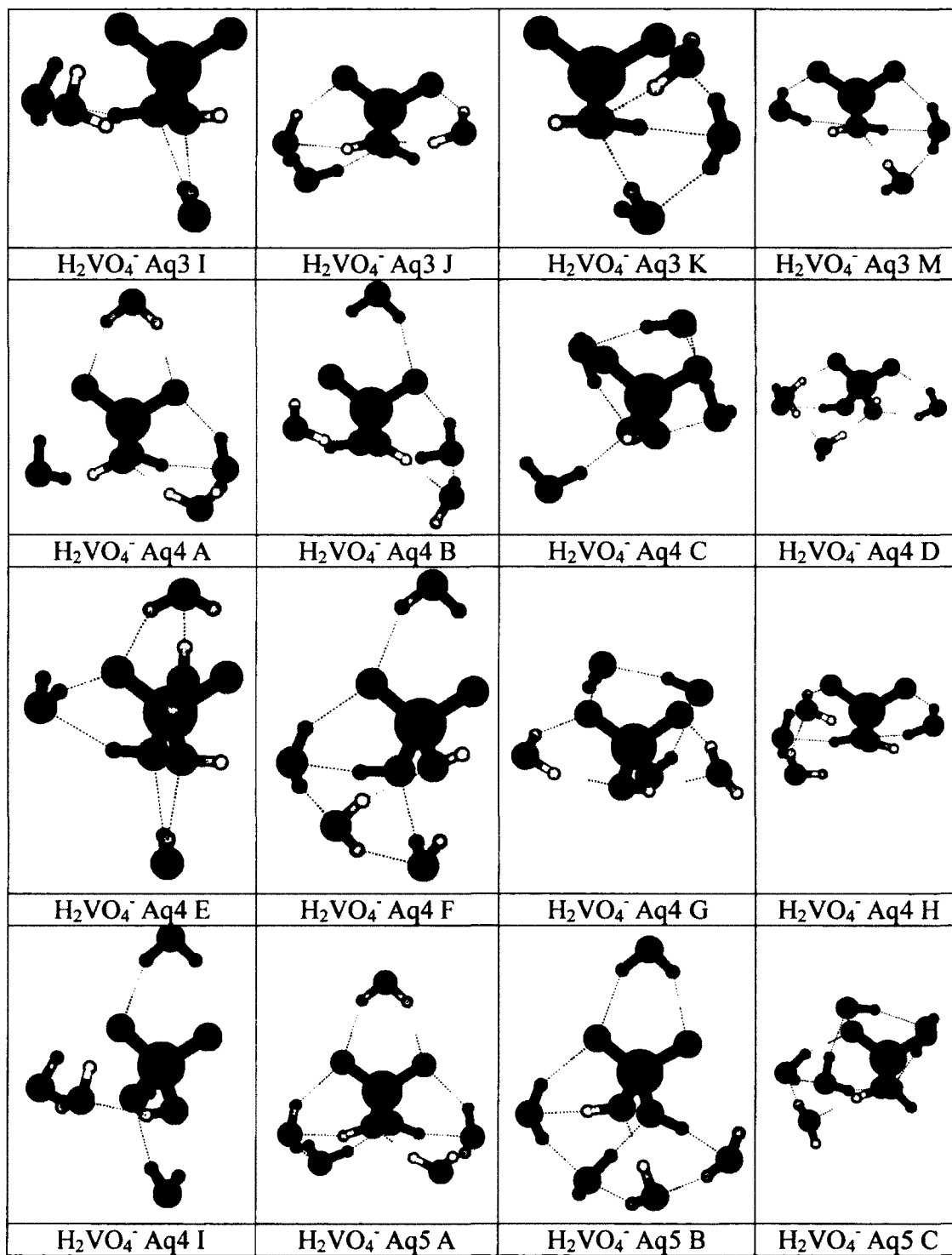
C9. Calculated energies of $C_2 H_2 VO_4^- \cdot 5H_2O$

Method/Basis set	Energy, H
HF/6-31G*	-1623.633248
HF/6-31+G*	-1623.681946
MP2-FC/6-31*	-1625.675027
MP2-FC/6-31+G*	-1625.779379
B3LYP/6-31+G*	-1628.535157

C10. Calculated energies for $C_1 H_2 VO_4^- \cdot 6H_2O$

Method/Basis set	Energy, H
HF/6-31G*	-1699.662363
RHF/6-31+G*	-1699.718300
MP2 /6-31G*	-1701.892197
MP2 /6-31+G*	-1702.008373
B3LYP/6-31+G*	-1704.979544





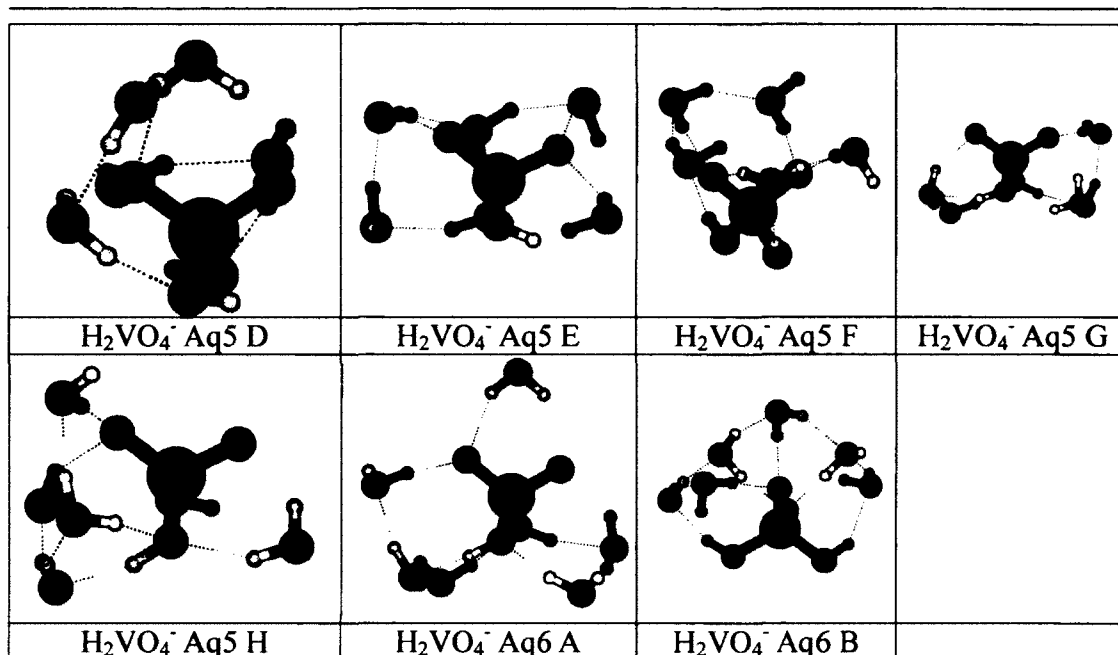


Figure C. Local Minima of $\text{H}_2\text{VO}_4^- n\text{H}_2\text{O}$, with $n=0-6$.

C11. Calculated energies of $\text{C}_s \text{H}_2\text{VO}_4^-$
Aq1 A

Method/Basis set	Energy, H
HF/6-31G*	-1319.499412
HF/6-31+G*	-1319.535599
MP2-FC/6-31*	-1320.768141
MP2-FC/6-31+G*	-1320.843188
B3LYP/6-31+G*	-1322.753128

C12. Calculated energies of $\text{C}_1 \text{H}_2\text{VO}_4^-$
Aq2 A

Method/Basis set	Energy, H
HF/6-31G*	-1395.534049
HF/6-31+G*	-1395.574737
MP2-FC/6-31*	-1396.988005
MP2-FC/6-31+G*	-1397.073328
B3LYP/6-31+G*	-1399.198412

C13. Calculated energies of $\text{C}_2 \text{H}_2\text{VO}_4^-$
Aq2 B

Method/Basis set	Energy, H
HF/6-31G*	-1395.574895
HF/6-31+G*	-1396.989544
MP2-FC/6-31*	-1397.07686
MP2-FC/6-31+G*	-1399.19852
B3LYP/6-31+G*	-1395.574895

C14. Calculated energies of $\text{C}_1 \text{H}_2\text{VO}_4^-$
Aq2 C

Method/Basis set	Energy, H
HF/6-31G*	-1395.534416
HF/6-31+G*	-1395.572807
MP2-FC/6-31*	-1396.993283
MP2-FC/6-31+G*	-1397.074723
B3LYP/6-31+G*	-1399.198336

C15. Calculated energies of $C_2 H_2 VO_4^-$
Aq2 D

Method/Basis set	Energy, H
HF/6-31G*	-1395.530226
HF/6-31+G*	-1395.574669
MP2-FC/6-31*	-1396.990399
MP2-FC/6-31+G*	-1397.075514
B3LYP/6-31+G*	1399.198661

C16. Calculated energies of $C_1 H_2 VO_4^-$
Aq2 E

Method/Basis set	Energy, H
HF/6-31G*	-1395.534182
HF/6-31+G*	-1395.572389
MP2-FC/6-31*	-1396.998195
MP2-FC/6-31+G*	-1397.077228
B3LYP/6-31+G*	-1399.198415

C17. Calculated energies of $C_1 H_2 VO_4^-$
Aq2 F

Method/Basis set	Energy, H
HF/6-31G*	-1395.527589
HF/6-31+G*	-1395.573217
MP2-FC/6-31*	-1396.985211
MP2-FC/6-31+G*	-1397.067989
B3LYP/6-31+G*	-1399.198272

C18. Calculated energies of $C_1 H_2 VO_4^-$
Aq2 G

Method/Basis set	Energy, H
HF/6-31G*	-1395.531245
HF/6-31+G*	-1395.571643
MP2-FC/6-31*	-1396.993129
MP2-FC/6-31+G*	-1397.074936
B3LYP/6-31+G*	-1399.198439

C19. Calculated energies of $C_1 H_2 VO_4^-$
Aq3 A

Method/Basis set	Energy, H
HF/6-31G*	-1471.567004
HF/6-31+G*	-1471.610144
MP2-FC/6-31*	-1473.219110
MP2-FC/6-31+G*	-1473.308416
B3LYP/6-31+G*	-1475.642753

C20. Calculated energies of $C_1 H_2 VO_4^-$
Aq3 B

Method/Basis set	Energy, H
HF/6-31G*	-1471.563099
HF/6-31+G*	-1471.608692
MP2-FC/6-31*	-1473.216282
MP2-FC/6-31+G*	-1473.309119
B3LYP/6-31+G*	-1475.641810

C21. Calculated energies of $C_1 H_2 VO_4^-$
Aq3 C

Method/Basis set	Energy, H
HF/6-31G*	-1471.564555
HF/6-31+G*	-1471.610436
MP2-FC/6-31*	-1473.212446
MP2-FC/6-31+G*	-1473.308424
B3LYP/6-31+G*	-1475.640579

C22. Calculated energies of $C_1 H_2 VO_4^-$
Aq3 D

Method/Basis set	Energy, H
HF/6-31G*	-1471.564976
HF/6-31+G*	-1471.608957
MP2-FC/6-31*	-1473.221880
MP2-FC/6-31+G*	-1473.309089
B3LYP/6-31+G*	-1475.646600

C23. Calculated energies of $C_1 H_2 VO_4^-$
Aq3 E

Method/Basis set	Energy, H
HF/6-31G*	-1471.563228
HF/6-31+G*	-1471.608539
MP2-FC/6-31*	-1473.209850
MP2-FC/6-31+G*	-1473.309089
B3LYP/6-31+G*	-1475.641412

C24. Calculated energies of $C_1 H_2 VO_4^-$
Aq3 F

Method/Basis set	Energy, H
HF/6-31G*	-1471.561290
HF/6-31+G*	-1471.605957
MP2-FC/6-31*	-1473.213961
MP2-FC/6-31+G*	-1473.308146
B3LYP/6-31+G*	-1475.642240

C25. Calculated energies of $C_2 H_2 VO_4^-$
Aq3 G

Method/Basis set	Energy, H
HF/6-31G*	-1471.563386
HF/6-31+G*	-1471.611521
MP2-FC/6-31*	-1473.210113
MP2-FC/6-31+G*	-1473.306929
B3LYP/6-31+G*	-1475.641109

C26. Calculated energies of $C_2 H_2 VO_4^-$
Aq3 H

Method/Basis set	Energy, H
HF/6-31G*	-1471.563474
HF/6-31+G*	-1471.609560
MP2-FC/6-31*	-1473.214226
MP2-FC/6-31+G*	-1473.311179
B3LYP/6-31+G*	-1475.639832

C27. Calculated energies of $C_1 H_2 VO_4^-$
Aq3 I

Method/Basis set	Energy, H
HF/6-31G*	-1471.565455
HF/6-31+G*	-1471.608306
MP2-FC/6-31*	-1473.218998
MP2-FC/6-31+G*	-1473.309600
B3LYP/6-31+G*	-1475.641082

C28. Calculated energies of $C_1 H_2 VO_4^-$
Aq3 J

Method/Basis set	Energy, H
HF/6-31G*	-1471.566138
HF/6-31+G*	-1471.610486
MP2-FC/6-31*	-1473.217310
MP2-FC/6-31+G*	-1473.309814
B3LYP/6-31+G*	-1475.642965

C29. Calculated energies of $C_1 H_2 VO_4^-$
Aq3 K

Method/Basis set	Energy, H
HF/6-31G*	-1471.564493
HF/6-31+G*	-1471.606947
MP2-FC/6-31*	-1473.219376
MP2-FC/6-31+G*	-1473.310644
B3LYP/6-31+G*	-1475.640982

C30. Calculated energies of $C_1 H_2 VO_4^-$
Aq3 M

Method/Basis set	Energy, H
HF/6-31G*	-1471.564523
HF/6-31+G*	-1471.606815
MP2-FC/6-31*	-1473.222210
MP2-FC/6-31+G*	-1473.311743
B3LYP/6-31+G*	-1475.642557

C31. Calculated energies of $C_1 H_2 VO_4^-$
Aq4 A

Method/Basis set	Energy, H
HF/6-31G*	-1547.597641
HF/6-31+G*	-1547.646691
MP2-FC/6-31*	-1549.440241
MP2-FC/6-31+G*	-1549.540498
B3LYP/6-31+G*	-1552.085479

C32. Calculated energies of $C_1 H_2 VO_4^-$
Aq4 B

Method/Basis set	Energy, H
HF/6-31G*	-1547.595973
HF/6-31+G*	-1547.645259
MP2-FC/6-31*	-1549.440195
MP2-FC/6-31+G*	-1549.539361
B3LYP/6-31+G*	-1552.084262

C33. Calculated energies of $C_1 H_2 VO_4^-$
Aq4 C

Method/Basis set	Energy, H
HF/6-31G*	-1547.597142
HF/6-31+G*	-1547.643131
MP2-FC/6-31*	-1549.440041
MP2-FC/6-31+G*	-1549.541100
B3LYP/6-31+G*	-1552.086138

C34. Calculated energies of $C_1 H_2 VO_4^-$
Aq4 D

Method/Basis set	Energy, H
HF/6-31G*	-1547.595937
HF/6-31+G*	-1547.642155
MP2-FC/6-31*	-1549.443292
MP2-FC/6-31+G*	-1549.541839
B3LYP/6-31+G*	-1552.084681

C35. Calculated energies of $C_1 H_2 VO_4^-$
Aq4 E

Method/Basis set	Energy, H
HF/6-31G*	-1547.593399
HF/6-31+G*	-1547.641992
MP2-FC/6-31*	-1549.432875
MP2-FC/6-31+G*	-1549.535118
B3LYP/6-31+G*	-1552.082051

C36. Calculated energies of $C_1 H_2 VO_4^-$
Aq4 F

Method/Basis set	Energy, H
HF/6-31G*	-1547.600158
HF/6-31+G*	-1547.646638
MP2-FC/6-31*	-1549.444176
MP2-FC/6-31+G*	-1549.545459
B3LYP/6-31+G*	-1552.088298

C37. Calculated energies of $C_1 H_2 VO_4^-$
Aq4 G

Method/Basis set	Energy, H
HF/6-31G*	-1547.594143
HF/6-31+G*	-1547.642400
MP2-FC/6-31*	-1549.436493
MP2-FC/6-31+G*	-1549.534938
B3LYP/6-31+G*	-1552.081443

C38. Calculated energies of $C_1 H_2 VO_4^-$
Aq4 H

Method/Basis set	Energy, H
HF/6-31G*	-1547.595736
HF/6-31+G*	-1547.643451
MP2-FC/6-31*	-1549.442188
MP2-FC/6-31+G*	-1549.546486
B3LYP/6-31+G*	-1552.089063

C39. Calculated energies of $C_1 H_2 VO_4^-$
Aq4 I

Method/Basis set	Energy, H
HF/6-31G*	-1547.596686
HF/6-31+G*	-1547.644766
MP2-FC/6-31*	-1549.438688
MP2-FC/6-31+G*	-1549.540269
B3LYP/6-31+G*	-1552.083973

C40. . Calculated energies of $C_1 H_2 VO_4^-$
Aq5 A

Method/Basis set	Energy, H
HF/6-31G*	-1623.631638
HF/6-31+G*	-1623.682499
MP2-FC/6-31*	-1625.665784
MP2-FC/6-31+G*	-1625.776011
B3LYP/6-31+G*	-1625.776011

C41. Calculated energies of $C_1 H_2 VO_4^-$
Aq5 B

Method/Basis set	Energy, H
HF/6-31G*	-1623.630437
HF/6-31+G*	-1623.681636
MP2-FC/6-31*	-1625.667717
MP2-FC/6-31+G*	-1625.777929
B3LYP/6-31+G*	-1628.531424

C42. Calculated energies of $C_1 H_2 VO_4^-$
Aq5 C

Method/Basis set	Energy, H
HF/6-31G*	-1623.627821
HF/6-31+G*	-1623.679284
MP2-FC/6-31*	-1625.667999
MP2-FC/6-31+G*	-1625.669773
B3LYP/6-31+G*	-1628.535150

C43. Calculated energies of $C_1 H_2 VO_4^-$
Aq5 D

Method/Basis set	Energy, H
HF/6-31G*	-1623.630456
HF/6-31+G*	-1623.680671
MP2-FC/6-31*	-1625.665656
MP2-FC/6-31+G*	-1625.770275
B3LYP/6-31+G*	-1628.527374

C44. Calculated energies of $C_1 H_2 VO_4^-$
Aq5 E

Method/Basis set	Energy, H
HF/6-31G*	-1623.625217
HF/6-31+G*	-1623.679603
MP2-FC/6-31*	-1625.656171
MP2-FC/6-31+G*	-1625.773344
B3LYP/6-31+G*	-1628.532877

**C45. Calculated energies of $C_1 H_2VO_4^-$
Aq5 F**

Method/Basis set	Energy, H
HF/6-31G*	-1623.626416
HF/6-31+G*	-1623.678576
MP2-FC/6-31*	-1625.654553
MP2-FC/6-31+G*	-1625.764115
B3LYP/6-31+G*	-1628.529308

**C46. Calculated energies of $C_1 H_2VO_4^-$
Aq5 G**

Method/Basis set	Energy, H
HF/6-31G*	-1623.633058
HF/6-31+G*	-1623.682644
MP2-FC/6-31*	-1625.673473
MP2-FC/6-31+G*	-1625.778434
B3LYP/6-31+G*	-1628.534616

**C47. Calculated energies of $C_2 H_2VO_4^-$
Aq5 H**

Method/Basis set	Energy, H
HF/6-31G*	-1623.626135
HF/6-31+G*	-1623.681034
MP2-FC/6-31*	-1625.668217
MP2-FC/6-31+G*	-1625.77338
B3LYP/6-31+G*	-1628.531148

**C48. Calculated energies of $C_2 H_2VO_4^-$
Aq6 A**

Method/Basis set	Energy, H
HF/6-31G*	-1699.662574
HF/6-31+G*	-1699.718169
MP2-FC/6-31*	-1701.891477
MP2-FC/6-31+G*	-1702.007958
B3LYP/6-31+G*	-1704.977617

C49. Calculated energies of $C_2 H_2VO_4^-$ Aq6 B

Method/Basis set	Energy, H
HF/6-31G*	-1699.662847
RHF/6-31+G*	-1699.718102
MP2 /6-31G*	-1701.890499
MP2 /6-31+G*	-1702.006708
B3LYP/6-31+G*	-1704.976164

C50. Energy Comparison of $VO(OH)_4^-$ and $H_2VO_4^- \cdot H_2O$

	$VO(OH)_4^-$	$H_2VO_4^- \cdot H_2O$
PCM B3LYP/cc-pVTZ	-1323.06037538	-1323.08385675
PCM CCSD(T)/cc-pVTZ	-1321.4496629	-1321.4762368

C51. The calculated V=O bond Lengths of $\text{H}_2\text{VO}_4^- \cdot n\text{H}_2\text{O}$, $n = 0-6$.

Name of Complex	MP2 V=O Bond Length, Å	B3LYP V=O Bond Length, Å
H_2VO_4^-	1.6711	1.624462
$\text{H}_2\text{VO}_4^- \cdot \text{H}_2\text{O}$	1.672147 1.666877	1.627904
$\text{H}_2\text{VO}_4^- \cdot 2\text{H}_2\text{O}$	1.626427 1.626075	1.665038 1.669425
$\text{H}_2\text{VO}_4^- \cdot 3\text{H}_2\text{O}$	1.668481 1.666442	1.626 1.625946
$\text{H}_2\text{VO}_4^- \cdot 4\text{H}_2\text{O}$	1.670474	1.62699
$\text{H}_2\text{VO}_4^- \cdot 5\text{H}_2\text{O}$	1.669259 1.671027	1.625544 1.630646
$\text{H}_2\text{VO}_4^- \cdot 6\text{H}_2\text{O}$	1.669608 1.676798	1.642436 1.638664

C52. The calculated V-O bond lengths of $\text{H}_2\text{VO}_4^- \cdot n\text{H}_2\text{O}$, $n = 0-6$.

Name of Complex	MP2 V-O Bond Length, Å	B3LYP V-O Bond Length, Å
H_2VO_4^-	1.916696	1.859739
$\text{H}_2\text{VO}_4^- \cdot \text{H}_2\text{O}$	1.9032 1.93092	1.847962
$\text{H}_2\text{VO}_4^- \cdot 2\text{H}_2\text{O}$	1.859197 1.840859	1.941354 1.914945
$\text{H}_2\text{VO}_4^- \cdot 3\text{H}_2\text{O}$	1.921949 1.92007	1.862306 1.8351
$\text{H}_2\text{VO}_4^- \cdot 4\text{H}_2\text{O}$	1.908965	1.850721
$\text{H}_2\text{VO}_4^- \cdot 5\text{H}_2\text{O}$	1.888793 1.926115	1.847858 1.843149
$\text{H}_2\text{VO}_4^- \cdot 6\text{H}_2\text{O}$	1.866398 1.911633	1.822263 1.816651

C53. The calculated V- -O bond lengths of $\text{H}_2\text{VO}_4^- \cdot n\text{H}_2\text{O}$, $n = 0-6$.

Name of Complex	MP2 V-O Bond Length, Å	B3LYP V-O Bond Length, Å
$\text{H}_2\text{VO}_4^- \cdot \text{H}_2\text{O}$	3.709333	3.549921
$\text{H}_2\text{VO}_4^- \cdot 2\text{H}_2\text{O}$	3.710864	3.39346
	3.612102	3.884324
$\text{H}_2\text{VO}_4^- \cdot 3\text{H}_2\text{O}$	3.718842	3.80275
	3.462056	3.801837
	3.588574	3.901118
$\text{H}_2\text{VO}_4^- \cdot 4\text{H}_2\text{O}$	3.767519	3.76892
	3.430191	3.361116
$\text{H}_2\text{VO}_4^- \cdot 5\text{H}_2\text{O}$	3.745671	3.885426
	3.427313	3.372496
	3.703936	3.747245
	3.725951	3.670073
$\text{H}_2\text{VO}_4^- \cdot 6\text{H}_2\text{O}$	3.417031	3.915168
	3.877505	3.775523
	3.582872	3.842129
	3.41636	3.407041
	3.765499	3.67776
	3.734187	3.746151
	3.742266	3.762818

C54. The MP2/6-31+G* calculated vibrational frequencies of $\text{H}_2\text{VO}_4^- \cdot n\text{H}_2\text{O}$, $n = 0-6$.

Name of Complex	MP2 V=O Bond Length, Å		
	Wavenumber, cm^{-1}	Mode	
H_2VO_4^-	160	A	Deformation
	209	A	Deformation
	230	B	Deformation
	252	B	Deformation
	335	A	Deformation
	561	A	Sym Stretch V-O
	590	B	Asym Stretch V-O
	939	A	Sym Stretch V=O
	979	B	Asym Stretch V=O

$\text{H}_2\text{VO}_4^- \cdot \text{H}_2\text{O}$	173	A	Deformation
	179	A	Deformation
	223	A	Deformation
	250	A	Deformation
	271	A	Deformation
	556	A	Sym Stretch V-O
	600	A	Asym Stretch V-O
	943	A	Sym Stretch V=O
984	A	Asym Stretch V=O	
$\text{H}_2\text{VO}_4^- \cdot 2\text{H}_2\text{O}$	182	A	Deformation
	219	A	Deformation
	268	A	Deformation
	301	A	Deformation
	330	A	Deformation
	545	A	Sym Stretch V-O
	574	A	Asym Stretch V-O
	946	A	Sym Stretch V=O
984	A	Asym Stretch V=O	
$\text{H}_2\text{VO}_4^- \cdot 3\text{H}_2\text{O}$	166	A	Deformation
	222	A	Deformation
	248	A	Deformation
	282	A	Deformation
	320	A	Deformation
	562	A	Sym Stretch V-O
	594	A	Asym Stretch V-O
	947	A	Sym Stretch V=O
988	A	Asym Stretch V=O	
$\text{H}_2\text{VO}_4^- \cdot 4\text{H}_2\text{O}$	190	A	Deformation
	192	B	Deformation
	249	B	Deformation
	321	A	Deformation
	330	A	Deformation
	566	A	Sym Stretch V-O
	603	B	Asym Stretch V-O
	937	A	Sym Stretch V=O
	1003	B	Asym Stretch V=O

$\text{H}_2\text{VO}_4^- \cdot 5\text{H}_2\text{O}$	226	A	Deformation
	258	A	Deformation
	282	A	Deformation
	298	A	Deformation
	328	A	Deformation
	335	A	Deformation
	555	A	Sym Stretch V-O
	573	A	Asym Stretch V-O
	611	A	Asym Stretch V-O
	919	A	Sym Stretch V=O
942	A	Asym Stretch V=O	
997	A	Asym Stretch V=O	
$\text{H}_2\text{VO}_4^- \cdot 6\text{H}_2\text{O}$	205	A	Deformation
	252	A	Deformation
	260	A	Deformation
	284	A	Deformation
	312	A	Deformation
	338	A	Deformation
	739	A	Sym Stretch V-O
	770	A	Asym Stretch V-O
	830	A	Asym Stretch V-O
	1043	A	Stretch V=O

C55. The B3LYP/6-31+G* calculated vibrational frequencies of $\text{H}_2\text{VO}_4^- \cdot n\text{H}_2\text{O}$, $n=0-6$.

Name of Complex	B3LYP V=O Bond Length, Å		
	Wavenumber, cm^{-1}	Mode	
H_2VO_4^-	189	A	Deformation
	229	A	Deformation
	259	B	Deformation
	280	B	Deformation
	363	A	Deformation
	664	A	Sym Stretch V-O
	649	B	Asym Stretch V-O
	1001	A	Sym Stretch V=O
	1015	B	Asym Stretch V=O
$\text{H}_2\text{VO}_4^- \cdot \text{H}_2\text{O}$	233	A	Deformation
	260	B	Deformation
	290	A	Deformation
	316	B	Deformation
	375	A	Deformation
	647	B	Sym Stretch V-O
	660	A	Asym Stretch V-O
	996	A	Sym Stretch V=O
	999	B	Asym Stretch V=O
$\text{H}_2\text{VO}_4^- \cdot 2\text{H}_2\text{O}$	242	A	Deformation
	255	A	Deformation
	291	A	Deformation
	325	A	Deformation
	371	A	Deformation
	660	A	Sym Stretch V-O
	678	A	Asym Stretch V-O
	999	A	Sym Stretch V=O
	1005	A	Asym Stretch V=O
$\text{H}_2\text{VO}_4^- \cdot 3\text{H}_2\text{O}$	216	A	Deformation
	253	A	Deformation
	270	A	Deformation
	298	A	Deformation
	334	A	Deformation
	365	A	Deformation
	643	A	Sym Stretch V-O
	679	A	Asym Stretch V-O
	1001	A	Sym Stretch V=O
	1008	A	Asym Stretch V=O

$\text{H}_2\text{VO}_4^- \cdot 4\text{H}_2\text{O}$	213	B	Deformation
	236	A	Deformation
	288	B	Deformation
	329	B	Deformation
	330	A	Deformation
	345	A	Deformation
	650	B	Sym Stretch V-O
	651	A	Asym Stretch V-O
	933	B	Sym Stretch V=O
	989	B	Asym Stretch V=O
	995	A	Asym Stretch V=O
1062	B	Asym Stretch V=O	
$\text{H}_2\text{VO}_4^- \cdot 5\text{H}_2\text{O}$	223	A	Deformation
	238	A	Deformation
	294	A	Deformation
	333	A	Deformation
	348	A	Deformation
	362	A	Deformation
	654	A	Sym Stretch V-O
	663	A	Asym Stretch V-O
	975	A	Sym Stretch V=O
	993	A	Asym Stretch V=O
	999	A	Asym Stretch V=O
1069	A	Asym Stretch V=O	
$\text{H}_2\text{VO}_4^- \cdot 6\text{H}_2\text{O}$	263	A	Deformation
	308	A	Deformation
	323	A	Deformation
	331	A	Deformation
	370	A	Deformation
	682	A	Sym Stretch V-O
	697	A	Asym Stretch V-O
	950	A	Asym Stretch V-O
	967	A	Sym Stretch V=O
	983	A	Asym Stretch V=O
	1051	A	Asym Stretch V=O

Chapter VI**D1. Mechanism I energies calculated at the B3LYP/cc-PVTZ**

H_3VO_4	H_3O^+	(A)	(B)	(C)
-1246.99633	-76.699109	-1323.759527	-1323.704366	-1323.746148

D2. Mechanism I energies calculated at the PCM B3LYP/cc-PVTZ

H_3VO_4	H_3O^+	(A)	(B)	(C)
-1247.06177	-76.85710024	-1323.9480858	-1323.896277	-1323.9437931

D3. Mechanism II energies calculated at the B3LYP/cc-PVTZ

H_2VO_4^-	H_3O^+	{A}	{B}	$\text{H}_3\text{VO}_4 \cdot \text{H}_2\text{O}$
-1246.46992	-76.699109	-1323.40083	-1400.33392	-1323.52034672

D4. The B3LYP/6-31+G* Calculated energies of solvated penta coordinate H_4VO_5^-

<A>		<C1>	<C2>
-3157.384097	-3157.395673	-3157.869007	-3157.86060

D5. The PCM B3LYP/6-31+G* Calculated energies of solvated penta coordinate H_4VO_5^-

<A>		<C1>	<C2>
-3157.476225	-3157.48627521	-3157.925791	-3157.915656

D6. The Energies of $\text{H}_2\text{VO}_4^- \cdot 34\text{H}_2\text{O}$ (tetra) and $\text{H}_4\text{VO}_5^- \cdot 33\text{H}_2\text{O}$ (penta)

Tetra	Penta	PCM Tetra	PCM Penta
-3845.39099467	-3845.389736	-3845.491494	-3845.479458

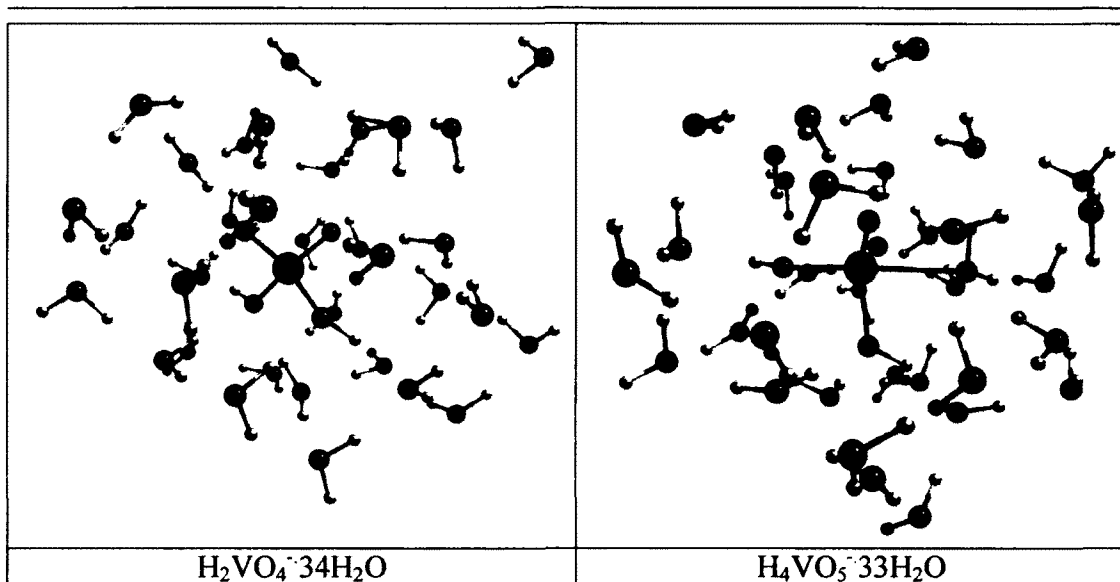


Figure D. The B3LYP/6-31+G* calculated geometries of $\text{H}_2\text{VO}_4^{2-} \cdot 34\text{H}_2\text{O}$ and $\text{H}_4\text{VO}_5^- \cdot 33\text{H}_2\text{O}$



**Saint Mary's
University**

Halifax, Nova Scotia
Canada B3H 3C3

Patrick Power Library

tel 902.420.5534

fax 902.420.5561

web www.stmarys.ca

Copyright Permission Notice

Documentation regarding permissions for the use of copyrighted material in this thesis is on file at the Saint Mary's University Archives. Contact us if you wish to view this documentation:

Saint Mary's University, Archives
Patrick Power Library
Halifax, NS
B3H 3C3

Email: archives@smu.ca
Phone: 902-420-5508
Fax: 902-420-5561